Title
WAVELENGTH MODULATION SPECTROSCOPY OF SOME SEMICONDUCTORS AND METALS

Author
Stokes, Jeffrey Andrew.

Publication Date
1973-03-01

WAVELENGTH MODULATION SPECTROSCOPY OF SOME SEMICONDUCTORS AND METALS

Jeffrey Andrew Stokes
(Ph. D. Thesis)

March 1973

Prepared for the U. S. Atomic Energy Commission under Contract W-7405-ENG-48

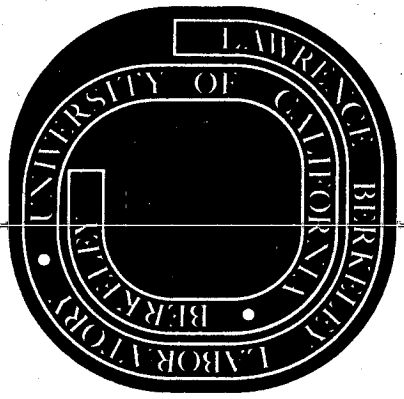

LBL-1125
c.1

DISCLAIMER

Table of Contents

WAVELENGTH MODULATION SPECTROSCOPY OF SOME SEMICONDUCTORS AND METALS

Jeffrey Andrew Stokes

Inorganic Materials Research Division, Lawrence Berkeley Laboratory
and Department of Physics; University of California
Berkeley, California

ABSTRACT

Three types of experiment were performed on a wavelength modulation spectrometer with spectral range from 1.5 to 6.0 eV. The spectrometer is described, as well as the uniaxial stress apparatus used in one of the experiments.

The derivative reflectivity spectra measured at 5°, 77°, and 300°K for the noble metals (Cu, Ag, Au) and for two III-V semiconductors (GaP, InP) are presented and discussed. The results are interpreted with the help of pseudopotential band structure calculations carried out concurrently by other workers. The data for GaP and InP are compared with previous measurements on the other III-V compounds.

Taking advantage of the sensitivity of the wavelength modulation technique, the derivative reflectivity of GaAs in the E_0' region was obtained for uniaxial stresses up to 8 kbars in the (111) direction and up to 9 kbars in the (001) direction. A theoretical treatment of the effects of stress perturbation is presented and is used to interpret the experimental curves. We have found that the dominant structure in the E_C' region arises from $\Delta_5^v \rightarrow \Delta_5^c$ transitions.

I. INTRODUCTION

The wavelength modulation technique, along with other types of modulation spectroscopy,[1] has provided the means for a detailed examination of the optical spectrum of semiconductors. Not only have new structures been seen in derivative reflectivity[2] and absorption spectra,[3] but other new information has been obtained from these spectra: accurate location of critical points,[2,4] evidence of hyperbolic excitons,[5] spin-orbit splittings of bands,[2,4] energies of indirect gaps,[6] and accurate measurements of temperature and pressure shifts.[7,8,9] In the present work we have extended applications of the wavelength modulation spectrometer to the study of metals (Cu, Ag, Au), as well as measuring the derivative reflectivity for two III-V semiconductors (GaP, InP) not covered by Zucca,[10] who built the apparatus. We will present curves of (1/R)dR/dE for these crystals in the range 2.0 to 6.0 eV at 5°, 77°, and 300°K. Like Zucca, Shen, et.al.,[11] we have correlated our results with empirical pseudopotential calculations carried out concurrently by C. Y. Fong, Y. Tsang, C. V. de Alvarez, J. Walter, and M. L. Cohen.[12,13,14,15] Also, we report derivative reflectivity curves for the E_0' region of GaAs at 5°K under uniaxial stresses of up to 8 kbars in the (111) direction and 9 kbars in the (001) direction. This extends earlier work on the uniaxial stress dependence of E_0' structures of Si[8] and Ge (diamond structure compounds).

One of the goals of optical studies of semiconductors and other crystals is the determination of the band structure $\mathcal{E}(\underset{\sim}{k},\ell)$ and hopefully

of the dipole matrix elements between states of the crystal, $\langle \psi_{\underset{\sim}{k},\ell} | \underset{\sim}{p} | \psi_{\underset{\sim}{k},\ell'} \rangle$. The optical properties of a crystal are derived from its dielectric function, which is a tensor for a non-cubic crystal or in a uniaxially-stressed cubic crystal. In the framework of the one-electron, random phase, and self-consistent field approximations, the dielectric function can be written[16] as

$$\underset{\approx}{\varepsilon}(\underset{\sim}{q},\omega) = \underset{\approx}{1} + \frac{4\pi e^2}{m^2\omega^2\Omega} \sum_{\underset{\sim}{k},\ell,\ell'} \frac{\left[f_0(\mathcal{E}_{\underset{\sim}{k}+\underset{\sim}{q},\ell'}) - f_0(\mathcal{E}_{\underset{\sim}{k},\ell})\right] (u_{\underset{\sim}{k},\ell} | \underset{\sim}{\pi} | u_{\underset{\sim}{k}+\underset{\sim}{q},\ell'}) (u_{\underset{\sim}{k}+\underset{\sim}{q},\ell'} | \underset{\sim}{\pi} | u_{\underset{\sim}{k},\ell})}{\hbar\omega - (\mathcal{E}_{\underset{\sim}{k}+\underset{\sim}{q},\ell'} - \mathcal{E}_{\underset{\sim}{k},\ell}) + \frac{i\hbar}{\tau_{\underset{\sim}{k}+\underset{\sim}{q},\ell';\ \underset{\sim}{k},\ell}}} - \frac{4\pi Ne^2}{m\omega^2\Omega} \underset{\approx}{1} , \tag{1a}$$

where

$$\underset{\sim}{\pi} \equiv \underset{\sim}{p} + \hbar\underset{\sim}{k} + \frac{1}{2}\hbar\underset{\sim}{q} , \tag{1b}$$

and

$$|\psi_{\underset{\sim}{k},\ell}\rangle = \frac{1}{\Omega^{1/2}} u_{\underset{\sim}{k},\ell}(\underset{\sim}{x}) e^{i\underset{\sim}{k}\cdot\underset{\sim}{x}} \tag{1c}$$

Here $\underset{\approx}{1}$ is the unit dyadic, ω and $\underset{\sim}{q}$ are the frequency and wave vector of the light wave, Ω is the volume of the crystal, $f_0(\mathcal{E}_{\underset{\sim}{k},\ell})$ is the Fermi distribution, $\mathcal{E}_{\underset{\sim}{k},\ell}$ is the energy of a state with wave vector $\underset{\sim}{k}$ in band ℓ, $(1/\Omega^{1/2})u_{\underset{\sim}{k},\ell}(\underset{\sim}{x})$ is the Bloch function of this state, $\underset{\sim}{p}$ is the momentum operator, and $\tau_{\underset{\sim}{k}+\underset{\sim}{q},\ell';\ \underset{\sim}{k},\ell}$ is the relaxation time due to random processes such as impurity and phonon scattering. N is the total number of electrons in the crystal. (The last term in Eq. (1a), involving N, does not have significance

by itself, as it is exactly cancelled by certain terms in the previous sum.) $\underset{\approx}{\varepsilon}(\underset{\sim}{q},\omega)$ as given in Eq. (1a) is quite general and applies to both longitudinal and transverse optical waves, except that certain local field effects have not been included.[16] In cubic crystals the dyadic $\langle \underset{\sim}{\pi} \rangle \langle \underset{\sim}{\pi} \rangle$ becomes the unit dyadic for small $\underset{\sim}{q}$, and $\underset{\approx}{\varepsilon}(0,\omega)$ can be treated as a scalar. In treating our experiments, the $\underset{\sim}{q}$-dependence of $\varepsilon(q,\omega)$ can be neglected, because the wavelength of the light is 500-1000 times greater than the spatial period of the lattice. Specific forms of $\varepsilon(0,\omega)$ will be exhibited later in connection with particular applications.

The reflectivity at normal incidence and absorption are given by,

$$R = \frac{(n-1)^2 + k^2}{(n+1)^2 + k^2} \tag{2a}$$

$$\eta = 2nk\,\frac{\omega}{c} \tag{2b}$$

where the real and imaginary parts of the index of refraction N are

$$n = \sqrt{\frac{\varepsilon_1 + \sqrt{\varepsilon_1^2 + \varepsilon_2^2}}{2}} \tag{3a}$$

$$k = \sqrt{\frac{-\varepsilon_1 + \sqrt{\varepsilon_1^2 + \varepsilon_2^2}}{2}} \tag{3b}$$

or

$$N = n + ik = \sqrt{\varepsilon} = \sqrt{\varepsilon_1 + i\varepsilon_2} \tag{4}$$

Clearly, from a measurement of R or η it is virtually impossible to obtain all the detailed information about the tremendous number of electronic states of the crystal. Because these states lie in broad, overlapping bands, $\varepsilon(\omega)$, along with all the quantities derived from it, is a rather featureless function of ω except at certain points, e.g., points of high symmetry. These points correspond to critical points (maxima, minima, and saddle points) in the joint density of states between two bands ℓ and ℓ' and are called van Hove singularities. Even so, $\varepsilon(\omega)$ itself is continuous at a van Hove singularity. It is in the slope of $\varepsilon(\omega)$ with respect to ω where the singularity appears, the discontinuity being semi-infinite or infinite. Even this discontinuity in slope is wiped out by damping effects, etc. Thus, in Eq. (1), when $\hbar/\tau_{\ell\ell'}$ is greater than zero the slope of $\varepsilon(\omega)$ undergoes a finite change over an energy range $\hbar/\tau_{\ell\ell'}$. However, for realistic relaxation times, corresponding to $\hbar/\tau_{\ell\ell'} \sim .001$ to .01 eV, this change in slope can still be rather sudden and large in magnitude compared to the background derivative.

Any sudden changes in the slope of $\varepsilon(\omega)$ carry over into the slope of $R(\omega)$, but in the spectrum of $R(\omega)$ itself the critical points are hard to pick out, just as with $\varepsilon(\omega)$. There are numerous such critical points in the near infrared, visible, and ultraviolet regions of the spectrum, but only three or four of them create major peaks in $R(\omega)$. The rest appear as shoulders on these peaks or not at all. Thus we would like to have an experiment which gives us $dR(\omega)/d\omega$, in order to reveal more of these critical points. This has been accomplished most directly by the use of wavelength modulation,[2,4] and indirectly by other modulation techniques such as piezoreflectivity,[1] and by mathematical differentiation of the reflectance spectrum.[17]

The energies of critical points, however, are the only real hard information about the band structure to be obtained from a reflectivity spectrum. We would like to know more than the energies of certain band edges; we want to know their location in $\underset{\sim}{k}$-space, the shape of the bands in between, and the transition probabilities between bands at each point in the zone: in short, $\mathcal{E}_{\underset{\sim}{k},\ell}$ and the matrix elements. As remarked earlier, however, we cannot work backwards from $R(\omega)$ to untangle $\varepsilon(\omega)$ because there are too many pairs of states in $\underset{\sim}{k}$-space with the same energy difference. Rather, it would be more practical to start from a theoretical band structure and calculate the reflectivity and its derivative for comparison with experiment. This is not as easy as it sounds, because of the large number of states in a crystal and because of the interaction of the electrons with each other. In order to get anywhere, one usually makes some assumptions and then calculates the band structure. But where do we start? What assumptions do we make? And, having made those assumptions and arrived at a calculated $R(\omega)$, how do we alter those assumptions in small, quantitative ways to produce a better fit of $R(\omega)$ or $dR(\omega)/d\omega$ with experiment?

At present, the most successful method of computing band structure appears to be the empirical pseudopotential method.[18] As will be described, our wavelength modulation results have been correlated with pseudopotential calculations of $R'(\omega)/R(\omega)$. The critical point energies used to adjust the pseudopotential parameters came both from our measurements and from others. In general the agreement is very promising.

The hope is that, as pseudopotential theory and modulation experiment interact, the calculated $R(\omega)$ and $R'(\omega)/R(\omega)$ will eventually agree with the measured $R(\omega)$ and $R'(\omega)/R(\omega)$. When this point is reached, we will probably have a good idea of $\mathcal{E}_{\underset{\sim}{k},\ell}$ and the matrix elements throughout the Brillouin zone.

In Chapter II we describe the design and operation of the wavelength modulation reflectance spectrometer, as well as an apparatus for applying a uniaxial stress to the sample.

In Chapter III we present the $R'(\omega)/R(\omega)$ data for the three noble metals, Cu, Ag, and Au. In Chapter IV the data for GaP and InP are described.

Chapter V gives a theoretical discussion of the effects of uniaxial stress on the E_0' region of GaAs and presents our derivative reflectivity data taken under (111) and (001) uniaxial stresses.

In order to predict the shape of structure a given critical point will produce in the optical spectrum, we have borrowed a procedure from electroreflectance theory.[19] The basis of this procedure is the belief that in the immediate neighborhood of a critical point the structure due to that critical point will dominate the spectrum. In other words, the sudden changes in slope of ε_1 and ε_2 produce a sudden change of slope in $R(\omega)$ that can be distinguished from a slow background variation of the slope. The shape of ε_1^1 and ε_2^1 at each type of critical point is well understood, and their contribution to R'/R can be deduced from

$$\frac{\Delta R}{R} = \alpha(\varepsilon_1, \varepsilon_2)\Delta\varepsilon_1 + \beta(\varepsilon_1, \varepsilon_2)\Delta\varepsilon_2 \qquad (5)$$

The hope is that α and β are smooth functions of ω and indeed they are. Seraphin and Bottka have calculated these functions from experimental ε_1 and ε_2 for Si, Ge, and GaAs.[19] The variation in α and β is roughly the same for these and other semiconductors. We have used this fact to aid in identifying the type of critical point responsible for various structures in semiconductor spectra.

Quantities similar to α and β have been calculated for the noble metals,[20] and are likewise fairly smooth.

In practice, this lineshape or "edgeshape" analysis is similar to the decomposition scheme of Zucca,[10] but we have taken a more sophisticated approach to the lineshapes, whereas he decomposed the spectra into structures approximating the derivative of a bell-shaped curve. Yet his method produces reasonable agreement with other measurements such as electroreflectance as to the major critical point energies. This is apparently a coincidence. It turns out that our predicted lineshapes for the major critical points in semiconductor spectra, those at E_0, E_1, E_2, and for an M_1 point at E_0', are all qualitatively similar to his lineshape. For other, weaker, critical points the lineshapes are significantly different. Our method has the advantages that: (1) we can eliminate one or more of the critical point types (M_0, M_1, M_2, or M_3) as being responsible for a particular structure; (2) we know what part of the structure represents the

location of the critical point; (3) we know what part of a structure to examine for exciton effects and what part not to. Shaklee, et.al.[5] has used this approach to deduce that hyperbolic excitons cause the low-temperature downward sharpening of E_1 structures in the III-V compounds. Theoretical calculations of R'/R from pseudopotential band structures show that our approach is valid wherever the one-electron approximation can be successfully applied. In fact, one of the useful features of such theoretical curves is that they tell us what kind of lineshape to look for in the experimental spectrum, and they also tell us how big it should be.

It is envisioned that a detailed approach to the line shapes of critical points in regions of the spectrum above the gap will yield information about the lifetime broadening $\tau_{\ell\ell'}$, where the concept is valid. This has already been successfully done for E_0 in GaP.[21]

II. EXPERIMENTAL DESCRIPTION

The wavelength modulation spectrometer is the same as that built and used by Ricardo R. L. Zucca[10] and Y. R. Shen with a few minor changes to be described below. For the stress experiments, we used the apparatus built by Jackson Koo[8] and R. Zucca, also modified slightly to conform to the particular situation.

A. The Wavelength Modulation Spectrometer

1. Principles

The system consists of three main segments: first, a monochromater modified to produce a wavelength-modulated beam; second, a conventional double-beam reflectance spectrometer; third, a dewar with the sample inside, capable of cooling the sample to temperatures between 1.5°K and room temperature. Figure 1 gives the layout of the apparatus. The light source at (A), a 75-watt PEK xenon short-arc lamp, or a 400-watt FAL quartz-iodine projection lamp, is focused by the spherical mirror (B) onto a narrow slit at (C). This slit, 0.1 to 0.5 mm wide, is reimaged, by spherical mirror (E), at (F) in the plane of the entrance slit of the Jarrell-Ash 0.5 m monochromater. Plane mirror (D) actually oscillated about an axis perpendicular to the paper, with a frequency of 1,000 hz. The result is that the image of (C) at (F) oscillates back and forth in the plane of the entrance slit, the jaws of the slit being opened wide to allow for the oscillation.

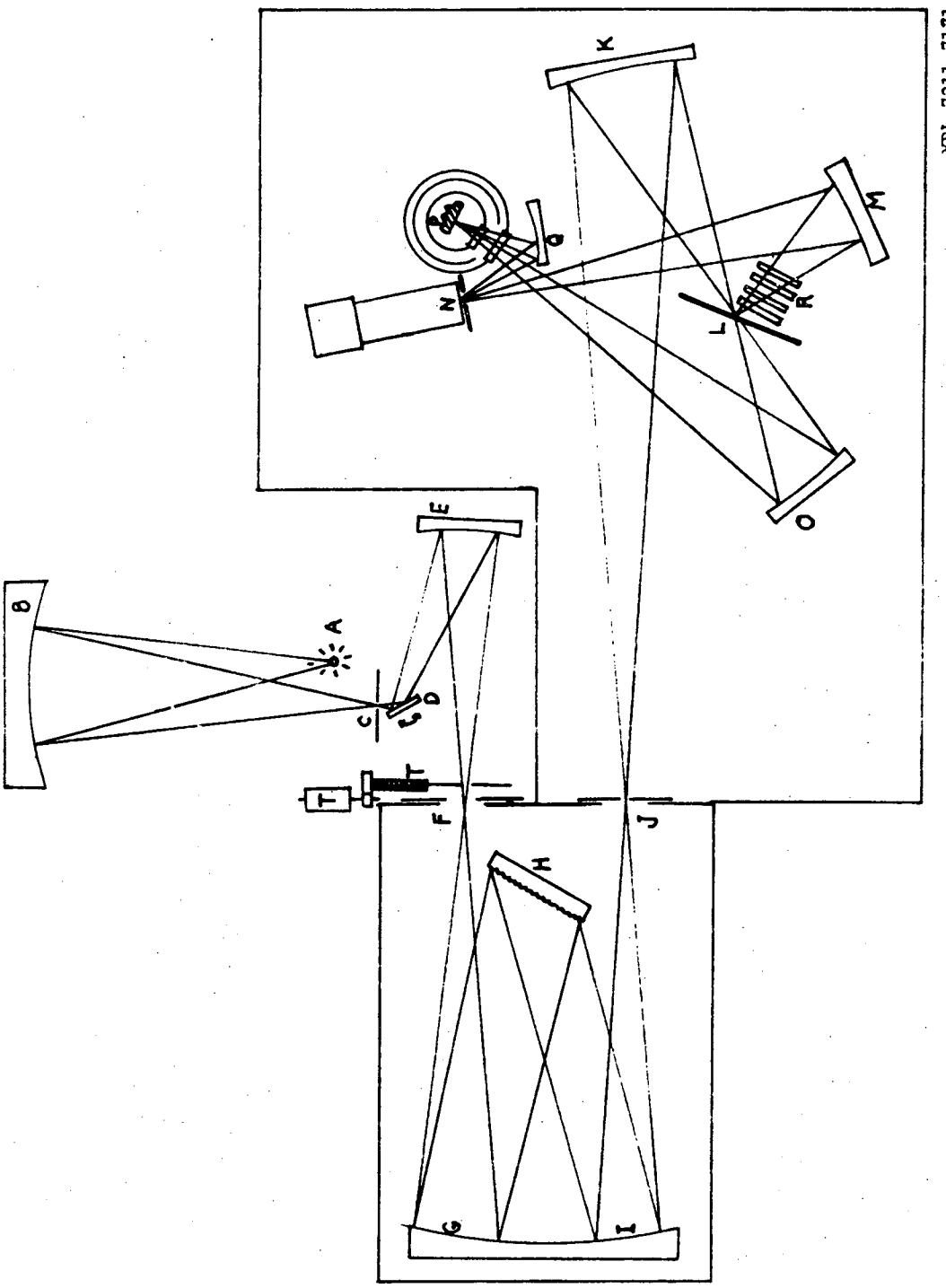

Fig.1. Wavelength modulation reflectance spectrometer.

Inside the monochromater, the back mirror forms the beam into a parallel beam (G-H); because of the oscillation of beam (F-G), the angle of the parallel beam (G-H) with respect to the grating oscillates also at 1,000 hz. The result is that the parallel beam of light (H-I) diffracted at a particular angle to the grating is oscillating in wavelength. This particular beam is focused at (J), and out of all this we get a beam, emerging from the 0.1-to 0.5 mm-wide exit slit at (J), that is oscillating in wavelength but fixed in space. λ oscillates about a central wavelength λ_0 that is determined by the angle of the grating. Thus,

$$\lambda(t) = \lambda_0 + \Delta\lambda \cos \omega t \qquad (5)$$

describes the beam emerging from the monochromater. The grating is adjusted so that the dial reading equals λ_0.

After emerging from the monochromater, the beam is focused by a small spherical mirror (K) to a small image at (L). What follows is based on the following principle: the beam is split into two equal parts and both parts undergo the same number of reflections from Al mirror surfaces before recombining, except that one beam also undergoes a reflection from the sample surface. The "separation" of the beam is accomplished by a chopper mirror at (L), which throws the whole beam first one way, (L) to (M) to (N), and then the other way, (L) to (O) to (P) to (Q) to (N). Thus when the beam travels by the first path, known as the reference channel, it undergoes two mirror reflections (Al + 480 Å MgF_2) at (L) and (M); when the beam travels the other path,

the sample channel, it undergoes two mirror reflections at (O) and (Q) plus being reflected from the sample at (P). Thus the intensities of the two beams when they reach the photomultiplier window at (N) differ by a factor of $R(\lambda_0)$, the reflectivity of the sample. The four quartz plates at (R) in the reference beam equalize the effect of the two quartz dewar windows through which the sample beam must pass twice. An auxiliary baffle at (S) is adjustable and allows us to cut down the height of the image on the sample, so it will fit.

The signal received by the photomultiplier thus has a square waveform upon which is superimposed a 1,000 hz. oscillation, as shown in Fig. 2. The reflection of a wavelength-modulated beam by a dispersive medium gives rise to an intensity modulation at the same frequency. This a.c. signal is proportional to the wavelength derivative of the reflectivity of the dispersive medium. Unfortunately, the many optical components including the lamp and the photomultiplier have dispersion of their own, and the result is a large background signal appearing in both the sample and reference channels. The actual signal due to $dR/d\lambda$ of the sample, which appears in the sample channel, may be only 10^{-4} of the background signal. Eliminating this background is the central concern in the design of the wavelength modulation spectrometer.

The various signals must first be separated. The scheme for this appears in Fig. 2. An electronic switch, synchronous with the chopper-mirror, sends the sample and reference parts of the electronic signal into separate electronic channels. (Sample/hold circuits maintain the d.c. level in each channel between the periods when the synchronous

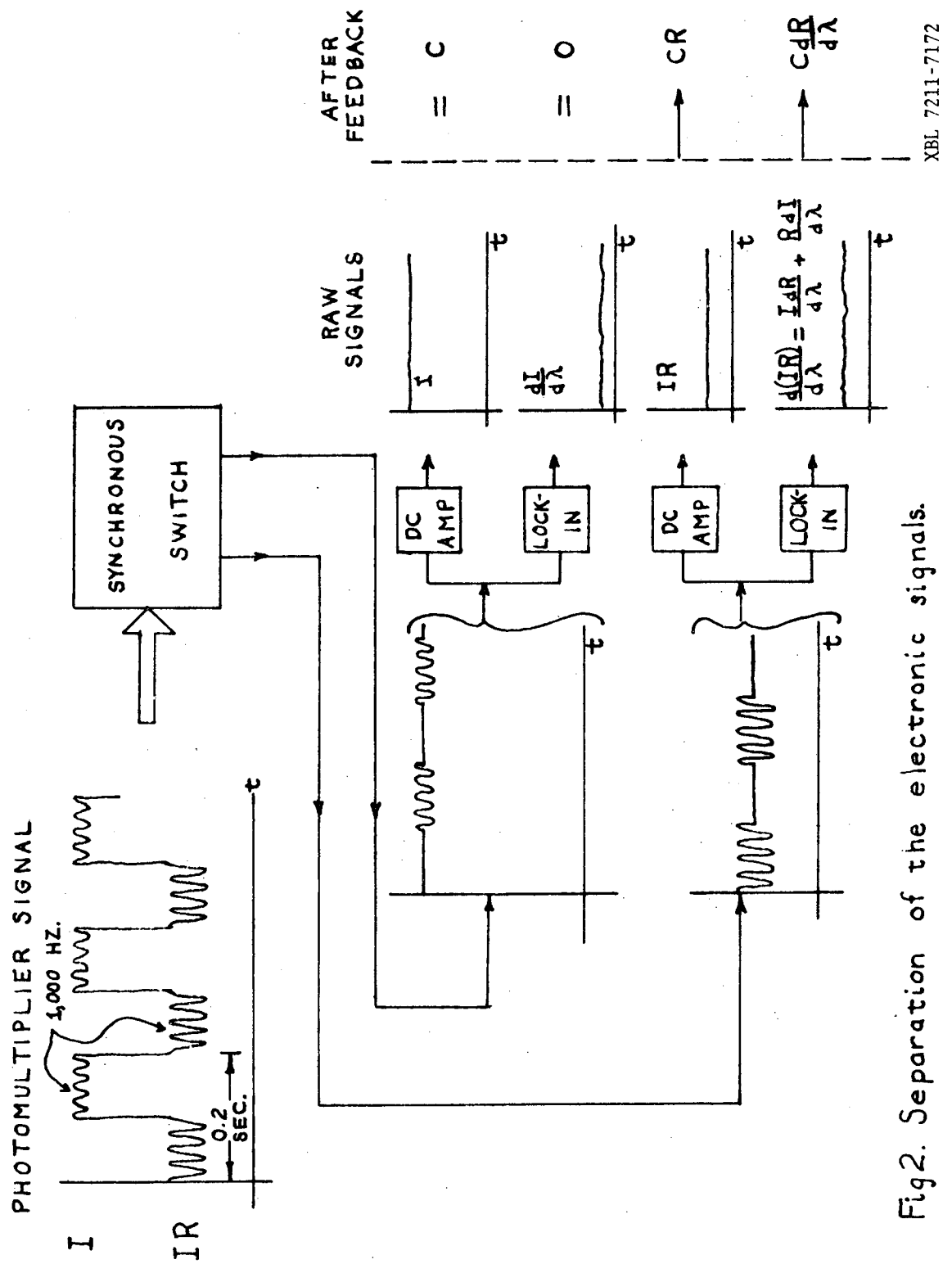

Fig2. Separation of the electronic signals.

switch is feeding the signal into that particular channel.) In each channel the d.c. level is read by a d.c. amplifier and the 1,000 hz. signal in each is read by a lock-in amplifier (PAR HR-8). The raw signals are now separated, as shown at the right of Fig. 2.

Two feedback loops are used. The first is to normalize the d.c. spectrum and is equivalent to dividing the sample beam by the reference beam to get $R(\lambda_0)$. To do this the power supply is controlled by feedback so as to keep $I(\lambda_0)$ equal to a constant, C. The sample channel d.c. signal then becomes $CR(\lambda_0)$. At the same time, the reference a.c. signal drives a motorized baffle which moves into the beam at (T) in Fig. 1 until the reference a.c. signal becomes zero. Then the sample a.c. signal is equal to $CdR/d\lambda$. R and $dR/d\lambda$ are recorded simultaneously on Moseley strip-chart recorders as functions of λ_0.

It turns out that one or both of the sample channel signals (a.c. and d.c.) can be used for the feedback loops instead. In the previous usage of the machine[10,2] IR was held constant rather than I, while $dI/d\lambda$ was held to zero as described above. If this is done, we have

REFERENCE	d.c.	I	$\longrightarrow C/R$
	a.c.	$dI/d\lambda$	$= 0$ (feedback)
SAMPLE	d.c.	IR	$= C$ (feedback)
	a.c.	$\frac{IdR}{d\lambda} + \frac{RdI}{d\lambda}$	$\longrightarrow \frac{C}{R}\frac{dR}{d\lambda}$

(6)

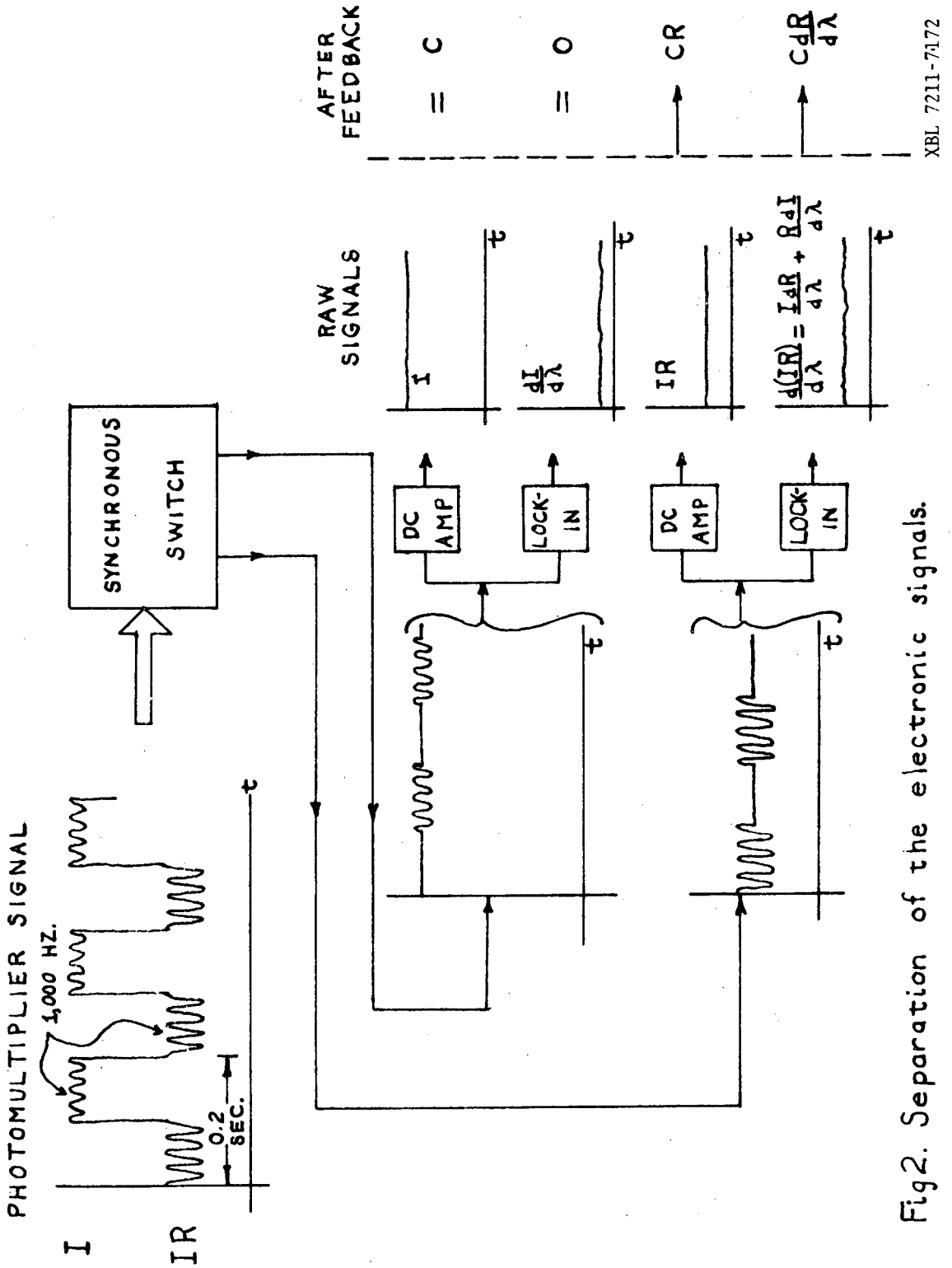

Fig2. Separation of the electronic signals.

switch is feeding the signal into that particular channel.) In each channel the d.c. level is read by a d.c. amplifier and the 1,000 hz. signal in each is read by a lock-in amplifier (PAR HR-8). The raw signals are now separated, as shown at the right of Fig. 2.

Two feedback loops are used. The first is to normalize the d.c. spectrum and is equivalent to dividing the sample beam by the reference beam to get $R(\lambda_0)$. To do this the power supply is controlled by feedback so as to keep $I(\lambda_0)$ equal to a constant, C. The sample channel d.c. signal then becomes $CR(\lambda_0)$. At the same time, the reference a.c. signal drives a motorized baffle which moves into the beam at (T) in Fig. 1 until the reference a.c. signal becomes zero. Then the sample a.c. signal is equal to $CdR/d\lambda$. R and $dR/d\lambda$ are recorded simultaneously on Moseley strip-chart recorders as functions of λ_0.

It turns out that one or both of the sample channel signals (a.c. and d.c.) can be used for the feedback loops instead. In the previous usage of the machine[10,2] IR was held constant rather than I, while $dI/d\lambda$ was held to zero as described above. If this is done, we have

$$\begin{array}{lll} \text{REFERENCE} & \text{d.c.} \quad I & \longrightarrow C/R \\ & \text{a.c.} \quad dI/d\lambda & = 0 \text{ (feedback)} \\ \text{SAMPLE} & \text{d.c.} \quad IR & = C \text{ (feedback)} \\ & \text{a.c.} \quad \frac{IdR}{d\lambda} + \frac{RdI}{d\lambda} & \longrightarrow \frac{C}{R}\frac{dR}{d\lambda} \end{array} \qquad (6)$$

Curves of $(1/R)dR/d\lambda$ are convenient because they are not affected by any experimental defect which changes $R(\lambda_0)$ by a constant factor, and also because the logarithmic derivative of R fits into Kramers-Kronig formulas. The data for GaP, InP, Cu, and Au were taken with the apparatus in this configuration.

IR = C cannot be used, however, when R is very low because the feedback has to increase the photomultiplier voltage too much to maintain IR = C and the system saturates. This was the case for Ag, which, with our resolution, has a reflectivity of 1-2% near 3.9 eV. So we used a third configuration, namely

$$\begin{array}{lll} \text{REFERENCE} & \text{d.c.} & I \;\big|\; = C \text{ (feedback)} \\ & \text{a.c.} & dI/d\lambda \longrightarrow \frac{-C}{R}\frac{dR}{d\lambda} \\ \text{SAMPLE} & \text{d.c.} & IR \longrightarrow CR \\ & \text{a.c.} & \frac{IdR}{d\lambda} + \frac{RdI}{d\lambda} \;\big|\; = 0 \text{ (feedback)} \end{array} \qquad (7)$$

This gives us the logarithmic derivative without driving the photomultiplier up to a high voltage. Also, the curves of R are more convenient than $R.^{-1}$

The fourth configuration gives C/R and $C\frac{d}{d\lambda}(1/R)$.

The dewar, a Janis Research Dewar, cools the sample by a flow of He gas, from a liquid He reservoir, past the sample holder. The temperature is regulated by balancing the current in a small heater against a valve which controls the rate of flow of He. Thus the sample is never in the liquid and the light can get to it freely

through the two suprasil quartz windows of the vacuum jacket. The temperature can be held at any value between 4.2°K and 300°K with an error of about 1°, but most of our work was at liquid He (~5°), liquid N_2 (~77°), and room (~300°) temperatures.

The 1,000 hz. oscillating mirror, purchased from American Time Products (Bulova), is driven by a tuning fork which is the tank part of a resonant circuit. By adjusting the amplitude of the oscillation, by changing the distance between the mirror and the slit (C), and by correctly focusing (C) on the plane of the entrance slit, the depth of modulation $\Delta\lambda$ can be set between 12 Å and 50 Å, peak-to-peak.

Suprasil quartz windows, a grating blazed at 1900 Å, a suprasil quartz envelope for the xenon lamp, a 480 Å coating of MgF_2 on all the aluminum mirrors, and an EMI 9558 QB photomultiplier allowed data to be taken out to 6.1 eV or 2000 Å in the uv. This wide range allowed us to see new structures in the spectra at higher energies than other modulation studies.

2. Modifications

The original wavelength modulation spectrometer[10] had a homemade oscillating mirror which worked well. Essentially a mirror mounted on two needle points and coupled to a piezoelectric bimorph, it had a moderately damped resonance near 100 hz. A sine wave of this frequency, amplified by a Bogen power amplifier up to around 200 volts, was used to drive the oscillator. However, between the measurements on GaP and InP, the power amplifier broke down, so the 1,000 hz. tuning-fork mirror was installed. The resulting signal was somewhat improved, because the tuning-fork oscillator is more stable, and

because it has a higher frequency so that 1/f noise is less. However, certain disadvantages need to be noted, in considering future modulation systems. First, this device has a minimum angular oscillation of 4.1° (p-p) which is necessary to sustain the resonant oscillations of the amplifier-tuning fork system. (The maximum is 7.2°.) Thus, although we needed finer resolution for the uv region, we were limited to a $\Delta\lambda$ of 12 Å. Second, while the mirror costs only $400, the response time of the manufacturer is quite slow, with delays up to many months for unknown reasons. The tuning-fork mirror appears to wear out after a few years, requiring higher and higher amplifier gains to start the oscillation. During the period of its functioning, however, this device provides very good wavelength modulation at medium resolution and requires no maintenance.

An improvement of major importance was carried out by fellow researchers, which made our measurements easier and also paves the way for building a vacuum ultraviolet spectrometer. This was the installation of a vacuum-ion pump in place of the oil-diffusion pump, and the replacement of the mechanical roughing pump with a cryopump containing zeolite. With this system, which provided a vacuum in the dewar jackets of 10^{-7} torr, there was absolutely no fear of the quartz windows becoming contaminated with oil at 5°. With the old pumps, this would happen within several hours.

The original sample holder[10] consisted of a flat brass surface upon which a semiconductor crystal was mounted with vacuum grease. This was satisfactory since the samples of Si, Ge, GaAs, InAs, GaSb, and InSb were flat, thin, and of uniform thickness. However, since

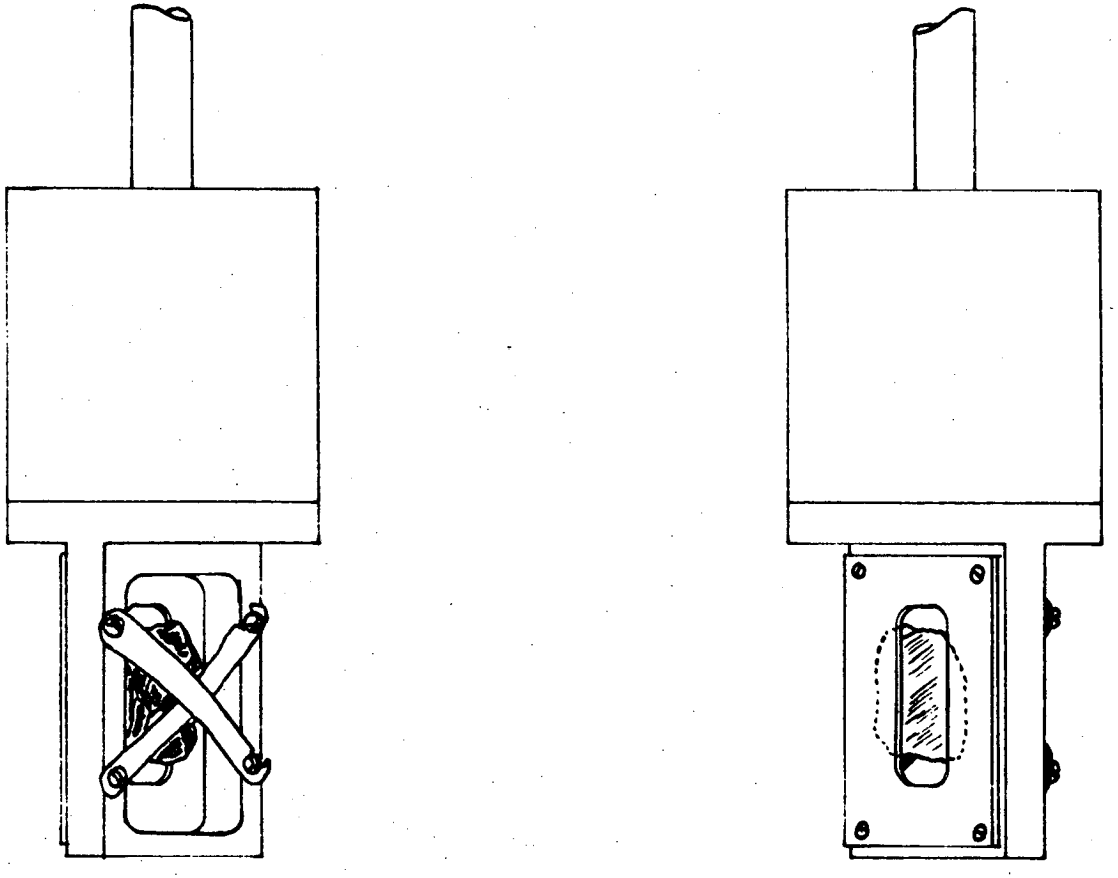

XBL 7211-7173

Fig.3. Sample holder for quick mounting of small samples.

some of the samples undertaken in this work were thick, with irregular back sides, a new method of holding the sample was sought. One of the designs used is shown in Fig. 3. In this sample holder, a mounted sample will always have its reflecting surface lying in the same plane. This plane is established by an anodized aluminum face plate, which can be easily changed for another face plate with a different hole in the front to accommodate smaller or larger samples. The sample is held against the inside of the face plate by two crossed phosphor bronze straps attached by screws. An advantage of this is that there is no vacuum grease, thus increasing the chances of keeping the system and the sample clean. Also, the sample holder was designed with speed and security of mounting in mind, since one wants to mount a sample quickly after chemical polishing and get it into the inert atmosphere in the dewar. To keep a small sample from sliding around under the straps, a block of teflon with a hole in it to fit the perimeter of the sample can be pre-cut and inserted behind the face plate. This sample holder is useful for samples prepared by cleavage, where the shape of the sample cannot always be predicted beforehand.

B. The Uniaxial Stress Apparatus

As mentioned before, we used the stress frame built by Jackson Koo and Ricardo R. L. Zucca[8] to apply uniaxial stresses to GaAs samples. Their design was based on that of Pollak and Cardona[22] except for the details of the brass plugs.

The sample holder is shown in Fig. 4. Our only modification of Koo's apparatus was to replace the steel piston and brass plug combination, also used by Pollak and Cardona, with a single brass piston on each end of the sample. As shown in the figure, the crystal is mounted with epoxy in holes in the end of each piston. Because of the permanence of epoxy it is necessary to machine new brass pistons for each sample. The larger brass pistons used in our experiment were easier to machine than the smaller brass plugs used by Koo, and the chance of misalignment was lessened. The central hole for the sample was drilled 1/32 in. deep with a flattened drill no more than .005 in. wider than necessary to accommodate the sample. A second reason for going to a single piston for each end is that the residual wobble of the system could be made smaller if there is only one piece to make instead of two. The piston diameter must be machined to a tolerance of two or three ten thousandths so that wobble is negligible but the piston still slides freely. The exact diameter must be established by trial and error but this is not difficult. The bottoms of the pistons were rounded, so that the top piston would not get stuck in its hole and so that the axis of the pistons would be determined entirely by their respective holes.

Careful orientation, cutting, and grinding of the crystal is required. This will be described later in connection with the experimental results for GaAs, along with the procedure for gluing and mounting the sample. For the stress to be uniform and to avoid shear stresses, the ends of the sample should be flat, smooth, and

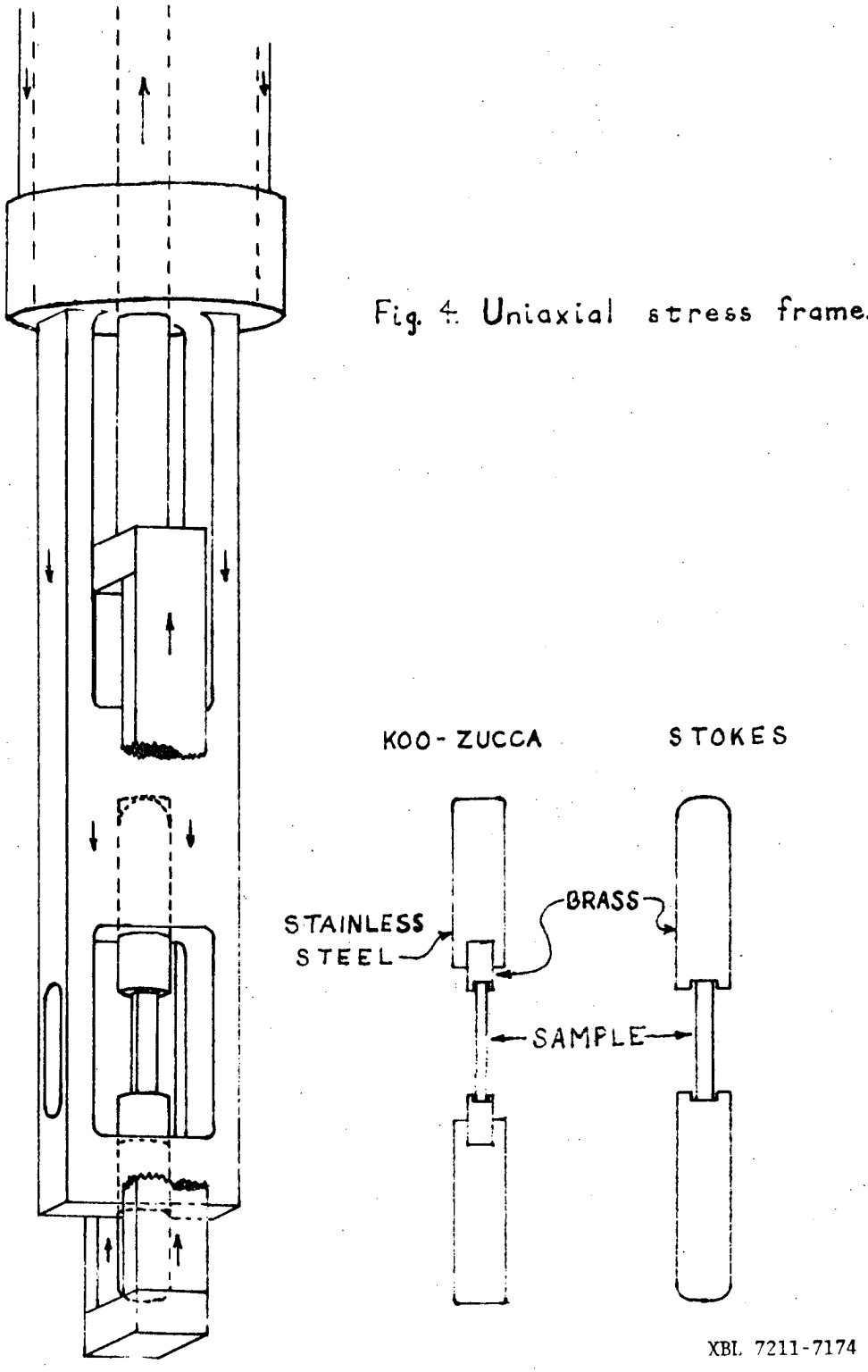

Fig. 4. Uniaxial Stress Frame.

parallel, and they should be perpendicular to the long edges of the sample. A sample for this device may have dimensions up to 13 mm by 2 mm by 2 mm.

The central rod of the stress frame is pulled on by a system of levers, designed so that the lever system pulls entirely against itself, with no strain or weight borne by the dewar. Also the sample can be raised and rotated with respect to the light beam, even while the sample is under stress. This is necessary because the support stem of the stress frame changes in length with temperature and stress. The force on the stem and the pull shaft can be as much as 700 lbs.

We turn now to theoretical and experimental discussions of the materials studied and a presentation of our results.

III. THE NOBLE METALS

A. Band Structure and Optical Properties

The band structure[12] for the outer electrons of copper (f.c.c.) is shown in Fig. 5. This was calculated by C. Y. Fong using the empirical pseudopotential method with four local pseudopotential form factors and four non-local parameters.[12,13] Similar band structures have been calculated for silver and gold.[14] These results, along with an early calculation of the Cu band structure by Segall,[23] as well as early experimental studies,[23] show that the filled d-bands in the noble metals lie just below and overlapping in energy with the conduction electron band. Thus in Fig. 5 there are 12 bands in each part of the zone (including both spins) which are filled by 10 electrons from the 3d orbitals of the free Cu atom and the one electron from the two 4s orbitals of the atom. The uppermost pair of bands are half-filled, up to the Fermi level E_F. The Fermi surface is roughly a sphere, touching the zone boundary in a small circle around L (the closest point of the boundary to Γ), and making a neck into the next zone.

Ignoring for the moment the 10 "d-bands", we would expect the electrons near the Fermi surface to give rise to optical properties appropriate to a free electron gas. In other words the Drude formula, which can be derived from (1), should be valid:[23,24]

$$\varepsilon(\omega) = 1 - \frac{\omega_{pa}^2}{\omega(\omega+i/\tau)} = 1 - \frac{\omega_{pa}^2}{(\omega^2+1/\tau^2)} + \frac{i}{\tau}\frac{\omega_{pa}^2}{\omega(\omega^2+1/\tau^2)} \qquad (8)$$

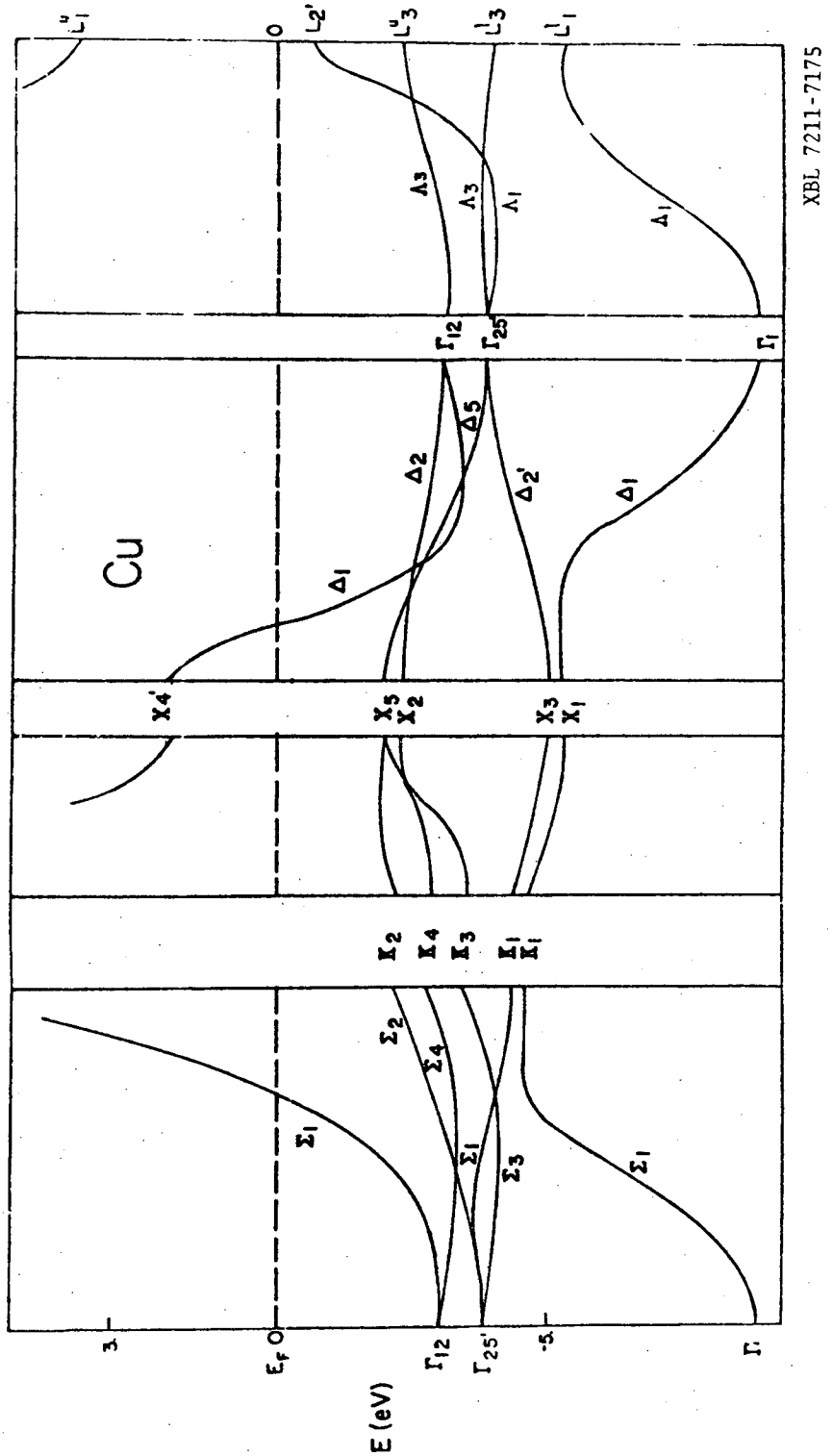

Fig. 5. Band Structure of Copper by the Empirical Pseudopotential Method.

where $\omega_{pa}^2 = 4\pi ne^2/m_a$ and n is the number of conduction electrons per unit volume, m_a^{-1} an average of the inverse effective mass over the filled portion of the conduction band,[23] and τ is a relaxation time due to phonons, electron-electron collisions, and other processes. The real and imaginary parts of this dielectric constant are shown in Fig. 6(a) (solid lines). The reflectivity arising from this $\varepsilon(\omega)$ is shown in Fig. 6(b) and the derivative in Fig. 6(c) (solid lines). The reflectivity remains nearly unity up to ω_{pa}, the "plasma frequency" for the conduction electrons, above which it drops sharply to zero.

If there were no d-bands, all three noble metals would be shiny and colorless, since $\hbar\omega_{pa}$ is around 9 eV for the conduction electrons. But the presence of the d-bands a few eV below the Fermi surface allows the possibility of interband transitions at energies below 9 eV. $\varepsilon_1(\omega)$ and $\varepsilon_2(\omega)$ resulting from these interband transitions can just be added to the curves for the free electrons, as indicated by the dashed lines in Fig. 6(a). Thus the dielectric constant becomes, using (1) to calculate the interband or "bound electron" contribution,[23]

$$\varepsilon(\omega) = 1 - \frac{\omega_{pa}^2}{\omega(\omega+i/\tau)} - \frac{1}{m}\left(\frac{e}{\pi}\right)^2 \frac{1}{3}\int d^3k \sum_{\ell,\ell',\mu}{}' \frac{f_o(\mathcal{E}_{\tilde{k},\ell})\left(\frac{2}{\hbar\omega_{\ell'\ell^m}}\right)|p_{\ell'\ell}{}^{\mu}|^2}{[(\omega + i/\tau_{\ell\ell'})^2 - \omega_{\ell\ell'}{}^2]} \qquad (9)$$

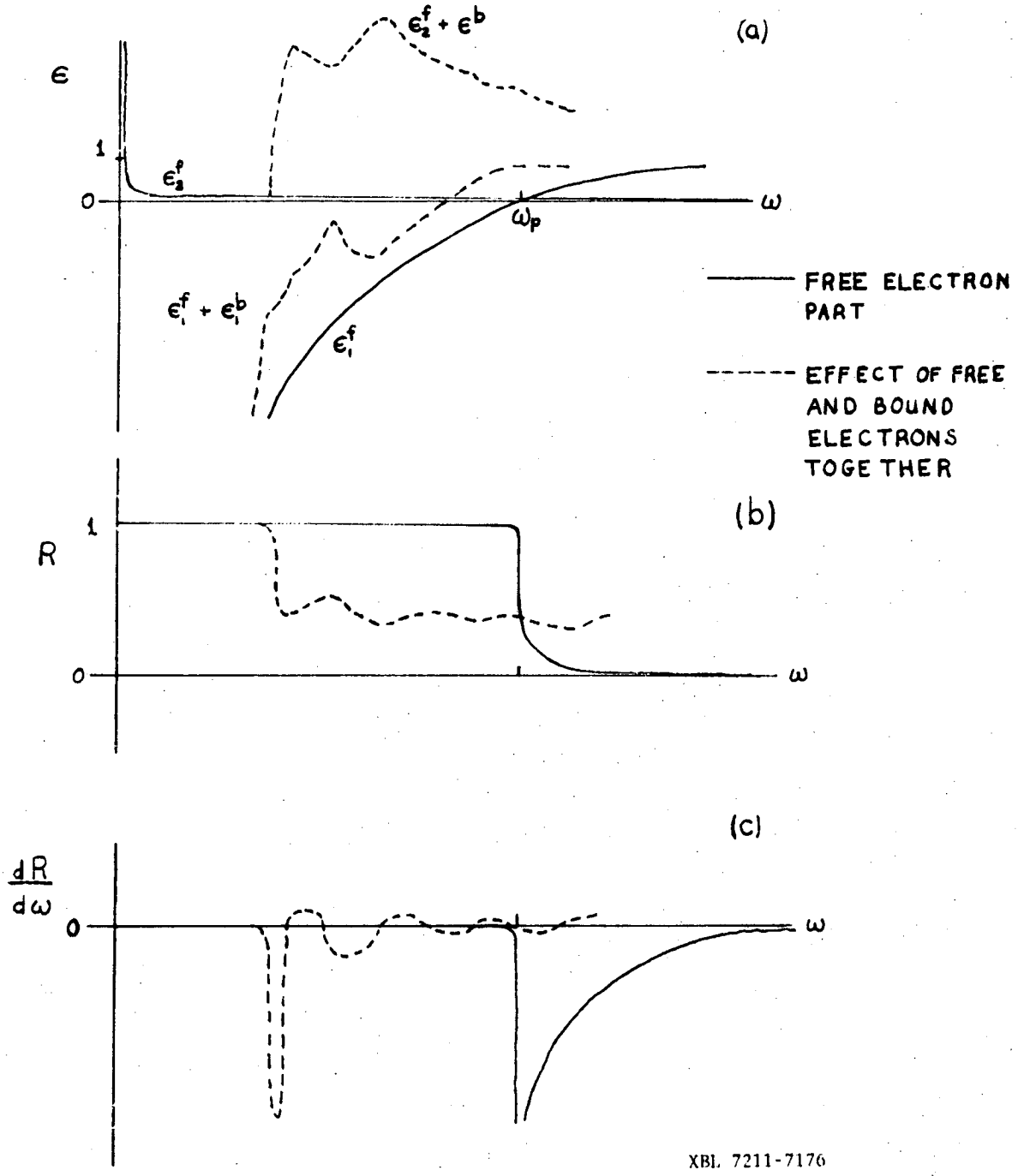

Fig. 6. Illustration of the optical properties of a typical noble metal.

where $P^{\mu}_{\ell\ell'}$ is the matrix element of p_μ between Bloch functions of bands ℓ and ℓ' at $\underline{k}$, and $\omega_{\ell'\ell}$ is the energy difference between the two bands at $\underline{k}$, and $\mu = x,y,z$. The effect of the interband transitions is to cut into the Drude free-electron high reflectivity before ω_{pa} is reached, and to add structure in the region above this cut according to the details of the interband spectrum. Three types of interband transitions give rise to structure in the optical spectra: (1) critical points; (2) osculating points, which result from transitions to or from the Fermi surface at points where it is parallel to the surface of constant interband energy; and (3) volume effects, which result from transitions over large regions of the Brillouin zone where two bands are separated by nearly the same energy. As indicated in Fig. 6(c) (dashed line), a positive swing of the derivative spectrum after the large dip is evidence that interband transitions are occuring, since the Drude theory alone (solid line) gives a derivative that is always negative.

There is also the possibility that the incoming photons in a reflectivity measurement will excite collective oscillations in the electron gas known as plasma oscillations, with a resultant absorption of energy from the incident beam and a lowering of the reflectivity. When $\varepsilon_2 \ll 1$, relatively undamped volume (bulk) plasmons can propagate near the frequency where $\varepsilon_1 = 0$; similarly, if $\varepsilon_1 = -1$, surface plasmons can propagate along the interface between a metal and a vacuum.[25,26]

The volume plasmon is a longitudinal plasma density wave with an associated electric field that is also longitudinal. With normally

incident light on an optically flat surface the transverse E-field of the incident light cannot couple with the longitudinal field of the plasmon. It has been predicted theoretically[27] that with non-normal incidence, light polarized parallel to the plane of incidence can generate volume plasmons at frequencies $\omega \geq \omega_p$ in "thick foils" (e.g., crystals). However, the calculated effect on reflectivity is still quite small. Further, the sharp dip in R at the interband threshold and the interband transitions above and in the vicinity of ω_p would effectively mask the rather smooth spectral dependence expected for the volume plasmon generation.[27] It is possible that, in a near-normal incidence reflectivity experiment like ours, surface roughness may enhance production of volume plasmons by presenting a surface of varying orientation to the incoming light beam. Nevertheless, since the effect of plasmon generation on R is small, particularly near normal incidence, we do not expect to notice any effect in our spectra.

Surface plasmons, which might be compared to water waves, contain fields which are both tangential and normal to the metal surface;[25] thus any external light wave may couple with a surface plasmon. However, the phase velocity along the metal-vacuum surface of light in vacuum is greater than that of the surface plasmon, so for a smooth surface coupling cannot occur.[28] It has been observed that surface roughness induces coupling,[26,29,30] with a consequent noticeable effect on optical properties including reflectivity. The surface plasmon frequency (at large k_{sp}) occurs somewhat below ω_p, in a region of smooth, high

reflectivity. However, a glance at the curves of ε_1 and ε_2 given by Ehrenreich, et.al[23] for the noble metals shows that favorable conditions exist only for Ag; namely, ε_2 is small when $\varepsilon_1 = -1$. Surface roughness can relax the momentum conservation requirement and allow an incident light wave to transfer energy into surface plasma modes.[26] The long wavelength surface plasmon frequency for silver should be around 3.6 eV.[23] The occurrence of a dip in R around this energy should indicate an r.m.s. surface roughness of at least 10 Å.[26,29] As we shall see, such a dip was observed in our spectra.

B. Samples and Surface Preparation

The preparation of a metallic crystal for measurement requires great care because of the softness of the material. Mechanical abrasion or cutting with a diamond saw rapidly generates dislocations throughout the crystal, broadening and shifting the structures in the spectra. Therefore "soft" methods must be used, such as spark cutting, electropolishing, and chemical lapping. Also great care must be taken to avoid knocking the crystal around, scratching the surface, or straining it during mounting.

The copper sample was a single crystal cut and prepared for cyclotron measurements,[13] which requires a greater degree of purity and perfection than optical measurements, so our sample was very good. This sample was electropolished using D. Lindholm's apparatus and following his technique exactly.[13] As with all samples, the Cu crystal was then immediately mounted in an inert atmosphere in the dewar.

The silver crystal[14] had also been used for cyclotron resonance studies.[31] The sample had been cut and electropolished by D. Howard[31] but the surface was black from years of oxide growth. In order to restore the surface to brightness it was lapped on a soft polishing cloth (Beuhler "Microcloth") wet with a suitable solution. The solution that worked best was that of J. M. Morabito, et.al.[32]

100 cc 0.2M KCN

2 cc 30% H_2O_2

WARNING:	Wear gloves, use fume hood. Cyanide is deadly poison. Never mix cyanides with acid because HCN develops!

This should be mixed just before use because the components go off as vapors (don't breathe them!) rendering it impotent. If gloves are worn, the crystal can be lightly moved around on the polishing cloth until a very shiny surface results. It is then rinsed in H_2O and CH_3OH, and quickly mounted. This chemical lapping solution seems to work best on (110) surfaces, as with our sample.

The gold crystal, from the batch of Mattera, et.al.,[33] had its reflecting surface lying in the (111) plane. The sample was prepared by dipping into semi-hot (~ 50°C) aqua regia (3 parts HCl in 1 part HNO_3) for about 1 sec., then rinsing quickly in methanol and mounting. Gold retains its polished surface better than the other two noble metals.

C. Experimental Results

The derivative spectra of Cu, Ag, and Au measured at He temperatures in Figs. 7, 8 and 9, along with the logarithmic derivative reflectivity calculated from the pseudopotential theory.[12,13,14] The overall agreement of theory and experiment is good, in particular in the region of the large dip in (1/R)dR/dE at the onset of interband transitions, except in the case of Ag, where the dip in the theory curve is .22 eV higher in energy than in the experimental curve. The reflectivity and its logarithmic derivative were obtained from the band energies and pseudowave-functions by first calculating R and its derviative. In calculating the matrix elements for $\varepsilon_2(\omega)$, the contributions of the p and s electrons of the outermost core shell (3s, 3p for Cu; 4s, 4p for Ag; 5s, 5p for Au) were explicitly included. With this step the agreement in the region of the interband onset is very good, but without it $\varepsilon_2(\omega)$ in this region is way too low as shown[12] in Fig. 10. In the case of silver, the theory and experiment curves agree in general shape, and it is anticipated that fitting the pseudopotential parameters to our data instead of to a photoemission "density of states"[14,34] will produce better agreement as to the energy of the onset.

In each of the spectra, the first structure that occurs as we move up in energy is a sharp negative dip in the slope, and right after each dip R'/R swings positive (Au and Ag) or goes through a sharp maximum just before it reaches zero (Cu). To the right of the large dip in each spectrum we find a variety of structures, which are

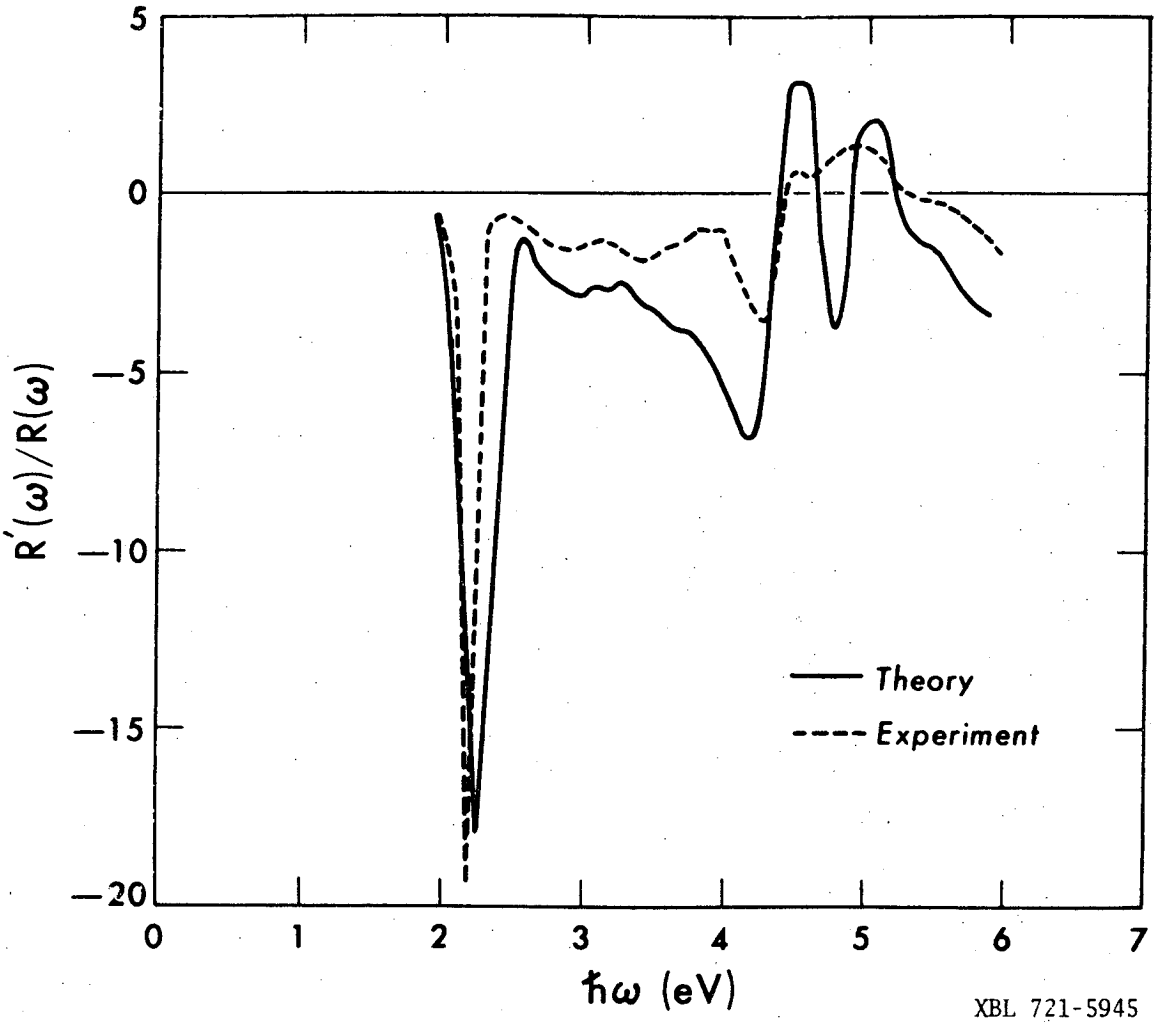

Fig. 7. Theoretical and Experimental Wavelength Modulation Spectra of Copper.

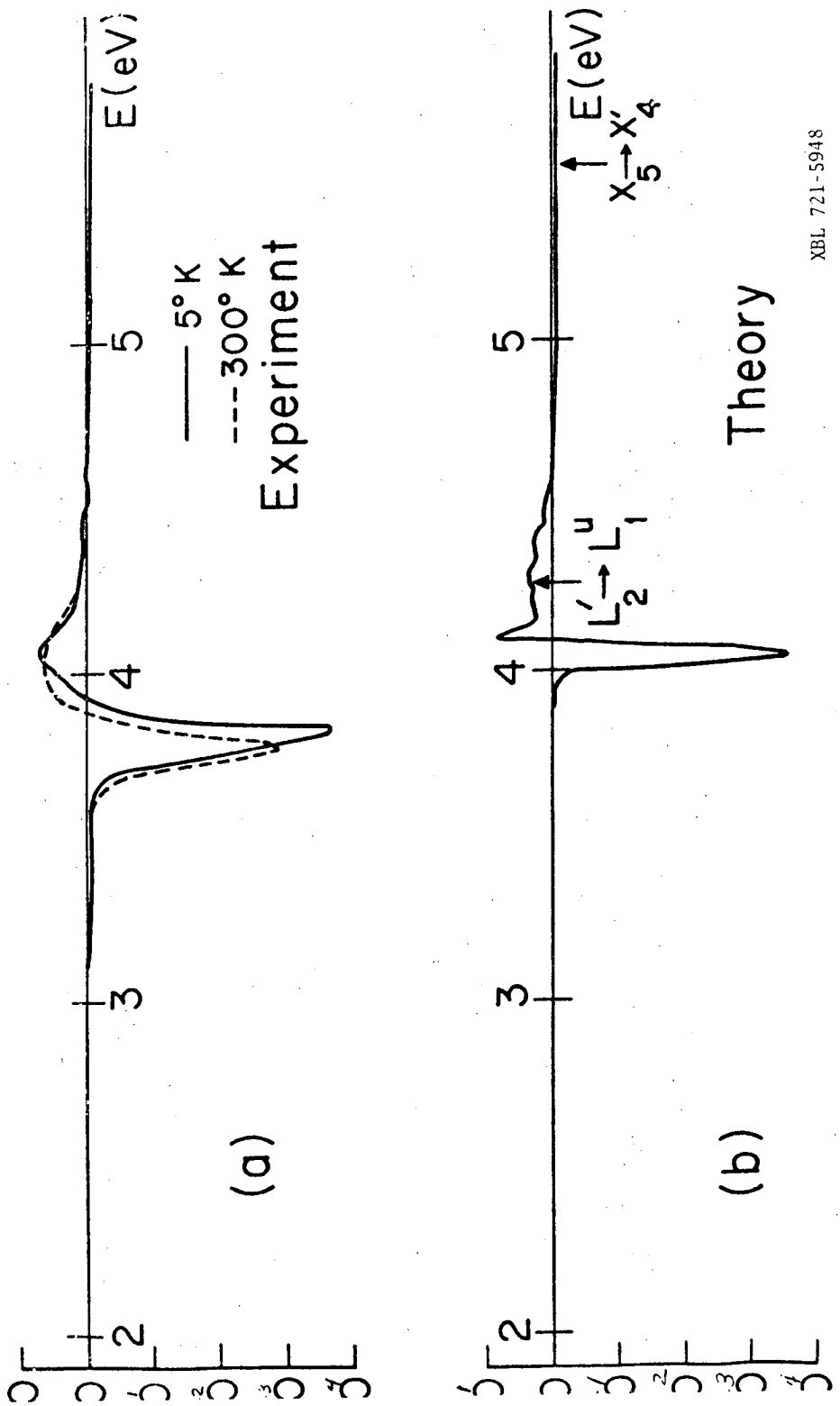

Fig. 8. Experimental and Theoretical Wavelength Modulation Spectra of Silver.

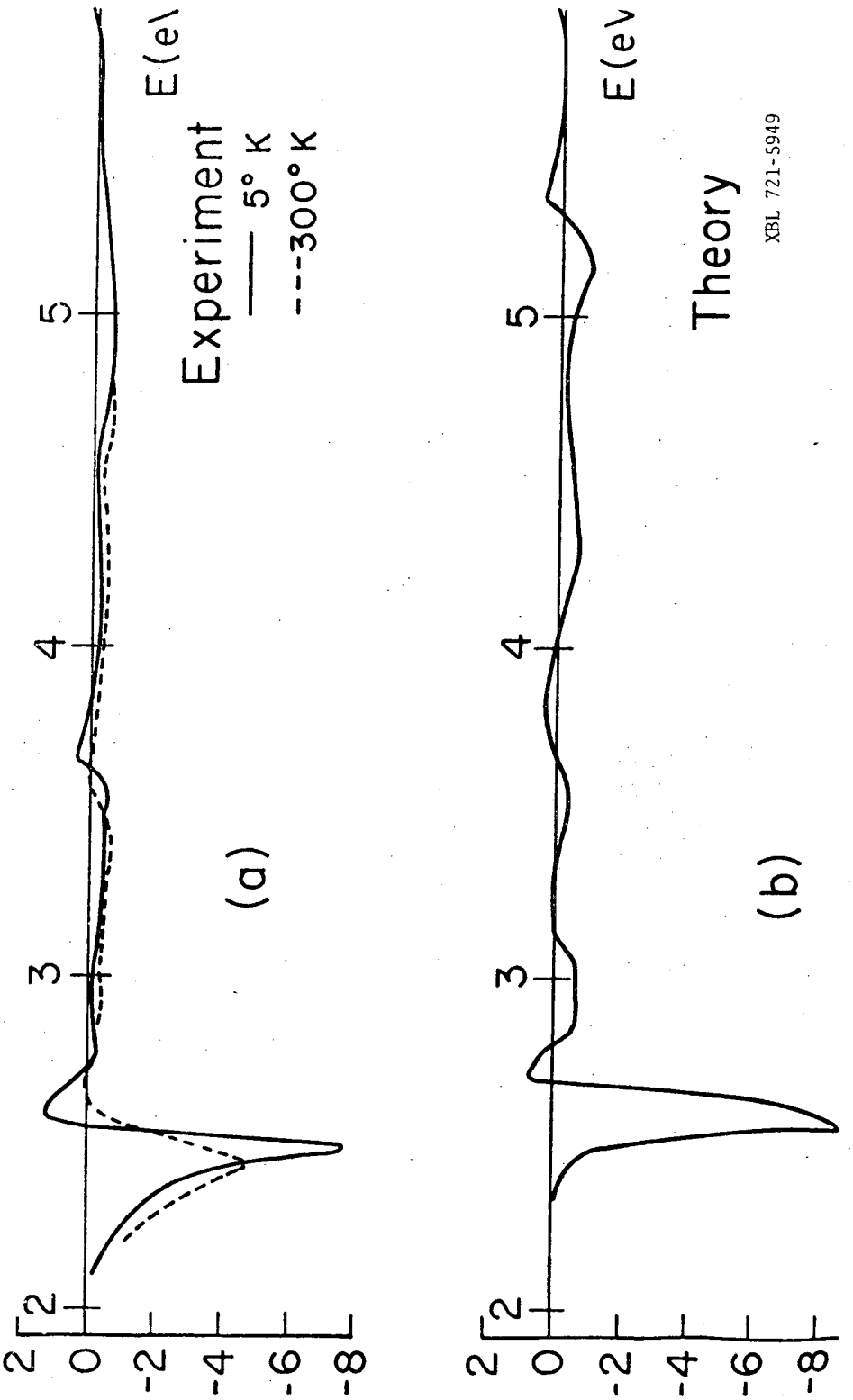

Fig. 9. Experimental and Theoretical Wavelength Modulation Spectra of Gold.

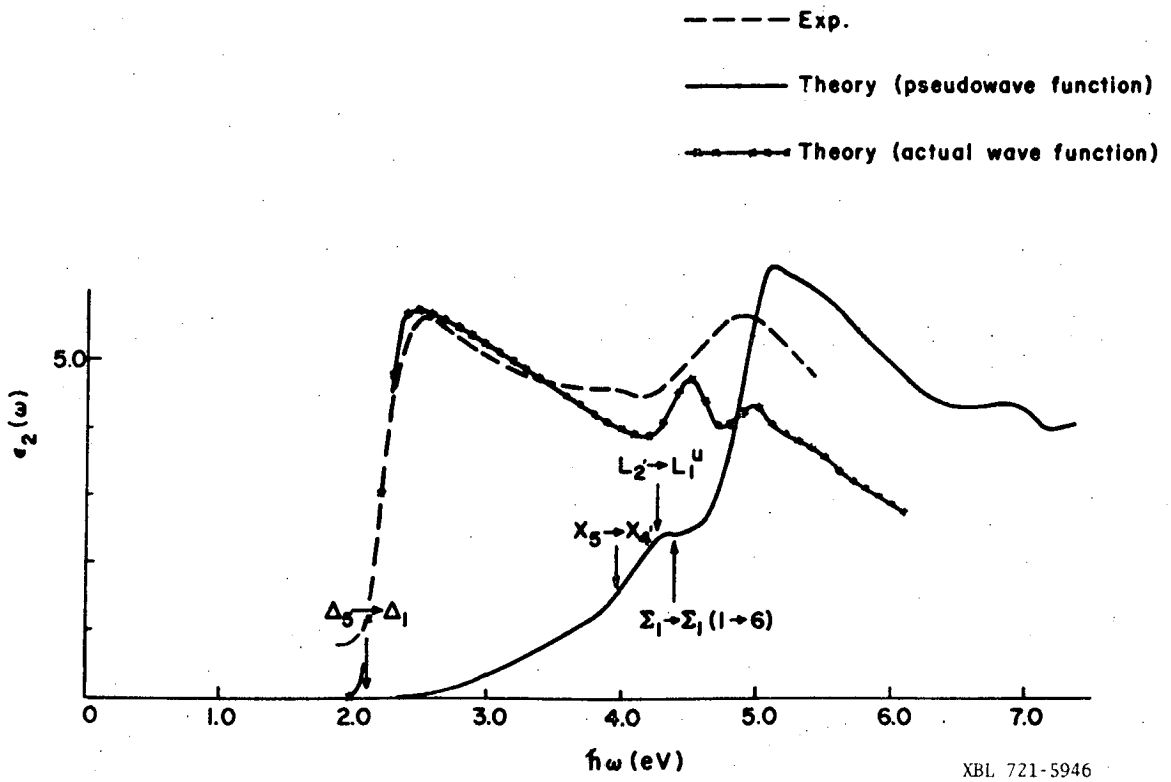

Fig. 10. Comparison of Theoretical Calculations of ε_2 at the Interband Threshold with an Experimental Result. (From Ref. 12; data is that of Gerhardt, et.al., as cited in Ref. 12.).

small in comparison to the dip, but there is not otherwise any striking similarity in the three spectra in this region.

Using the pseudopotential results as a guide, we can interpret some of the features of the experimental spectra. We start with copper[12] (Fig. 7). The large dip between 2.1 and 2.3 eV is produced by the lowest interband transitions, which originate from the bands just below the conduction band and end up on the Fermi surface. Most of these transition occur near Δ in the Brillouin zone. The bump in the data at 3.1 eV is explained by a volume effect, near X with final states in the conduction band just above the Fermi surface. Other volume effects and an osculating point ($\Sigma_1 - \Sigma_1$, band 3 to band 6, numbering the bands according to the single group notation) could acoount for the small structures at 3.6 eV and 3.8 eV. (We note that, because of the coarse mesh of points in the Brillouin zone used for calculating the joint density of states, volume effects may be emphasized in the theoretical result.) In the pronounced structure around 4.0 eV we can locate two critical points, on the basis of both the theory and our line-shape analysis scheme described in Chapter I. These are: an M_1 point, $X_5 - X_4$, (bands 4, 5 to band 6), at 3.97 ± .02 eV; an M_0 point, $L_2, - L_1^u$ (band 6 to band 7) at 4.32 ± .04 eV. Above 4.25 eV, the experimental spectrum agrees with the theory in shape but not in magnitude. We can tentatively assign the bumps near 4.5 and 5.0 eV to volume effects; also, an osculating point may contribute to the lower energy bump.

We next turn to gold,[14] because of its similarity to copper in many respects. (Fig. 9) The dip between 2.1 and 2.6 eV represents the onset of interband transitions, as with copper; these occur from the upper "d-bands" to the Fermi surface, mostly near Δ in the Brillouin zone. The shoulder at 3.0 eV corresponds to a volume effect. The cusp at 3.66 ± .05 eV is assigned to the X_5-X_4, M_1 critical point. In the theory it is at 3.84 eV. The theoretical band structure gives 3.94 eV as the energy of the L_2, - L_1^u M_0 critical point, but this is not seen in either the theoretical or experimental R'/R, and if it contributes at all it may be buried in the X_5 - X_4, structure. Higher energy structures in the data, at 4.6 and 5.6 eV, are probably volume effects.

For silver,[14] we have the same large dip, but its significance is somewhat different. First we notice that it is twice as large in energy, beginning at around 3.7 eV, beyond the visible. The L_2, - L_1^u M_0 critical point has about the same energy as the other metals, but this means that it is almost on top of the large dip instead of 1 or 2 eV above it (4.35 ± .05 eV in the data, 4.27 eV in the theory). On the other hand, the X_5 - X_4, M_1 point is about the right energy above the interband onset, as represented by the dip, but is therefore higher in energy than for Cu or Au (5.54 eV, from the theoretical band structure only). Finally, there is a small depression at 3.6 eV, probably resulting from the surface plasmon,[26,29] which we have said above is only reasonably possible in silver, and not likely in copper or gold.

All these differences between Ag and the other two metals can be related to the fact that the "d-bands" lie lower in Ag with respect to the Fermi surface than in Cu or Au, while the L_1^u valley remains about the same distance above the Fermi energy. The pseudopotential calculation confirms this. Thus the osculating points producing the dip and the X_5-X_4, point, all of which transitions initiate in the "d-bands", have higher energies in Ag by about 1.8 eV, while the $L_{2'}$-L_1^u transitions, initiating in the conduction band, have about the same energy in Ag as in Cu and Au. The fact that the interband onset in Ag is around 4 eV instead of 2 eV means that the bound electron part of ε_1 is higher up on the free-electron ε_1 curve (refer to Fig. 6a); this means that the total ε_1 can rise <u>above</u> 0 before the lowest osculating point energy (the interband onset) is reached, and hence also before ε_2 begins to rise from its relatively small free-electron value. ε_1 reaches -1 and 0, and even +1 before ε_2 increases substantially; thus the situation is right for the two kinds of plasmons to propagate. Further, consideration of the relation of R to ε_1 and ε_2 shows that in this situation the large dip in R to 1% or so comes near the energy at which ε_1 equals +1, which is right at or before the energy of the first interband transitions. (ε_1 "feels" the effect of the first osculating point well before it gets to it, but ε_2 is not affected until the point is reached, just as if the osculating point were an M_0 critical point.)[23]

The presence of surface plasmons (3.62 ± .02 eV) in our data is not surprising. The magnitude of this structure varied somewhat with repeated preparations of the sample surface, suggesting that our

lapping method leaves a residual surface roughness with variable reproducibility. Only 20 Å or so of rms roughness can produce a noticeable effect.[29] Also, we note that our beam is about 10° off normal incidence. (All the other structure in our spectra were reproducible.) Anomalies in the free carrier region of the noble metals have been observed by others,[20] and there is some debate as to their origin, but we will not pursue the question further here.

Table I summarizes the results for the noble metals. From the decent agreement of theory with experiment we can conclude, not surprisingly, that the transitions in a noble metal crystal are mostly direct,[12,34] and also that strong many-body effects are not needed to explain the gross features of the spectra near their absorption edges. The transitions listed are the main spectral features and are those discussed by most published works. More detailed studies of osculating point composition (such as that done by Ehrenreich, et.al.[23]), critical point composition, and lineshapes will no doubt be done in the future for this spectral region. With better resolution in our theory and experiment, as well as closer collaboration between the two, such a detailed analysis can be done with wavelength modulation reflectivity.

Table I. Energies of important transitions, determined from experiment. (5°K). (Energies are in eV.)

	Cu	Ag	Au
Transitions from d-bands to Fermi surface at absorption edge	2.1 (2.0-2.2)†	3.8 (3.75-4.0)	2.25±.1 (2.3-2.45)
X_5-X_4' (M_1)	3.97 (3.97-4.2)	5.54* (5.71-5.73)	3.66 (?) (3.5-4.2)
$L_2'-L_1^u$ (M_0)	4.25 (4.4-5.0)	4.35 (4.0-4.2)	3.94* (4.08-4.5)
Surface Plasmon Energy	-	3.62±.02 (3.60-3.65)	-
$\hbar\omega_p$	-	3.83±.02 (3.78-3.80)	-

†Parentheses indicate the range of values found in published studies of the noble metals, based on reflectivity,[23,29] absorption,[30] photoemission,[34,35] piezoreflectance,[36] and other studies.[26] In general these studies were done mostly at room temperature and on evaporated films.

*Theoretical value only, from pseudopotential band structure; any effect on the spectra of $(1/R)\,dR/dE$ is not seen, and therefore is less than 1 eV^{-1} in magnitude if any structure exists at all.

IV. SEMICONDUCTORS: GaP AND InP

The wavelength modulation technique is suited to the study of semiconductor and insulator crystals, because the optical structures are in general sharp and numerous. Also the detailed lineshapes in the derivative spectra are interesting because the effects of excitons and the spin-orbit interaction are clearly visible, more so than in the reflectivity. Our study of GaP and InP is a continuation of the III-V series studied by Zucca, Shen, Cohen, and Walter.[2,7,10,11,37,38]

A. Band Structure and Optical Properties

The band structures of GaP and InP are much like those of the other III-V compounds, with one important difference in the case of GaP. Of the six common and stable III-V compounds, only in GaP is the fundamental gap an indirect one, X_1^c being lower than Γ_1^c. Also, L_1^c is lower than Γ_1^c but not as low as X_1^c. The Γ-X indirect gap has been observed by wavelength modulated absorption.[3] Otherwise, GaP is similar to the other five. The possible interband transitions at symmetry points can be grouped into the usual spectral regions:[10,37] E_0, the fundamental direct gap at Γ; E_1, L_3-L_1 (M_0) and Λ_3-Λ_1 (M_1) transitions; E_0', transitions along the Δ direction, such as Δ_5-Δ_1 (M_0), Δ_5-Δ_1 (M_1), and X_5-X_1 (M_1); E_2, Σ_2-Σ_1 transitions (M_2). Often the E_0' and E_2 regions are mingled together in energy, and somewhere in this same region energy range the weak Γ_{15}-Γ_{15} transitions lie. At higher energies are E_1' transitions, $L_3(3,4)$-$L_3(6,7)$ (M_0) and $\Lambda_3(3,4)$-$\Lambda_3(6,7)$ (M_1), but for the lighter III-V's like GaP and InP

these are expected to be just beyond the 6 eV upper limit to the range of our spectrometer. The principal E_2 transition, $\Sigma_2(4)-\Sigma_1(5)$, is quite strong because the energy separation of the two bands near this point is more nearly constant over a wider range than for other critical points. Because of the strength of the E_2 transitions it is usually possible to pick it out in the spectrum and then look for the E_0' structures superimposed on it or adjacent to it.

For GaP the indirect transition would be found below the E_0 region, at 2.3 eV. It is impossible to see in a reflectivity spectrum, and almost invisible in reflectivity derivative spectra. The optical properties of these semiconductors in the E_0 through E_1' and higher regions are given by (10), without the Drude free electron term, as follows.[23]

$$\varepsilon(\omega) = 1 - \frac{1}{m}\left(\frac{e}{\pi}\right)^2 \frac{1}{3}\int d^3k \sum_{\ell,\ell',\mu}{}' \frac{f_0(\mathcal{E}_{k,\ell})\left(\frac{2}{\hbar\omega_{\ell'\ell^m}}\right)\left|p_{\ell'\ell}{}^{\mu}\right|^2}{\left[(\omega + i/\tau_{\ell'\ell})^2 - \omega_{\ell\ell'}{}^2\right]} \qquad (11)$$

The prime on the sum indicates that only transitions between different bands participate in the dielectric constant. At 0°K there can be no intraband transitions in a semiconductor because all bands are either completely filled or completely empty. This is taken care of by the Fermi distribution function, $f_o(\mathcal{E}_{k,\ell})$ in Eq. (11). For photon energies lower than the lowest gap a semiconductor is transparent because there are no final states to which to excite the electrons at these energies. In an undoped, good crystal there are also no free electrons, as there are in a metal, to follow the electric field and

radiate it back out of the sample. Because the indirect and direct gaps of GaP are so high (2.3, 2.5, and 2.8 eV) it is yellow in color and relatively transparent to red, orange, and yellow light. InP, on the other hand, is metallic in color like the other III-V compounds, since the fundamental gap is in the infrared (1.4 eV).

B. Samples and Surface Preparation

The single crystals of GaP and InP used in the experiment were kindly provided by Dr. L. M. Foster of IBM Research Laboratory, Yorktown Heights, N. Y. Both crystals were polished with abrasive powders of decreasing particle size, down to .05μ alumina (in H_2O), then chemically polished ("etched") and quickly mounted in the dewar so that exposure to the atmosphere was less than ten minutes.

The Gap sample, according to Dr. Foster, was vapor grown in a PCl_3 system on a GaAs substrate, which was later removed. The growth was on a (111A) surface. The sample has a conductivity of 10^{-8} cm^{-1} and is believed to be very pure, as is typical of growth on this orientation. For the chemical polish we used a 1:1 solution of HCl and HNO_3 for two minutes.[39] Because GaP is transparent in the yellow, we sought to minimize the error in measuring R'/R that would result in reflections from the back surface of the sample. When we got it, the back surface had already been roughened, but to reduce the effects of scattered light we decided to paint the back black. After chemical polishing we laid the sample down on several sheets of new, clean lens paper and carefully sprayed the back with black enamel. This dried in a few minutes, and then we mounted it in the dewar. After use, the black backing was easily cleaned off with acetone.

The InP sample was boat grown in near stoichiometric conditions. In order to get a piece of the right size for the sample holder, we cut off a slice with surface normal to the (001) direction and polished it down to .05μ alumina. Then it was chemically polished in a solution of 1 part Br_2 in 10 parts CH_3OH[40] and mounted for measurement.

The procedure of measurement is essentially that followed by R. Zucca[10] earlier. Resolution of the spectrometer was 50 Å.

C. Experimental Results

In Figs. 11 and 12 are the curves of (1/R)dR/dE for GaP and InP at 5°, 77°, and 300°K. Following Zucca[10] and Cardona[41] we have divided the spectra into the E_0, E_1, E_0' and E_2 regions. Note the sharpening of the structures and their shift to higher energy as the temperature decreases. The sharpening results from the decrease in relaxation effects, which are largely caused by phonons. Excitonic effects also can produce sharpening at low temperatures, as the screening due to thermal electrons and holes decreases. The shift to higher energy is the combined result of the decrease in lattice constant upon cooling, and the Debye-Waller effect, a smoothing and shallowing of the effective atomic potentials because of thermal motion of the nuclei.[37] Our results agree with existing data[3,21,17] in the E_0 and E_1 regions, and the origin of these structures is well understood.

For GaP, (Fig. 11) the double peaks at 2.8 to 3.0 eV represent the spin-orbit split direct gap at Γ, and the sharpening at 5° and 77° is due to Wannier excitons.[31] The E_1 peak is mainly the consequence

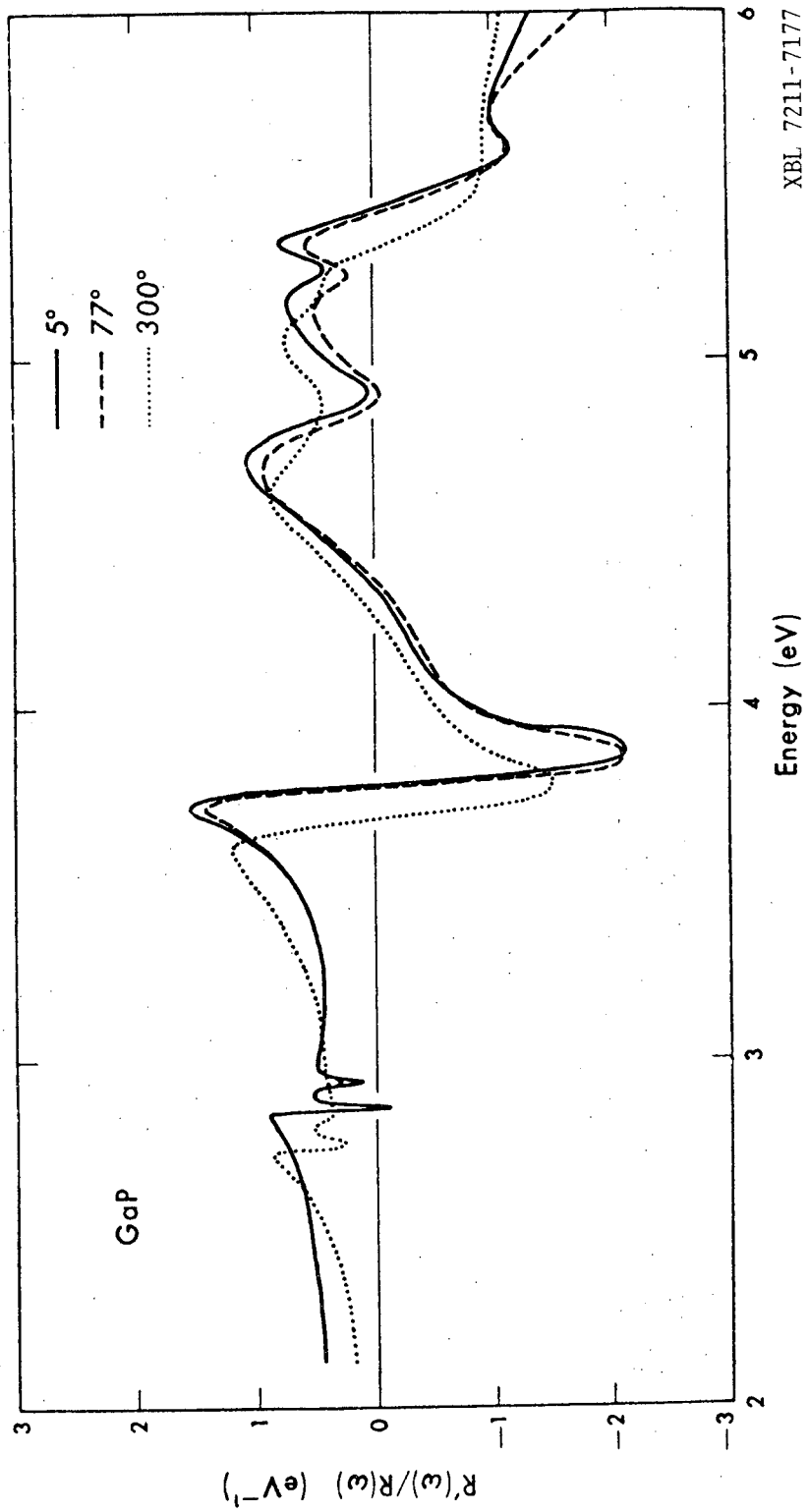

Fig. 11. Experimental Wavelength Modulation Spectra for GaP at Three Temperatures.

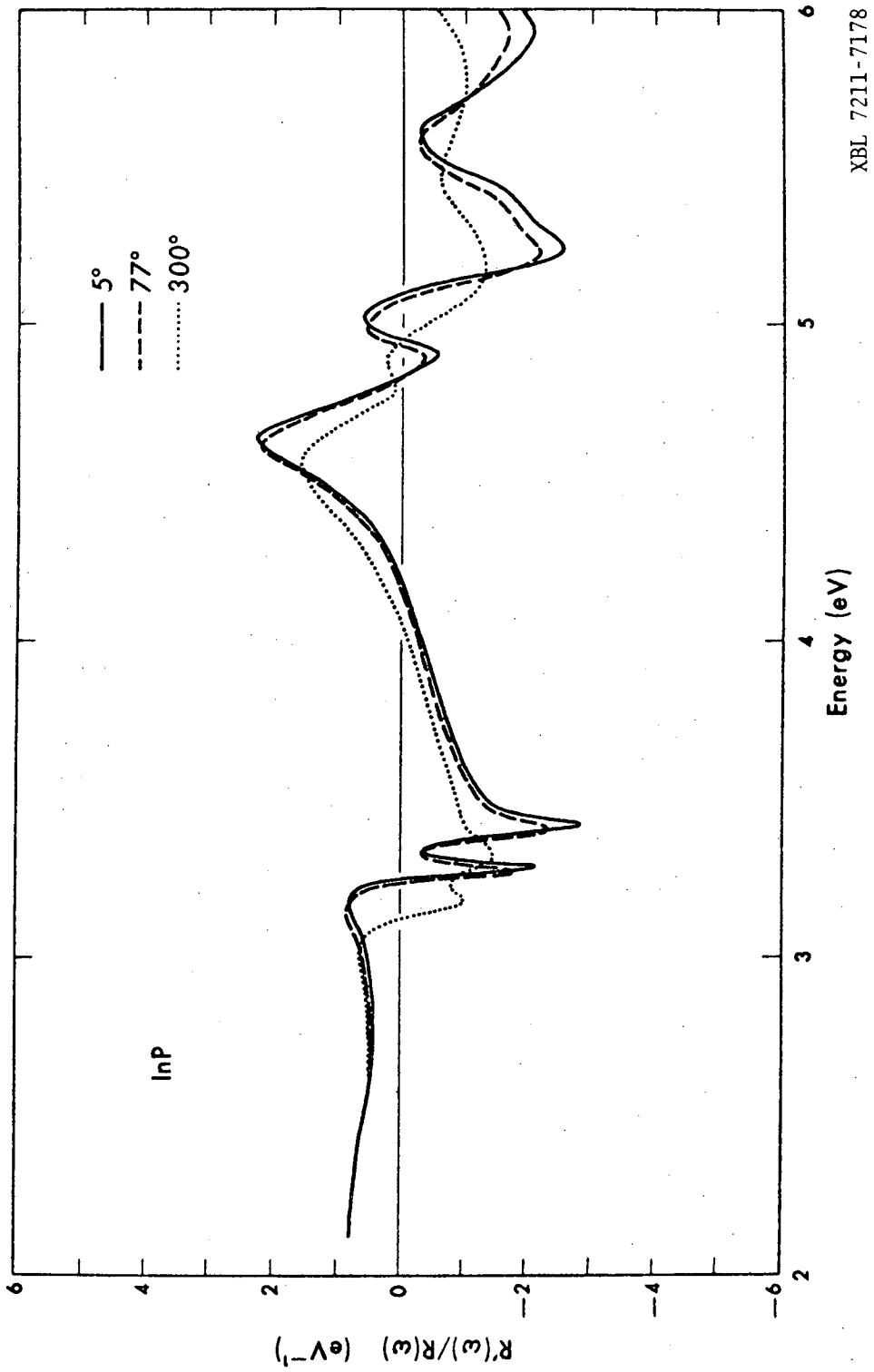

Fig. 12. Experimental Wavelength Modulation Spectra for InP at Three Temperatures.

of Λ_3-Λ_1 transitions, and the spin-orbit splitting of the valence band is small and hidden within our resolution, although we have seen a hint of it in the 5° data. The zero in the derivative at 5.3 to 5.4 eV corresponds to the large E_2 peak in the reflectivity, and the small structures just below it make up the E_0' region.

The E_0 region of InP is not really within the range of our spectrometer, since the band gap is at 1.42 eV. The data for the three temperatures is shown in Fig. 12. As with GaP, the E_1 peaks sharpen at low temperatures, but the sharpening is more dramatic, especially on the negative swings. The splitting of the E_1 peaks is evident. It looks like the general trend of the E_2 structure has superimposed on it the E_0' structures, so the two regions cannot be clearly separated on the basis of the data alone. Finally we note the appearance of a new small structure in the derivative at 5.3 eV for 77° and 5°K.

Our spectra agree well with those of Welkowsky and Braunstein,[4] except their magnitude is smaller, and with the GaP data of Stokowoski and Sell.[17]

D. Interpretation of the Results

In understanding the spectra for these two compounds, we combine three approaches: (1) comparison with the pseudopotential spectra and band structures; (2) comparison with the other III-V compounds; and (3) lineshape, or "edgeshape", analysis.

1. Comparison with Pseudopotential Calculations

In Fig. 13 we compare our modulated reflectivity of GaP at 300°C with that calculated by Walter and Cohen[15,38] for the same temperature.

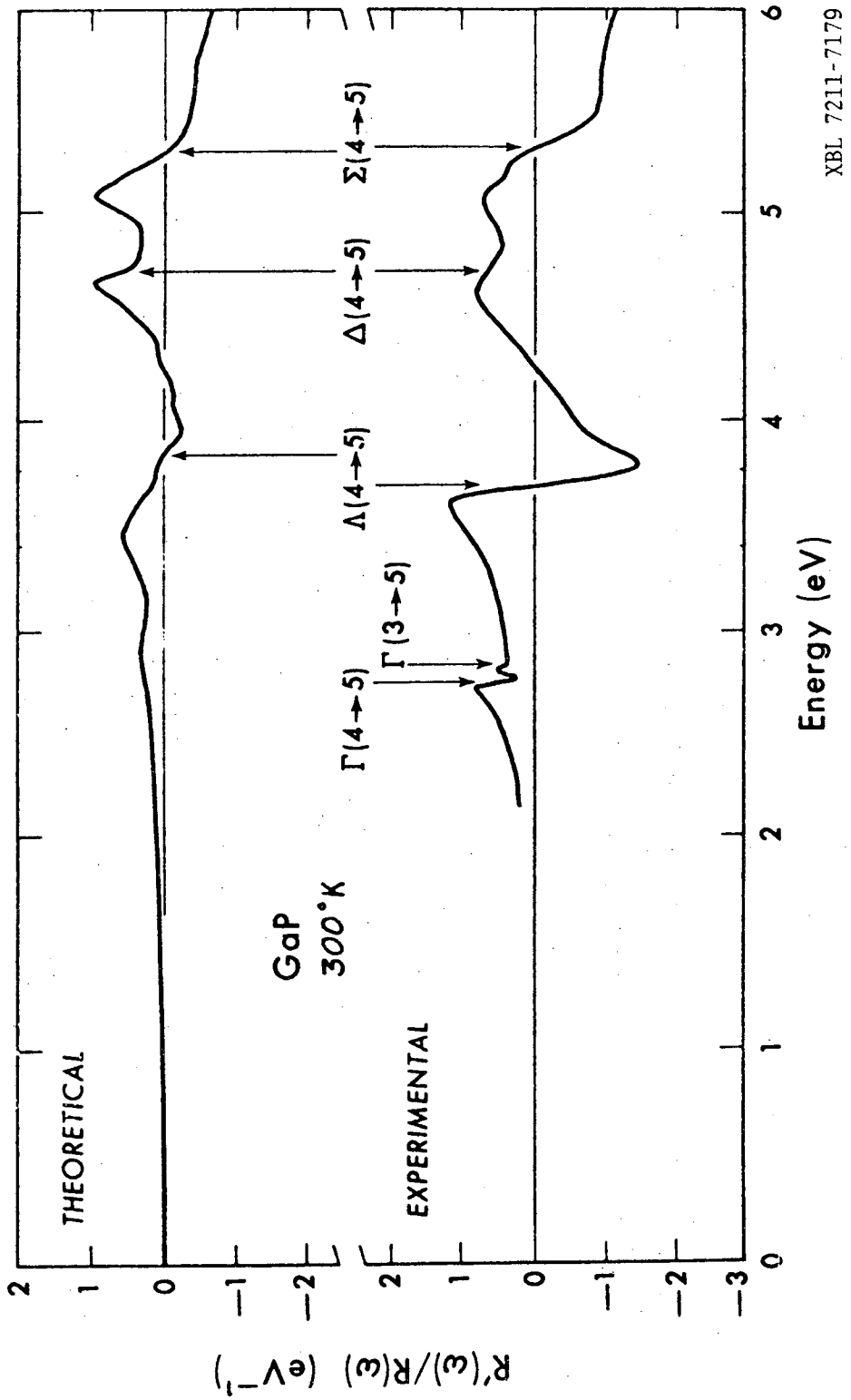

Fig. 13. Comparison of Theoretical and Experimental Wavelength Modulation Spectra of GaP (300°K).

Table 2. GaP Reflectivity Structure.[15,37]

Theory	Experiment	Location in zone	Symmetry	c_p energy
2.79 eV	2.78 eV	$\Gamma(4\text{-}5)(0,0,0)$	M_0	2.79 eV
	2.86			
3.70	3.69	$L(4\text{-}5)(0.5,0.5,0.5)$	M_0	3.40
		$\Lambda(4\text{-}5)(0.15,0.15,0.15)$	M_1	3.76
4.7	4.74	$\Delta(4\text{-}5)(0.71,0,0)$	M_0	4.50
		$X(4\text{-}5)(1,0,0)$	M_1	4.57
5.3	5.31	$\Delta(4\text{-}5)(0.30,0,0)$	M_3	4.72
		$\Sigma(4\text{-}5)(0.50,0.50,0)$	M_2	5.20

The experimental spectrum shows sharper structure at E_0 and E_1, which is to be expected because the theoretical computation did not take Coulomb effects between electron and holes into account. The theory shows that the E_0 peaks are the spin-orbit split direct gap at Γ and that the E_1 structure results from the M_1 point along Λ, with L_3-L_1 (M_0) contributing to the positive swing just before the main structure. In the theory the L and Λ transitions are .36 eV apart but the experiment suggests that they are closer together and not necessarily distinguishable with any resolution. The peak in the derivative is attributed to the combined effects of critical points along Δ while the zero in the derivative at 5.3 eV corresponds to the E_2 peak in R and is the result of the strong M_2 point along Σ. The small shoulder at 5.1 eV is real but does not have its counterpart in the theoretical curve. The comparable magnitude of theory and experiment in the E_0' and E_2 regions suggests that excitonic effects are not important for these transitions. The critical points determined from the theoretical band structure are tabulated in Table 2.[15,37]

De Alvarez[15] has calculated the empirical pseudopotential band structure for InP, in part using our own results for fitting the calculated curve. The derivative reflectivity (5°) she calculated is shown in Fig. 14, along with our experimental result for comparison. As with GaP, the E_1 structures are caused mostly by the M_1 critical point along Λ. The experimental curve shows more negative swing than positive around E_1, possibly indicating that the M_0 critical point (L_3-L_1) does not contribute as much here as in GaP. Comparison of the two curves in

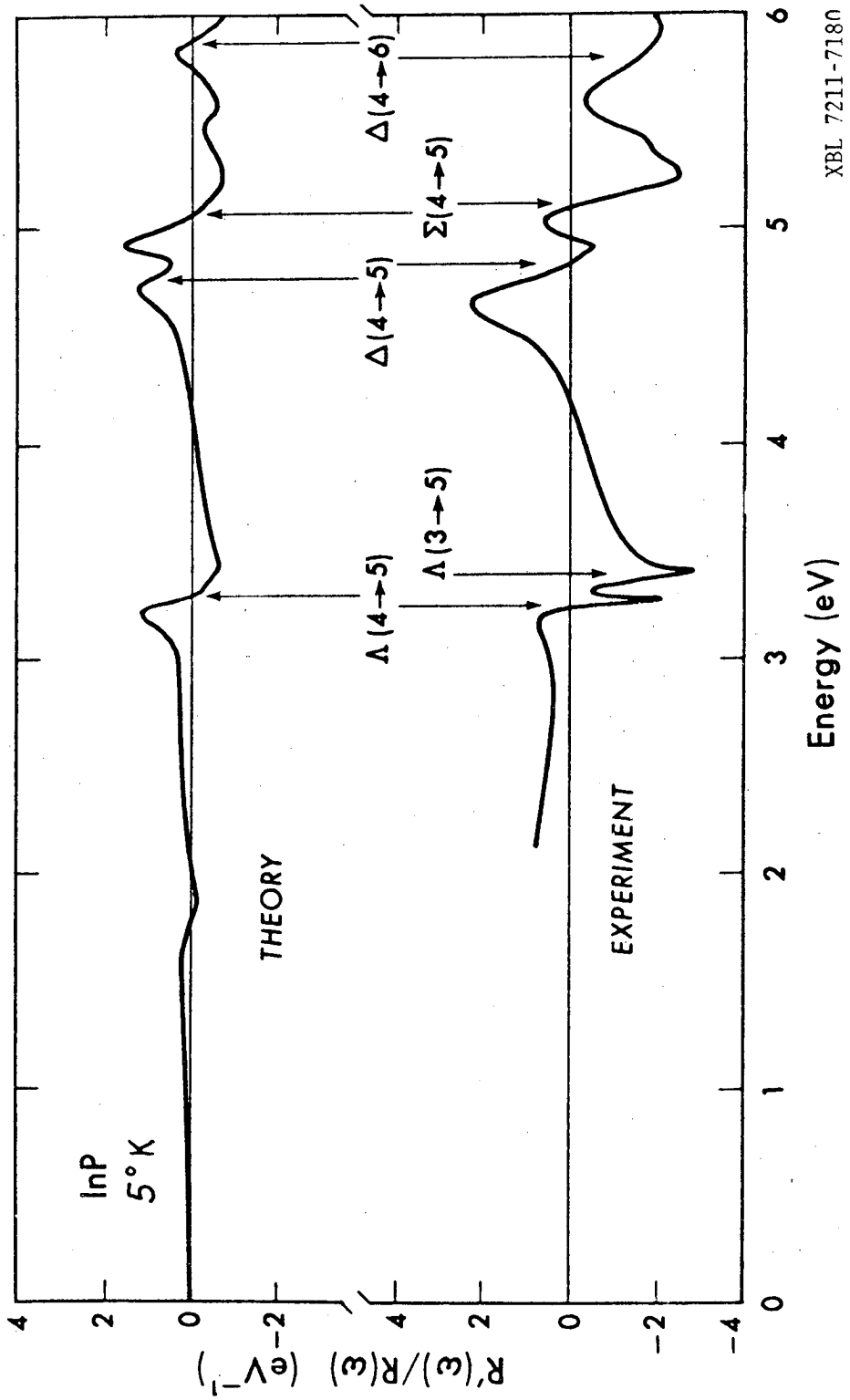

Fig. 14. Comparison of Theoretical and Experimental Wavelength Modulation Spectra of InP (5°K).

Table 3. InP Reflectivity Structure[a,15]

Theory	Experiment	Location in zone	Symmetry	c_p energy
1.43 eV[b]	1.42 eV[c]	Γ(4-5)(0,0,0)	M_0	1.5 eV
3.23[b]	3.24	L(4-5)(0.5,0.5,0.5)	M_0	3.2
3.37[b]	3.38	Λ(4-5)(0.3,0.3,0.3)	M_1	3.22
4.75	4.78	Δ(4-5)(0.8,0,0)	M_0	4.7
		X(4-5)(1.0,0,0)	M_1	4.71
		Volume near (4-5)(0.3,0,0)	-	4.88
5.06	5.10 (5.05)	Σ(4-5)(0.7,0.7,0)	M_2	5.02
5.48	(5.25)	Vol. (3-6)(0.3,0.1,0)	-	5.5
5.86	5.77(5.6)	Δ(4-6)(0.7,0,0)	M_1	5.77
6.47	(6.57)	L(4-6)(0.5,0.5,0.5)	M_0	6.2
		Λ(4-6)(0.4,0.4,0.4)	M_1	6.28

(a) Data in parentheses from Woolley-Vishnubhatla, Canad. J. Phys. 46, 1769 (1968). Other data from this paper's 5°K experiment.

(b) Corrected to include spin-orbit corrections.

(c) W. J. Turner, W. E. Reese and G. D. Pettit, Phys. Rev. 136, A1467 (1964).

the E_0' plus E_2 region reveals that: (1) the experimental peak at 4.65 eV is due mainly to the Δ (M_0) transitions near X, with possible contributions from a volume effect near (.3, 0, 0) and from transitions at X itself (M_1); (2) the structure between 4.9 and 5.3 eV is the E_2 peak, due to M_2 Σ_2-Σ_1 transitions; and (3) the peak below zero at 5.6 eV can be associated with Δ (M_1), transitions between bands 4 and 6, at (.7,0,0). A shoulder at 5.3 eV could be the volume effect reported in the theory. In Table 3 are the critical point energies from the band structure calculated for InP (5°K).[15]

2. Comparison with Other III-V Compounds

Examining the R'/R spectra[10] for the 6 common stable III-V compounds (GaP, GaAs, GaSb, InP, InAs, InSb) we immediately notice that we can group them into three similar pairs: GaP and GaAs, InP and InAs, GaSb and InSb. There are differences within each pair, such as in the magnitudes of the spin-orbit splittings resulting in one E_1 structure for GaP and two E_1 structures for GaAs, but the shape of and grouping of the various structures is similar within each of the pairs. In particular the E_0' and E_2 regions for the two pairs (GaP, GaAs) and (GaSb, InSb) are well separated, but in the pair (InP, InAs) the E_0' structures seem to be superimposed the E_2 structure. Spin-orbit splitting increases as we go down the periodic table, since χ_V becomes larger. The similarities within these pairs, as well as the more general similarities among all six, lend support to the assignments we made above on the basis of pseudopotential theory. E_0, E_1, and E_2 are thus well-understood, and a good idea of the makeup of E_0' is

available. However, sorting out the many small critical points that can occur in E_0' and above must wait for more finely resolved theoretical and experimental curves, as well as the use of special techniques such as uniaxial stress which we describe in the next chapter.

3. Edgeshape Analysis

The decomposition of the principal features of the spectra for GaP and InP into the lineshapes that are expected to occur, using the procedure described in the end of chapter 1 and Eq. (5), assists us in making assignments of transition energies. These assignments are summarized in Table 4. Also we have indicated whether the lineshape shows evidence of excitonic enhancement, based on the Toyozawa and Koster-Slater models[1] in which an edge of M_i character in ε_1 or ε_2 has some M_{i+1} character mixed into it by the Coulomb interaction. For example, the negative dip at 5.6 eV in GaP (Fig. 11) has the correct shape to be the exciton-enhanced part of E_2, and this dip also is absent at 300°K, as we would expect for exciton effects.

Table 4. Energies of important interband transitions as determined from experiment. (T=5°K)

		GaP		
E_0	Γ_8-Γ_6	M_0	2.85± .01 eV	ex.†
	Γ_7-Γ_6		2.92	
E_1	$L_{4,5}$-L_6	M_0	3.72± .04	
	L_6-L_6			
	Λ_4,Λ_5-Λ_6	M_1	3.78± .01	ex.
	Λ_6-Λ_6			
E_0'	Δ_5^{uv} - Δ_5^c (near X)	M_0	4.70± .06	
	Δ_5^{lv} - Δ_5^c			
	Δ_5^{uv} - Δ_5^c (near Γ)	M_3	4.91± .03	ex.
	Δ_5^{lv} - Δ_5^c			
	Σ-Σ or Δ-Δ near Γ		5.25	
E_2	Σ_3,Σ_4-Σ_3,Σ_4	M_2	5.45± .04	ex.
		InP		
E_1	$L_{4,5}$-L_6	M_0	3.2 ± .1 eV	
	L_6-L_6		-	
	Λ_4,Λ_5-Λ_6	M_1	3.25± .01	ex.
	Λ_6-Λ_6		3.38± .01	
E_0'	$\Delta_5^{uv},\Delta_5^{lv}$-$\Delta_5^c$ (near X)	M_0	4.64± .05	
	volume effect near (0.3,0,0)	-	4.75± .03	
E_2	Σ_3^v, Σ_4^v - Σ_3^c, Σ_4^c	M_2	5.12± .03	ex.
	$\Delta_5^{uv},\Delta_5^{lv}$ - Δ_5^c (bands 11,12)	M_1	5.77± .05	

† "ex." signifies that excitonic effects are discernible

V. DERIVATIVE REFLECTIVITY OF A UNIAXIALLY-STRESSED SEMICONDUCTOR: GaAs

When you have a hard, shiny object whose contents are unknown, one way to find out what's inside is to crush it and see what comes out. In this chapter we will take this approach to the E_0' region of the GaAs spectrum, the lowest spectral region whose critical point composition is not well agreed upon. Before examining GaAs in Sec. B, however, we will outline our method for predicting the stress dependence of semiconductor band structure.

A. Effect of Stress on Band Structure

1. Splitting of Degeneracies

Applying a uniaxial stress to a crystal usually lowers its symmetry, resulting in splitting of some of the degenerate states.* Degeneracies in a crystal fall into two categories: (1) states which have the same $\underset{\sim}{k}$ and the same energy, and (2) states which have the same energy but different $\underset{\sim}{k}$. We shall refer to these types of degeneracy as "local degeneracy" and "intervalley degeneracy," respectively, these terms referring to the geography of $\underset{\sim}{k}$-space rather than real space.

A stress which lowers the symmetry of the lattice also lowers the symmetry of the Brillouin zone, with the result that points, lines, and planes of the Brillouin zone originally equivalent by symmetry

---

*In our discussion of this problem we consider only symmetry-related degeneracies and leave out accidental degeneracies.

may no longer be equivalent; thus intervalley degeneracies may be split by stress. Similarly, the distortion of the lattice produces a distortion of the potential around each lattice point; thus degenerate states at the same $\underset{\sim}{k}$ may be split because the lobes of these wave functions no longer "feel" the same potential anymore.

We now examine in a more rigorous and detailed way the effects of stress on the point group of the crystal, the groups of the wave vectors, and the representations of these groups.

Let $G_0(0)$ be the point group of the crystal without stress. If we stress the crystal along an axis $\hat{s}$, the point group becomes $G_0(\hat{s})$. (Note that a stress along axis $\hat{s}$ is the same as one along $-\hat{s}$, since we are squeezing the crystal, i.e., pushing it from both sides.) Barring coincidences, $G_0(\hat{s})$ is a subgroup of $G_0(0)$. In order to determine $G_0(\hat{s})$ we keep only those elements of $G_0(0)$ which take $\hat{s}$ into $\hat{s}$ or $-\hat{s}$, i.e. those elements of $G_0(0)$ which do not change the stress axis. Thus, if $G_0(0)$ contains the inversion i, i will also be in $G_0(\hat{s})$.

The group of a particular wave vector $\underset{\sim}{k}$, denoted by $G_{\underset{\sim}{k}}(0)$, is found by taking all those elements of $G_0(0)$ which take $\underset{\sim}{k}$ into $\underset{\sim}{k}$, with $\underset{\sim}{k} + \underset{\sim}{g}$ being considered the same as $\underset{\sim}{k}$. ($\underset{\sim}{g}$ is a reciprocal lattice vector.) $G_{\underset{\sim}{k}}(\hat{s})$, the group of $\underset{\sim}{k}$ in the stressed crystal, is found in the same manner from $G_0(\hat{s})$, the point group of the stressed crystal. From these definitions it is clear that $G_{\underset{\sim}{k}}(\hat{s})$ contains no symmetry operations that are not in $G_{\underset{\sim}{k}}(0)$, and therefore it is a subgroup of $G_{\underset{\sim}{k}}(0)$ as well as of $G_0(\hat{s})$.

If $\underset{\sim}{k}$ lies along the stress axis $\hat{s}$, the application of stress does not change the group of $\underset{\sim}{k}$. We see this as follows. Since $G_0(\hat{s})$ includes all those members of $G_0(0)$ which take $\hat{s}$ into $\hat{s}$ and $-\hat{s}$, it includes all the elements of $G_{\underset{\sim}{k}}(0)$; thus, for $\underset{\sim}{k}$ parallel to $\hat{s}$, $G_{\underset{\sim}{k}}(\hat{s}) = G_{\underset{\sim}{k}}(0)$.* The representations labeling the states at $\underset{\sim}{k}$ are thus unchanged, and no local splitting occurs.

If $\underset{\sim}{k}$ is not parallel to $\hat{s}$, on the other hand, $G_{\underset{\sim}{k}}(\hat{s})$ will in general be smaller than $G_{\underset{\sim}{k}}(0)$. The representations Γ of $G_{\underset{\sim}{k}}(0)$ will break up into one or more representations Γ' of $G_{\underset{\sim}{k}}(\hat{s})$, and local splitting can thus occur.

The star of $\underset{\sim}{k}$ consists of all those wave vectors which are equivalent to $\underset{\sim}{k}$ by symmetry. If there is a state at $\underset{\sim}{k}$ with energy $E_{\underset{\sim}{k}}$, then there are states at the other wave vectors in the star of $\underset{\sim}{k}$ with the same energy. This is the intervalley degeneracy mentioned above. Under uniaxial stress, all the wave vectors in the star of $\underset{\sim}{k}$ may no longer be equivalent, because the crystal has lower symmetry. The original star of $\underset{\sim}{k}$ may break up into two or more stars, and the states in one are no longer degenerate by symmetry with the states in another; intervalley splitting thus occurs. The old star divides into new stars, the members of a given star having the same projection, $|\underset{\sim}{k}\cdot\hat{s}|$, on the stress axis. In order to label these new stars created by stress, we will use the following convention. If a state with wave vector $\underset{\sim}{k}$ belongs to the representation Σ of $G_{\underset{\sim}{k}}(0)$, then Σ will become Σ of $G_{\underset{\sim}{k}}(\hat{s})$ if $\underset{\sim}{k}$ is parallel to $\hat{s}$ (in which case $G_{\underset{\sim}{k}}(\hat{s}) = G_{\underset{\sim}{k}}(0)$); if $\underset{\sim}{k}$ is not parallel to $\hat{s}$, the representations will

*There are special exceptions for some cases when $\underset{\sim}{k}$ lies on the zone face; then $G_{\underset{\sim}{k}}(\hat{s})$ is smaller than $G_{\underset{\sim}{k}}(0)$. These do not affect our discussion.

be labeled Σ' for the first new star, Σ'' for the next new star, and so on, in order of decreasing $|\underset{\sim}{k}\cdot\hat{s}|$. Since Σ', Σ'', etc. are representations with $\underset{\sim}{k}$ not parallel to $\hat{s}$, their $G_{\underset{\sim}{k}}(\hat{s})$ may be lower in symmetry than $G_{\underset{\sim}{k}}(0)$, in which case local splitting may occur along these lines in $\underset{\sim}{k}$-space; at each $\underset{\sim}{k}$ within a given new star, however, the local splitting will be the same.

Table V gives the stars produced by various kinds of stress, along with their labels and multiplicity within the Brillouin zone.

The effect of (001) stress is to turn the face-centered cubic zinclende crystal (T_d) into a tetragonal crytal (D_{2d}); the labels in the second column of Table V thus correspond to the conventional symmetry labels for the tetragonal Brillouin zone, such as are found in Zak's book.[42] We will continue to use Δ, Δ', Λ', etc. because they are more convenient.

"Intervalley" and "local" splitting are often referred to in the literature as "interband" and "intraband" splitting, respectively. We feel that the use of the prefixes "inter" and "intra" is the reverse of what it should be, and therefore, to avoid creating any new confusion, we will stick to "intervalley" and "local".

Under stress a cubic crystal becomes uniaxial or biaxial and no longer has an isotropic dielectric tensor. The reflected light from such a crystal, even at normal incidence, becomes polarization dependent, and we would like to make use of the extra information this provides. Obtaining a detailed picture of this polarization dependence is one of the tasks of the quantum mechanical perturbation theory analysis, to be described in the next section.

Table V. The "stars of $\underline{k}$" in the unstressed and stressed crystals. (Beside the stress direction (xyz) we have indicated the point group of the stressed crystal, $G_0(\hat{s})$. The numbers in the body of the table indicate the multiplicity within the Brillouin zone of the stars.

(000) T_d	(111) C_{3v}	(001) D_{2d}	(110) C_{2v}
1 Γ	1 Γ	1Γ	1Γ
6 Δ	6 Δ'	2Δ, 4Δ'	4Δ', 2Δ''
8 Λ	2Λ, 6Λ'	8Λ'	4Λ', 4Λ''
12 Σ	6Σ', 6Σ''	8Σ', 4Σ''	2Σ, 8Σ', 2Σ''

2. Formal Theoretical Treatment

It is evident by now that the first step in the theoretical analysis of stress perturbation is to perform a thorough group theory analysis. This does not give us everything, but it provides a boundary within which to work and a check on the consistency of our results. Some information about polarization dependence is available from consideration of the representations involved, as well as immediate information about which levels split and which don't.

To do this, we first ask what the point group of the stressed crystal is and what the groups of the wave vectors in the stressed crystal are. Then we see how the old representations split up into the new representations of the groups in the stressed crystal. This is a straightforward process, unless the crystal is non-symmorphic, as with the diamond structure. In this case we must go into the language of space groups. In Si (O_h^7) some of the symmetry operations are rotations combined with non-primitive translations. It is not immediately obvious which of these complex operations survive when a particular stress is applied. However, in determining the space group of the new crystal the following theorem can be applied: if the space group operations, expressed as 3×3 orthogonal matrices plus vector translations, commute with 3×3 strain tensor (under matrix multiplication), then the operation is a symmetry operation of the stressed crystal. Then Zak's[42] book of character tables for the 230 space groups can be used to work out the groups of the wave vectors and the splittings of the bands. For our purposes, we need only think

about point groups, since the zinc blende space group (T_d^2) is symmorphic.

In order to get an idea of how much the splitting is and a more detailed picture of the polarization dependence, we go to a quantum mechanical perturbation treatment. Here, too, group theory is invaluable. From an analysis of the representations we move into an analysis of what happens to the basis functions of these representations, and the general laws of group theory provide important simplifications.

The states in a crystal are labelled by their wave vector $\underset{\sim}{k}$ and band index ℓ, and have the form,

$$\psi_{\underset{\sim}{k},\ell}(\underset{\sim}{x}) = u_{\underset{\sim}{k},\ell}(x)\ e^{i\underset{\sim}{k}\cdot\underset{\sim}{x}} \tag{12}$$

where $u_{\underset{\sim}{k},\ell}$ is the Bloch function, periodic with the period of the lattice. $u_{\underset{\sim}{k},\ell}(\underset{\sim}{x})$ is an eigenfunction of the Hamiltonian

$$H_o(\underset{\sim}{k},x) = \frac{p^2}{2m} + V(\underset{\sim}{x}) + \frac{\hbar}{m}\underset{\sim}{k}\cdot\underset{\sim}{p} = H_o(0,\underset{\sim}{x}) + \frac{\hbar}{m}\underset{\sim}{k}\cdot\underset{\sim}{p} \tag{13}$$

with energy eigenvalue $\mathcal{E}^{\circ}_{\underset{\sim}{k},\ell} - \frac{\hbar^2k^2}{2m}$, i.e.,

$$H_o(\underset{\sim}{k},\underset{\sim}{x})\ u_{\underset{\sim}{k},\ell}(\underset{\sim}{x}) = (\mathcal{E}^{\circ}_{\underset{\sim}{k},\ell} - \frac{\hbar^2k^2}{2m})\ u_{\underset{\sim}{k},\ell}(\underset{\sim}{x}) \tag{14}$$

Pikus and Bir[43] have shown that we can treat the effect of stress by adding to this $\underset{\sim}{k}\cdot\underset{\sim}{p}$ Hamiltonian a small perturbation Hamiltonian, as follows.

$$H(\underset{\sim}{k},\underset{\sim}{x}) = H_o\ (\underset{\sim}{k},\underset{\sim}{x}) + H'\ (\underset{\sim}{k},\underset{\sim}{x}) \tag{15}$$

Here

$$H'(\underset{\sim}{k},\underset{\sim}{x}) = e_{ij}\left\{\frac{-\hbar^2\partial^2}{\partial x_i\,\partial x_j} + \frac{\partial \mathcal{V}[\underset{\approx}{e},\ (1+\underset{\approx}{e})\underset{\sim}{x}]}{\partial e_{ij}}\bigg|_{e_{ij}=0} - \frac{\hbar}{m}\,p_i k_j\right\}, \tag{16}$$

which we abbreviate

$$H'(\underset{\sim}{k},\underset{\sim}{x}) = e_{ij}\left[\frac{-\hbar^2\partial^2}{\partial x_i\,\partial x_j} + V_{ij}(\underset{\sim}{x})\right] - e_{ij}\,\frac{\hbar}{m}\,p_i k_j$$

$$= e_{ij}\,[D_{ij}(\underset{\sim}{x}) + d_{ij}(\underset{\sim}{k},\underset{\sim}{x})]$$

$$= e_{ij}\,h_{ij}(\underset{\sim}{k},\underset{\sim}{x}) \tag{17}$$

(Sum over repeated indices.) e_{ij} is the ij<u>th</u> component of the strain tensor, determined by

$$e_{ij} = s_{ijkl}\,\sigma_{kl} \tag{18}$$

where σ_{kl} are the stress tensor components, s_{ijkl} the elastic compliance constants.[25]

$\mathcal{V}(\underset{\approx}{e},\underset{\sim}{x})$ is a self-consistent, one-electron potential, defined to be the exact or true potential in the crystal when it is strained a particular amount. As such, we really don't know what its behavior is until we have measured it or concocted a theory for it, so we will treat it phenomenologically. The V_{ij}'s can be considered the microscopic deformation potentials of the crystal. We know the transformation properties of the $V_{ij}(\underset{\sim}{x})$'s under group operations, so their exact

functional dependence on $\underset{\sim}{x}$ will not be important to us in our treatment. In this Hamiltonian, all the quantities labeled ij, including the product $p_i k_j$ when we allow $\underset{\sim}{k}$ to rotate, transform as $x_i x_j$ under the operations of a group, and this fact will be useful to us later. When $\underset{\sim}{k}$ is considered fixed, $p_i k_j$ transforms as x_i. Note that D_{ij}, d_{ij}, and h_{ij} are also operators, with $\underset{\sim}{k}$ as a parameter, since they contain $\underset{\sim}{p}$ and $\underset{\sim}{x}$.

Of course the Bloch functions that solve Eq. (15) are not really the Bloch functions in the stressed crystal. The reason is that Eq. (16) has the translational symmetry of the face-centered cubic crystal, while the stressed crystal has a lower degree of translational symmetry. The solutions of Eq. (15) would not fit into the stressed crystal unless we stretched them out in the identical way we stretched out the crystal potential, as follows,

$$u_{\underset{\sim}{k},\ell}(\underset{\sim}{x}) \rightarrow u_{\underset{\sim}{k}',\ell}[(1-\underset{\approx}{e})\underset{\sim}{x}] \tag{19}$$

where the new function belongs to $\underset{\sim}{k}' = (1-\underset{\approx}{e})\underset{\sim}{k}$. But the stretching process does not change the energy eigenvalue, so Eq. (15) gives us the correct energies. The perturbation Hamiltonian was derived[43] by considering the true Hamiltonian in the stressed crystal and compressing it by an inverse transformation to fit the lattice of the unstressed crystal. The result is that $H'(\underset{\sim}{k},\underset{\sim}{x})$ has the translational symmetry of the unstressed crystal, but the actual shape of the potential around a lattice point has, in general, a lower rotational symmetry than that of the original cubic potential. In shorter terms, Eq. (16) has the translational symmetry of unstressed crystal but the point group symmetry of the stressed crystal. In this process of

contraction the energy eigenvalue is not changed, but we can now expand the solution to the perturbed Hamiltonian Eq. (15) in terms of the Bloch functions of the unstressed crystal, since they both have the same spatial periodicity or "satisfy the same boundary conditions." In the above discussion tension is considered to be a positive strain; the strain in our experiments is thus negative.

The derivation of this perturbation Hamiltonian is well covered by Pikus and Bir and subsequent authors, and so we will not go further into the details of it. The Pikus-Bir Hamiltonian is the basis for almost all published treatments of the effects of stress on semiconductors, but various authors have cast it into different forms. We will use it in a fairly general form consistent with the language of group theory. Our treatment follows that of Kane[44] except that we remain with the one-electron band picture, while he treats the problem in terms of exciton states, or hole-electron excitations. Our approach is also similar to that of F. Cerdeira.[45]

We can write the Hamiltonian Eq. (16) in an irreducibly transforming manner,[44]

$$H'(\underset{\sim}{k},\underset{\sim}{x}) = \sum_{j,\alpha,s} e^{*}_{\alpha}(j)s \; h_{\alpha}^{(j)s} \qquad (20)$$

where (j) and α label a function which belongs to the α th row of the jth representation of the group of $\underset{\sim}{k}$ in the unstressed crystal. $h_{\alpha}^{(j)s}$ is a linear combination of the operators h_{ij} in Eq. (17); the operators h_{ij} have simply been regrouped in such a way that each group transforms

under the operations of $G_{\underset{\sim}{k}}(0)$ like some basis function α of the jth representation. When this is done, the strain coefficients regroup as well; the new strain coefficients, it turns out, belong to the complex conjugate of the jth representation of $G_{\underset{\sim}{k}}(0)$ and the αth row. For our purposes, $e_{\alpha}^{*(j)s} = e_{\alpha}^{(j)s}$, since the e_{ij} are real. s is a repetition index, necessary because sometimes more than one function belonging to (j,α) occurs. Its role will become clear later. Considered as a function of $\underset{\sim}{x}$ alone, with $\underset{\approx}{e}$ and $\underset{\sim}{k}$ as static parameters, this Hamiltonian is less symmetric than the unstressed crystal, because the basis functions $h_{\alpha}^{(j)s}$ by themselves do not have the full spatial symmetry of the point group to which they belong. As remarked before, however, the Hamiltonian still has the same spatial symmetry as the unstressed crystal, so we take as our unperturbed set of functions the Bloch functions of the unstressed crystal.

We now write out the Hamiltonian for a particular point (Γ) and line (Δ) of interest to us, casting it in the form of Eq. (20). At Γ, $H'(\underset{\sim}{k},\underset{\sim}{x})$ becomes, in terms of the basis functions of T_d,

$$
\begin{aligned}
H'(o,\underset{\sim}{x}) = {} & \frac{1}{\sqrt{3}}\ (e_{xx}+e_{yy}+e_{zz})\left[\frac{1}{\sqrt{3}}\ (D_{xx}+D_{yy}+D_{zz})\right] \\
& + \frac{1}{\sqrt{6}}\ (-e_{xx}-e_{yy}+2e_{zz})\left[\frac{1}{\sqrt{6}}\ (-D_{xx}-D_{yy}+2D_{zz})\right] \\
& + \frac{1}{\sqrt{2}}\ (e_{xx}-e_{yy})\left[\frac{1}{\sqrt{2}}\ (D_{xx}-D_{yy})\right] \\
& + \frac{1}{\sqrt{2}}\ (e_{yz}+e_{zy})\left[\frac{1}{\sqrt{2}}\ (D_{yz}+D_{zy})\right] + \frac{1}{\sqrt{2}}\ (e_{zx}+e_{xz})\left[\frac{1}{\sqrt{2}}\ (D_{zx}+D_{xz})\right] + \frac{1}{\sqrt{2}}\ (e_{xy}+e_{yx})\left[\frac{1}{\sqrt{2}}\ (D_{xy}+D_{yx})\right]
\end{aligned}
\tag{21}
$$

These six linear combinations of the D_{ij}'s transform as $h^{(1)}$, $h_1^{(3)}$, $h_2^{(3)}$, $h_x^{(5)}$, $h_y^{(5)}$, $h_z^{(5)}$ of T_d, respectively, where $h_\alpha^{(j)}$ is an operator belonging to the αth row of the jth representation of T_d. Note that e_{ij} equals e_{ji} in the absence of torque,[25] but that D_{ij} and d_{ij} do not necessarily equal D_{ji} and d_{ji}.

Similarly, along Δ,

$$H'(k\hat{z},\underset{\sim}{x}) = \left(\frac{e_{xx}+e_{yy}+e_{zz}}{\sqrt{3}}\right)\left(\frac{D_{xx}+D_{yy}+D_{zz}+d_{zz}}{\sqrt{3}}\right) + \left(\frac{-e_{xx}-e_{yy}+2e_{zz}}{\sqrt{6}}\right)\left(\frac{-D_{xx}-D_{yy}+2D_{zz}+2d_{zz}}{\sqrt{6}}\right)$$

$$+ e_{xy}\,[2\,\bar{D}_{xy}] + \frac{e_{xx}-e_{yy}}{\sqrt{2}}\left[\frac{1}{\sqrt{2}}\,(D_{xx}-D_{yy})\right]$$

$$+ (e_{zx}+e_{yz})\left[(\bar{D}_{zx}+\bar{D}_{zy}) + \frac{d_{xz}+d_{yz}}{2}\right] + (e_{zx}-e_{yz})\left[(\bar{D}_{zx}-\bar{D}_{zy}) + \frac{d_{xz}-d_{yz}}{2}\right], \qquad (22)$$

where

$$\bar{D}_{ij} \equiv \frac{D_{ij} + D_{ji}}{2} \qquad (23)$$

and, for $\underset{\sim}{k} = k\hat{z}$, the operator d_{ij} is given by:

$$d_{ij} = \frac{-\hbar}{m}\,k_j p_i = \frac{-\hbar}{m}\,k\,p_i \delta_{jz} \qquad (24)$$

Here $H'(k\hat{z},\underset{\sim}{x})$ is composed of six basis functions belonging to $\Gamma^{(1)}$, $\Gamma^{(2)}$, $\Gamma^{(3)}$, and $\Gamma^{(4)}$ of the group of $\Delta(C_{2v})$, namely $h^{(1)a}$, $h^{(1)c}$, $h^{(3)}$, $h^{(4)}$, $h^{(2)}$, in that order. Near Γ, the $\underset{\sim}{k}$-dependent d_{ij}'s are unimportant,[43] but away from Γ they may still be relatively small. We argue for this as follows. D_{ij} contains $p_i p_j$, which acts on the rapid

core oscillations giving something like $g_i g_j$, where $\underset{\sim}{g}$ is a reciprocal lattice vector, while d_{ij}, acting on the same state, would give a contribution like $g_i k_j$. Now the relevant $\underset{\sim}{g}$ here is approximately that which would label the band if we were using the extended zone scheme, and it would describe the spatial variation of in $u_{\underset{\sim}{k},\ell}$ in the n.f.e. limit. For all but the lowest bands, $g_i \sim \frac{1}{i}\frac{\partial}{\partial x_i} u_{\underset{\sim}{k},\ell}(\underset{\sim}{x})$ may be significantly greater than k_i, in which case $\langle d_{ij} \rangle \ll \langle D_{ij} \rangle$. Since, however, we are interested in Δ states not necessarily near Γ, we have for completeness' sake not dropped the d_{ij} terms from our calculation.

Equations (20) to (24) are very convenient for us to use. They allow us to work out the relative values of matrix elements of $H'(\underset{\sim}{k},\underset{\sim}{x})$ between the unperturbed wave functions, these latter also belonging to particular rows of representations in the group of $\underset{\sim}{k}$. To do this we make use of the coupling (Clebsch-Gordan) coefficients between the basis functions of two representations and those of the direct product representations. Thus,

$$\left(u_{\alpha_1}^{(j_1)}, H'(\underset{\sim}{k},\underset{\sim}{x})\, u_{\alpha_2}^{(j_2)}\right) = \sum_{j,\alpha,s} e_\alpha^{*(j)s} \left(u_{\alpha_1}^{(j_1)}, h_\alpha^{(j)s}\, u_{\alpha_2}^{(j_2)}\right) \qquad (25)$$

For $\Gamma^{(j)} \times \Gamma^{(j_2)} = \Sigma\, \Gamma^{(j')}$, we have

$$\left(u_{\alpha_1}^{(j_1)}, H'(\underset{\sim}{k},\underset{\sim}{x})\, u_{\alpha_2}^{(j_2)}\right) = \sum_{j,\alpha,s} e_\alpha^{*(j)s} \sum_{j',\alpha'} U_{\alpha\alpha_2,\alpha'}^{*jj_2,j'} \left(u_{\alpha_1}^{(j_1)}, v_{\alpha'}^{(j')s}\right)$$

$$= \sum_{j,\alpha,s} e_{\alpha}^{*(j)s} \sum_{j',\alpha'} \mathbf{U}^{*jj_2,j'}_{\alpha\alpha_2,\alpha'} \delta_{j'j_1} \delta_{\alpha'\alpha_1} \left(\!\!\left(u^{(j_1)}, v^{(j_1)s} \right)\!\!\right)$$

$$= \sum_{j,\alpha,s} e_{\alpha}^{*(j)s} \mathbf{U}^{*jj_2,j_1}_{\alpha\alpha_2,\alpha_1} \left(\!\!\left(u^{(j_1)}, v^{(j_1)s} \right)\!\!\right) \tag{26}$$

where the $v_{\alpha'}^{(j')s}$ are a set of orthogonalized, but not necessarily normalized basis functions defined by

$$h_{\alpha}^{(j)s} u_{\alpha_2}^{(j_2)} = \sum_{j',\alpha'} \mathbf{U}^{*jj_2,j'}_{\alpha\alpha_2,\alpha'} v_{\alpha'}^{(j')s} , \tag{27a}$$

and

$$\left(\!\!\left(u^{(j_1)}, v^{(j_1)s} \right)\!\!\right) \equiv \sum_{\alpha_1} \frac{\left(u_{\alpha_1}^{(j_1)}, v_{\alpha_1}^{(j_1)s} \right)}{\ell_{j_1}} \tag{27b}$$

is a reduced matrix element, independent of the row index α_1.[44,46] The repetition index s simply carries through the above manipulations, and need not disturb the reader. The coupling coefficients $\mathbf{U}^{jj_2,j_1}_{\alpha\alpha_2,\alpha_1}$ are tabulated in the tables of Koster, et.al.[47] These coupling coefficients play the same role in the point group as the Clebsch-Gordan coefficients play in the full rotation group; they relate the basis functions of a direct product representation to the binary products of the basis functions of the two original representations. With this machinery, and careful attention to the effects of time reversal symmetry,[46,48] we can reduce the stress-perturbation

calculations to a minimum number of matrix elements. This simplification comes about because many of the $U^{*jj_2,j_1}_{\alpha\alpha_2,\alpha_1}$ are zero.

The optical transition probability between two states in bands ℓ and ℓ' is proportional to the square of the modulus of $(u_{\underset{\sim}{k},\ell'}, \underset{\sim}{A}\cdot\underset{\sim}{p}\, u_{\underset{\sim}{k},\ell'})$. In the spirit of our group theoretical approach, we write $\underset{\sim}{A}\cdot\underset{\sim}{p}$ in the same form as Eq. (20). Usually the basis functions in this expression will correspond to light polarized either purely parallel to $\underset{\sim}{k}$ or purely perpendicular to $\underset{\sim}{k}$. Then it is a simple matter to get the relative magnitudes of the $\underset{\sim}{A} \parallel \underset{\sim}{k}$ and $\underset{\sim}{A} \perp \underset{\sim}{k}$ transitions by working out the matrix elements as in Eq. (26). For the total response of the crystal, we have to combine the effects of all the states in the star of $\underset{\sim}{k}$.

B. The E_0' Region of GaAs

1. Critical Point Composition

Previous investigations[4,10,11,37,49,50] indicate that the main transitions contributing to the E_0' regions of III-V semiconductors, including GaAs, occur between the uppermost valence bands and the lowest conduction band, along Δ in the Brillouin zone. Examination of a good calculated band structure for GaAs[37] shows why this is a reasonable conclusion. (Fig. 15.) From $(.3,0,0)\frac{2\pi}{a}$ (Δ) to $(1,0,0)\frac{2\pi}{a}$ (X) the conduction band is nearly parallel to the spin-orbit split valence bands. If we move out into the zone from a point on Δ, the interband energy increases in all directions; several kinds of critical points[37] contribute to the detailed structure of the E_0' region. In order of increasing interband energy, these are: an M_0 around (.6,0,0),

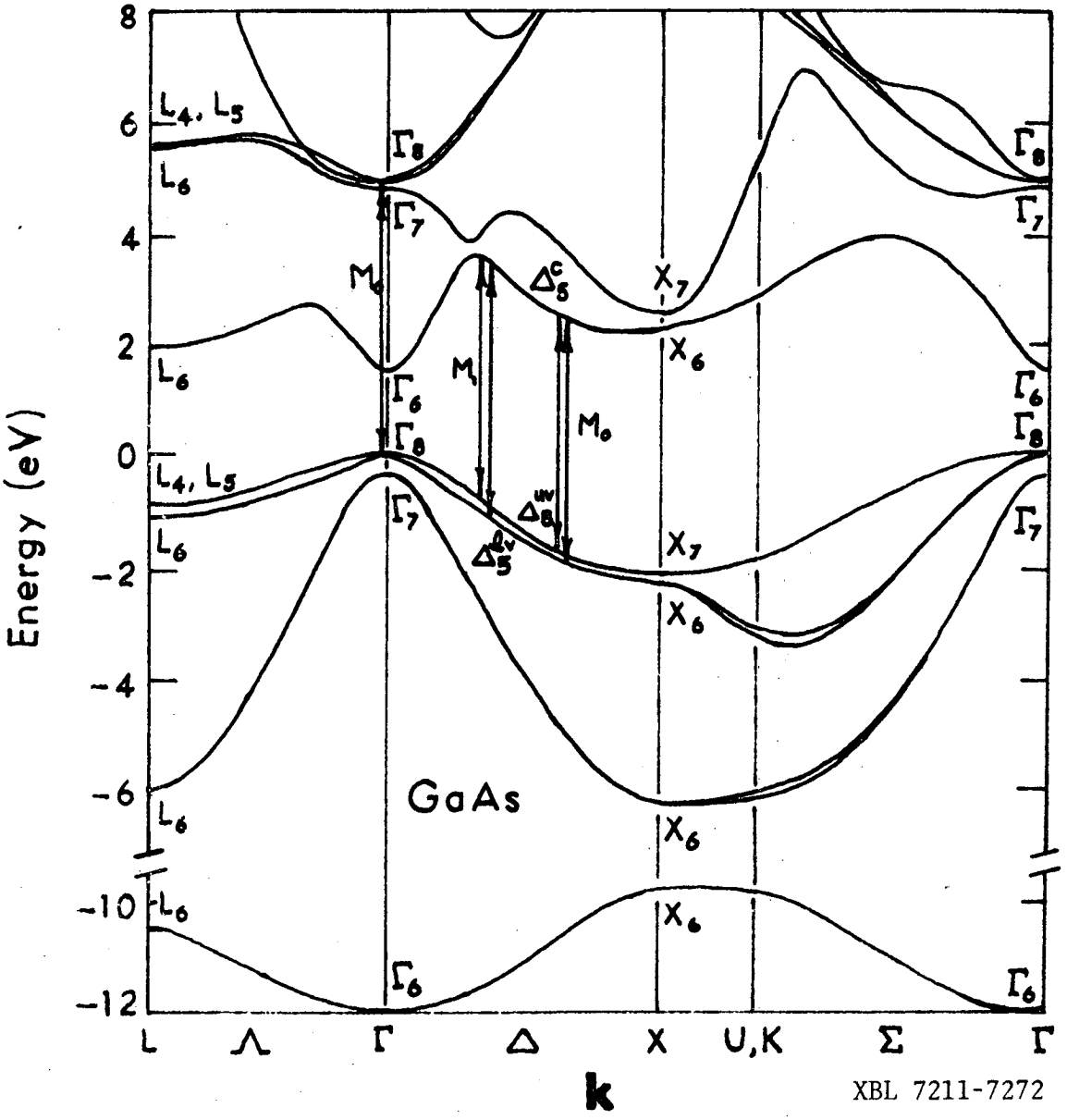

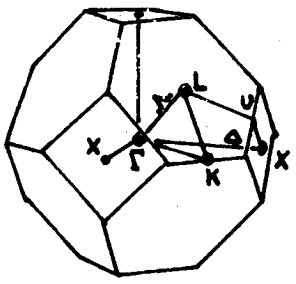

Fig. 15. Band structure of GaAs (ref. 37) showing important critical points contributing to the E_0' spectral region.

an M_1 around (.3,0,0)(near the "pseudocrossing" of the two lower comduction bands), a weaker M_1 point at X, and other weaker points at higher energies.

It has also been suggested that transitions at Γ can contribute structure in this region,[4] and the calculated band structure of Fig. 15 shows that the $\Gamma_8^v - \Gamma_7^c$ and $\Gamma_8^v - \Gamma_8^c$ energies lie in the E_0' region, at slightly higher energies than the presumed Δ transitions. At the same time, it is evident from the figure that the joint density of states near Γ is much less than that for Δ, so Γ peaks, if they occur, should be small and superimposed on the Δ structure. Using stressed samples in an experiment similar to ours, Sell and Kane[9] found this to be the case for the E_0' region of Ge; they observed the small Γ structures against the background of a larger Δ structure. Rehn and Kyser,[49] who analyzed the polarization dependence of transverse electroreflectance data, concluded that E_0' in GaAs results from Δ transitions; as Γ transitions give a zero polarization dependence, their analysis does not exclude the possibility of a small Γ contribution hidden in the Δ structure.

2. Polarization Dependence of the Reflectivity.

The polarization dependence of the reflected light from a uniaxially-stressed sample can help us pick out the symmetry of the transitions giving rise to peaks in E_0'. Therefore, we ask, what are the effects of (111) stress and (001) stress on peaks of Δ symmetry, and Λ symmetry? Also, what is the polarization dependence of the reflected light in these three cases? Figures 16-18 show the

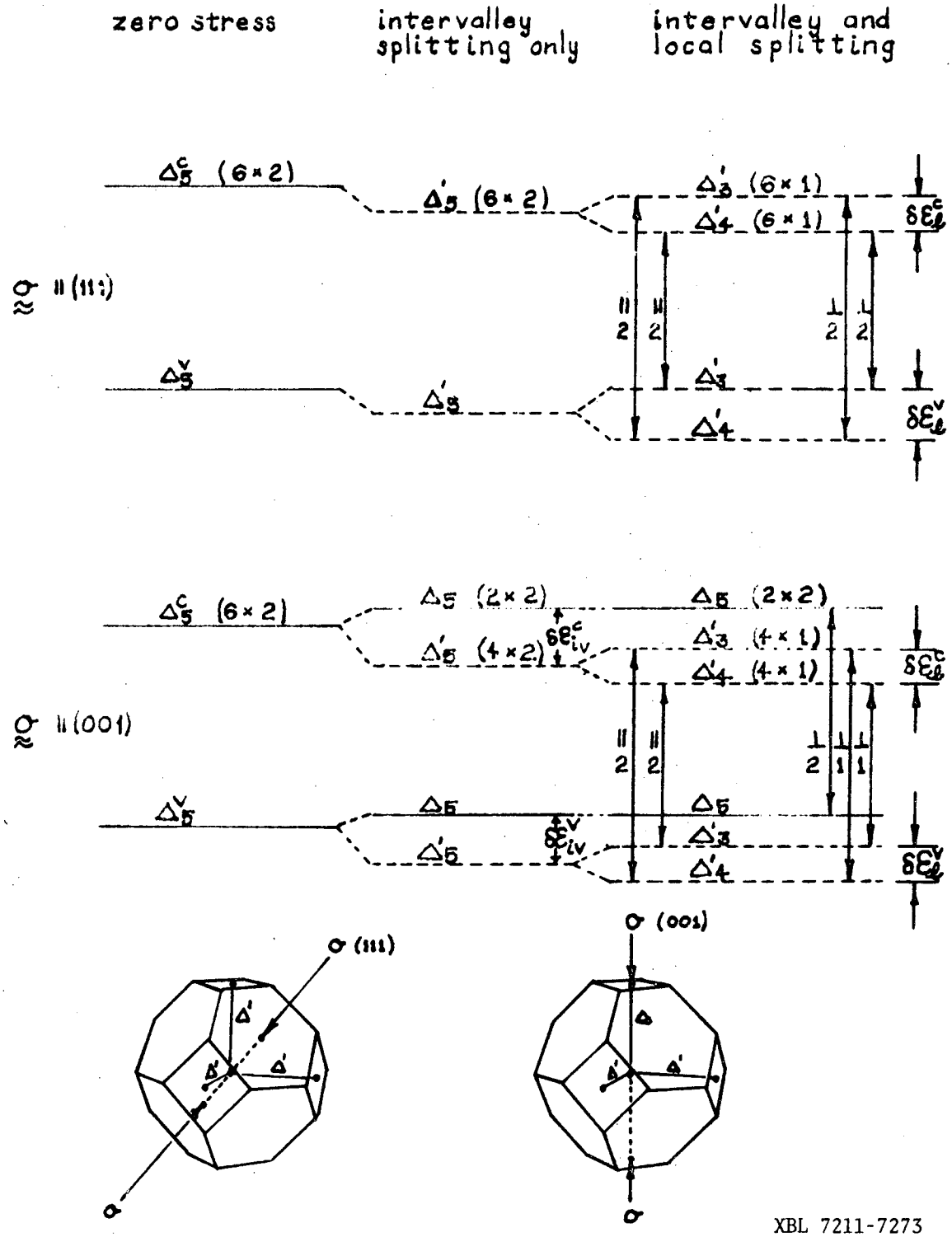

Fig. 16. Effect of (111) and (001) stresses on Δ_5 states, showing intervalley splitting ($\delta\varepsilon_{iv}$) and local splitting ($\delta\varepsilon_{\ell}$).

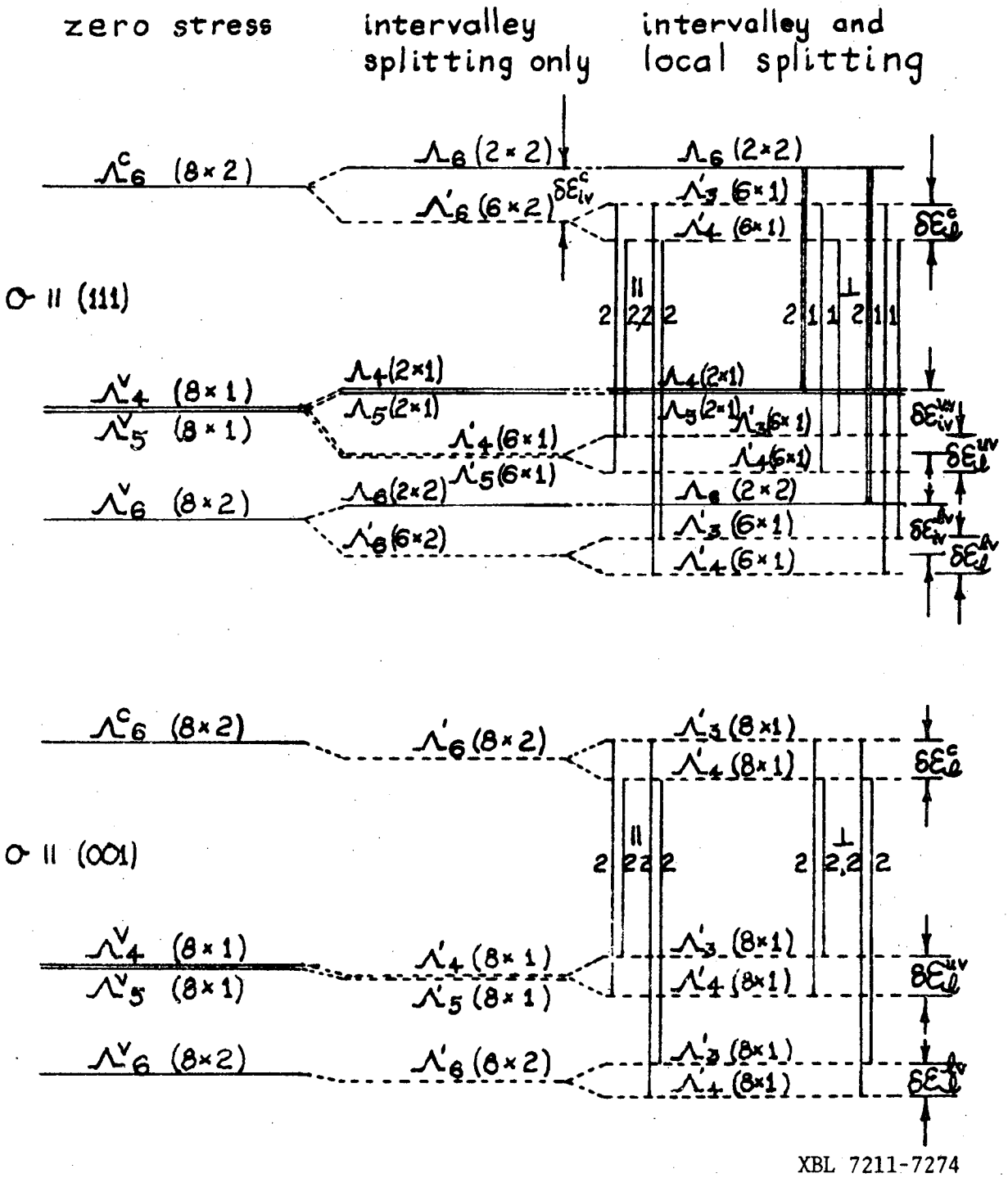

Fig. 17. Effect of (111) and (001) stresses on the bands at Λ, showing intervalley and local splittings. In the unstressed crystal, Λ_4 and Λ_5 are nearly degenerate; at L they are degenerate because of time-reversal symmetry.

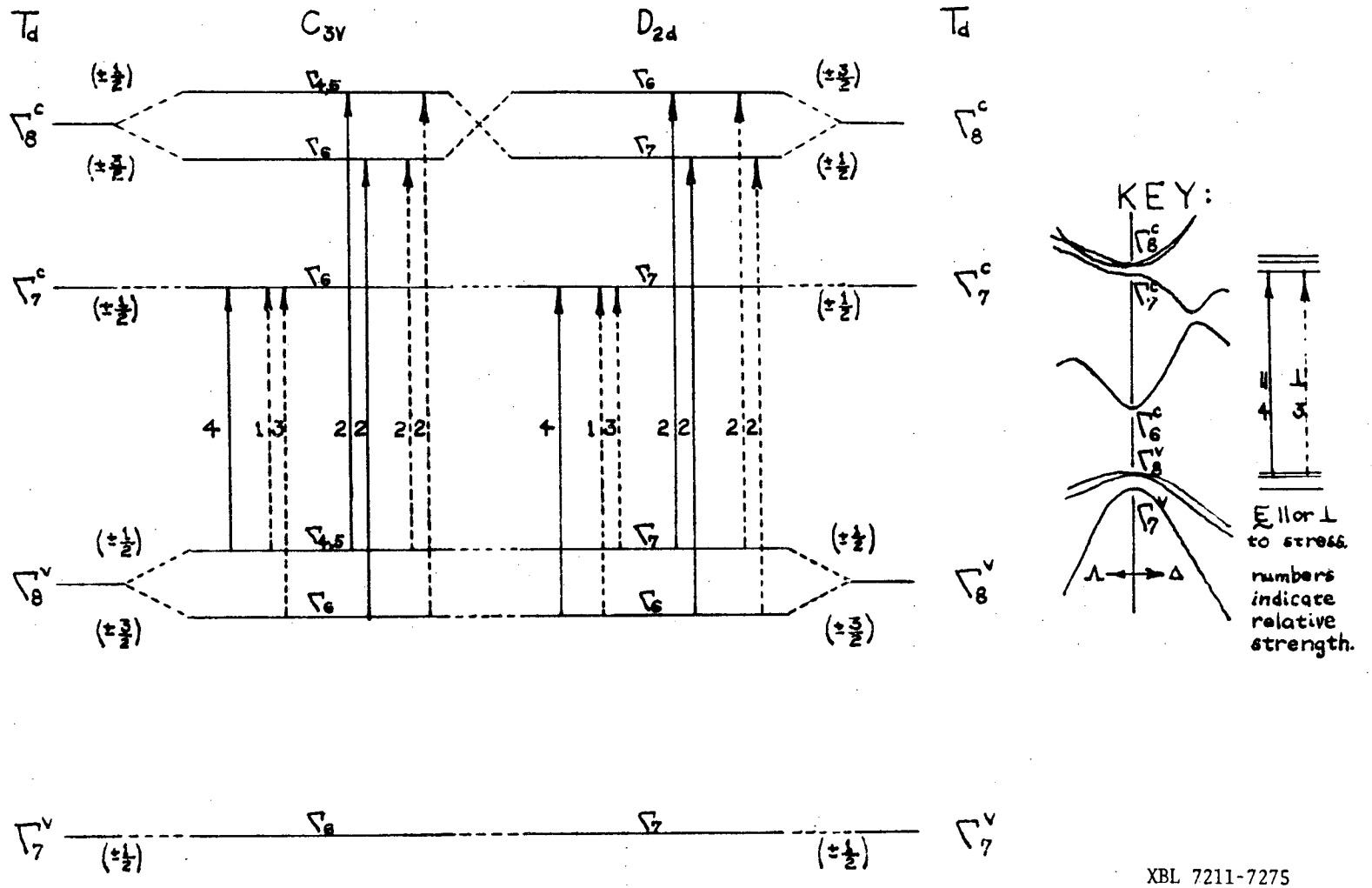

XBL 7211-7275

Fig. 18. Stress splitting and polarization dependence of Γ transitions. (After ref. 9.)

intervalley and local splittings of the conduction and valence bands along Δ, Λ, and Γ respectively for (111) and (001) stresses. The full horizontal lines indicate the energy levels for $\underset{\sim}{k}$ parallel to the stress axis; the dashed lines indicate the energy levels for those states with $\underset{\sim}{k}$ not parallel to the axis (the representations are labeled with primes). The numbers in parentheses beside the representations indicate the intervalley degeneracy multiplied by the local degeneracy. $||$ and $\perp$ indicate allowed transitions for light polarized $||$ and $\perp$ to stress, respectively. Beside these lines are numbers indicating relative strength.

The allowed dipole transitions shown are those allowed by group theory (symmetry) in the absence of spin-orbit interaction. The inclusion of this interaction mixes small amounts of other states into the unperturbed states, and thus "turns on" new dipole transitions. But since the spin-orbit interaction causes only small changes in the band energies of the Δ-states in question compared to the energy difference of the unperturbed bands, we expect the new allowed transitions to be significantly weaker than the original ones. Thus, in Figs. 16 and 17 we neglect the transitions turned on by the spin-orbit interaction. This simplification is borne out by experimental evidence for the $E_1(\Lambda)$ peaks in GaAs,[22] and we shall use it in our analysis. (Our own data on E_1, which we will not describe, agrees with ref. 22.)

On the basis of the information in Figs. 16-18 we can draw the following general conclusions about the behavior of the reflectance

in the low-strain limit, for spectral regions dominated by transitions in the different parts of the Brillouin zone: (a) If the main transitions between the upper valence bands and the lower conduction band occur along Δ, there should be a polarization dependence in R and R' for (001) stress but not for (111) stress. (b) If the transitions occur along Λ, polarization dependence is expected for (111) stress but not for (001) stress. (c) (i) For the lower Γ transitions, $\Gamma_8^v-\Gamma_7^c$, polarization dependence occurs for both stresses; (ii) for $\Gamma_8^v-\Gamma_8^c$, polarization dependence occurs only for (111) stress.

The exact shapes of the curves under stress depends on a number of factors: (1) the magnitudes and signs of the energy shifts and splittings; (2) the relative magnitudes of intervalley and local splitting; (3) the presence or absence of transitions in other parts of the zone; and (4) the types of critical points involved. Assuming that the dominant $\vec{\Delta}$-critical points in this region are the M_0 minimum at (.6,0,0) and the M_1 saddle point near the pseudocrossing, we have drawn in Fig. 19 the expected lineshapes for each of these, based on our lineshape analysis scheme outlined earlier. Under stress, these shapes should split into one or more similar shapes.

For X and X', the splitting and polarization dependence are the same as for Δ and Δ', except that no local splitting occurs for X'. Thus the Δ_3' and Δ_4' bands, split by stress, come together at X_5', as illustrated in Fig. 20. This is because the X-point of the zone has higher symmetry than the Δ-line and thus can support greater degeneracy of states. The absence of local splitting for X' can help us

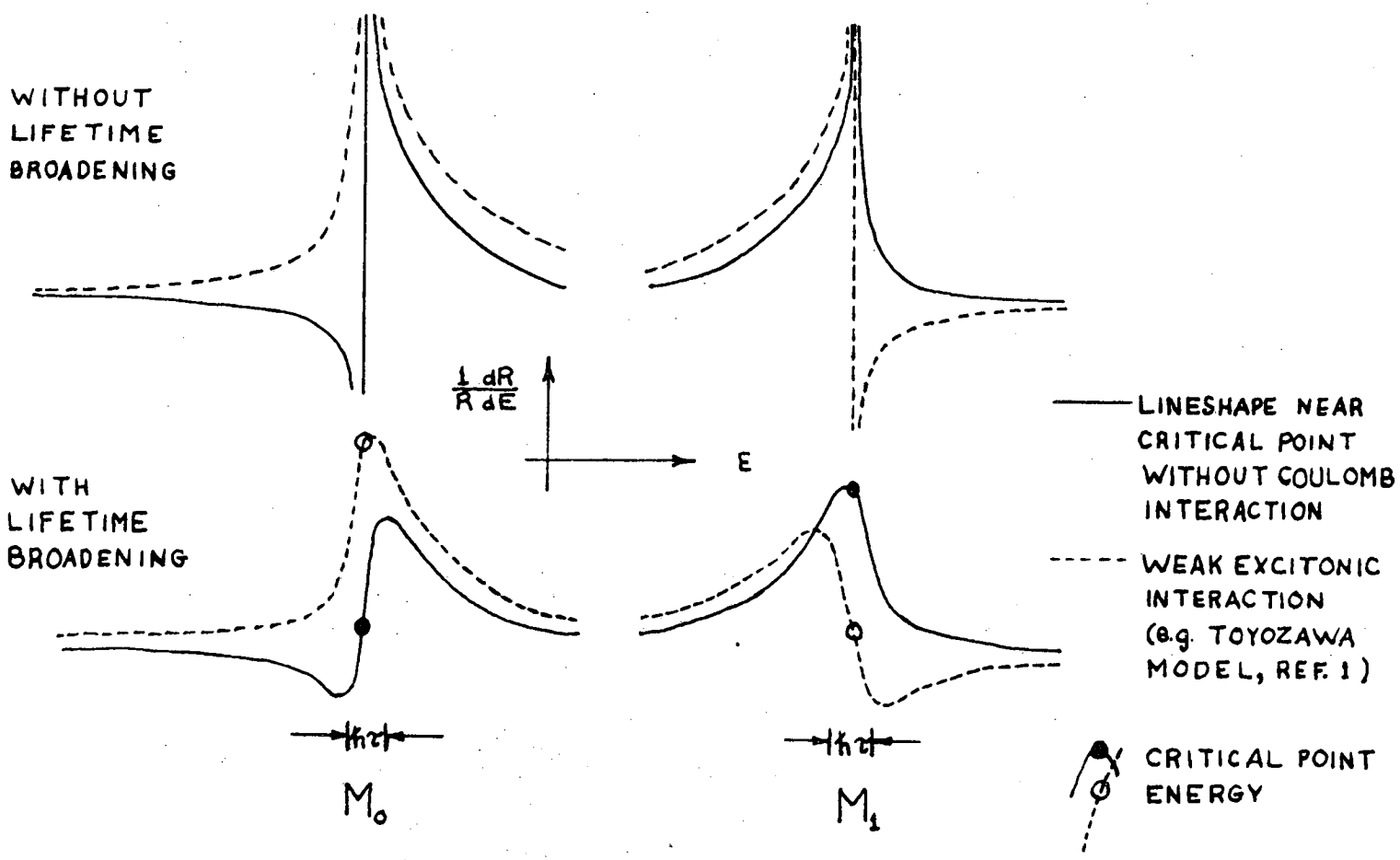

Fig. 19. Expected lineshapes in $\frac{1}{R}\frac{dR}{dE}$ of M_0 and M_1 edges in the E_0' region of GaAs.

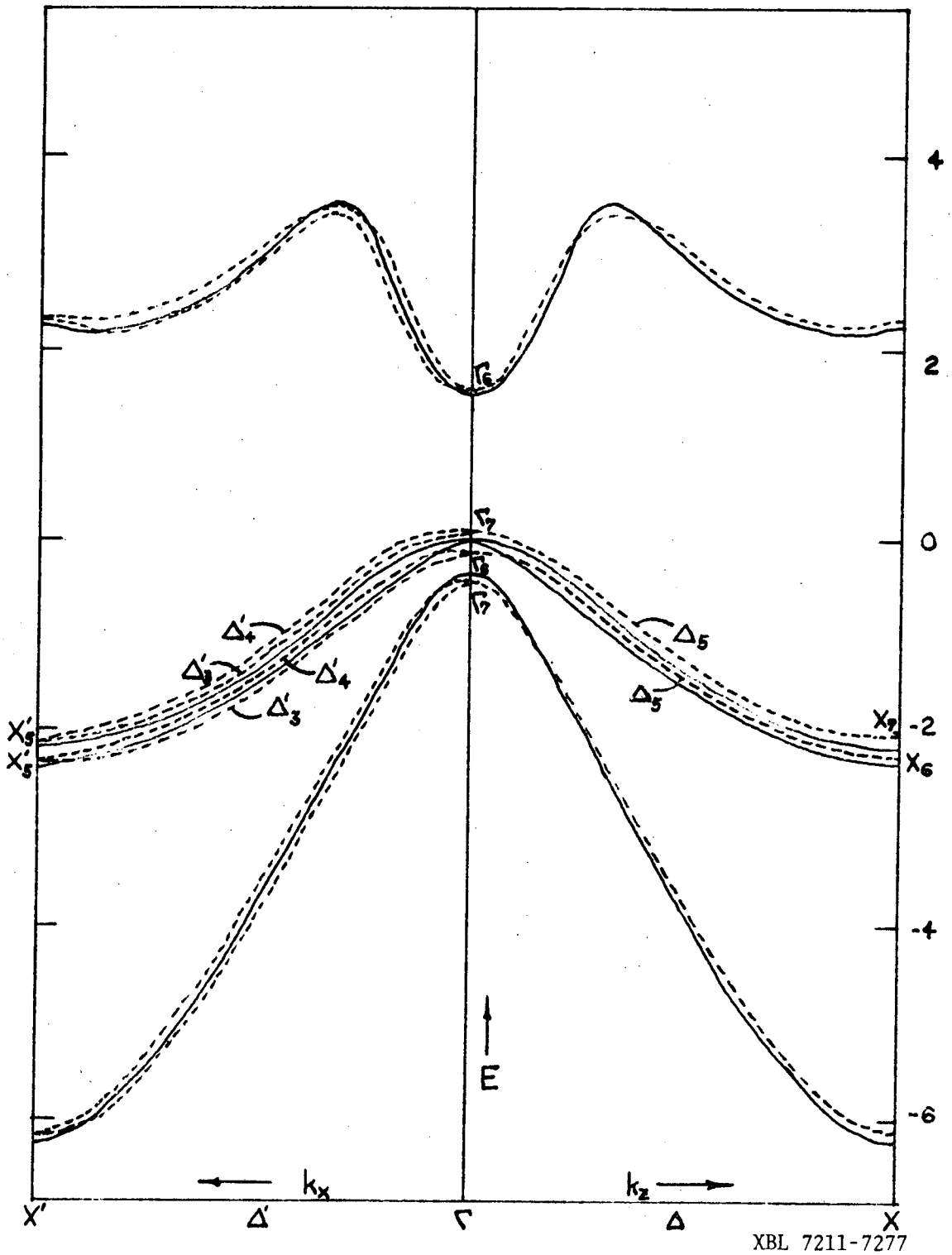

XBL 7211-7277

Fig. 20. Labelling of the bands along Δ and Δ' for a GaAs crystal under (001) stress.

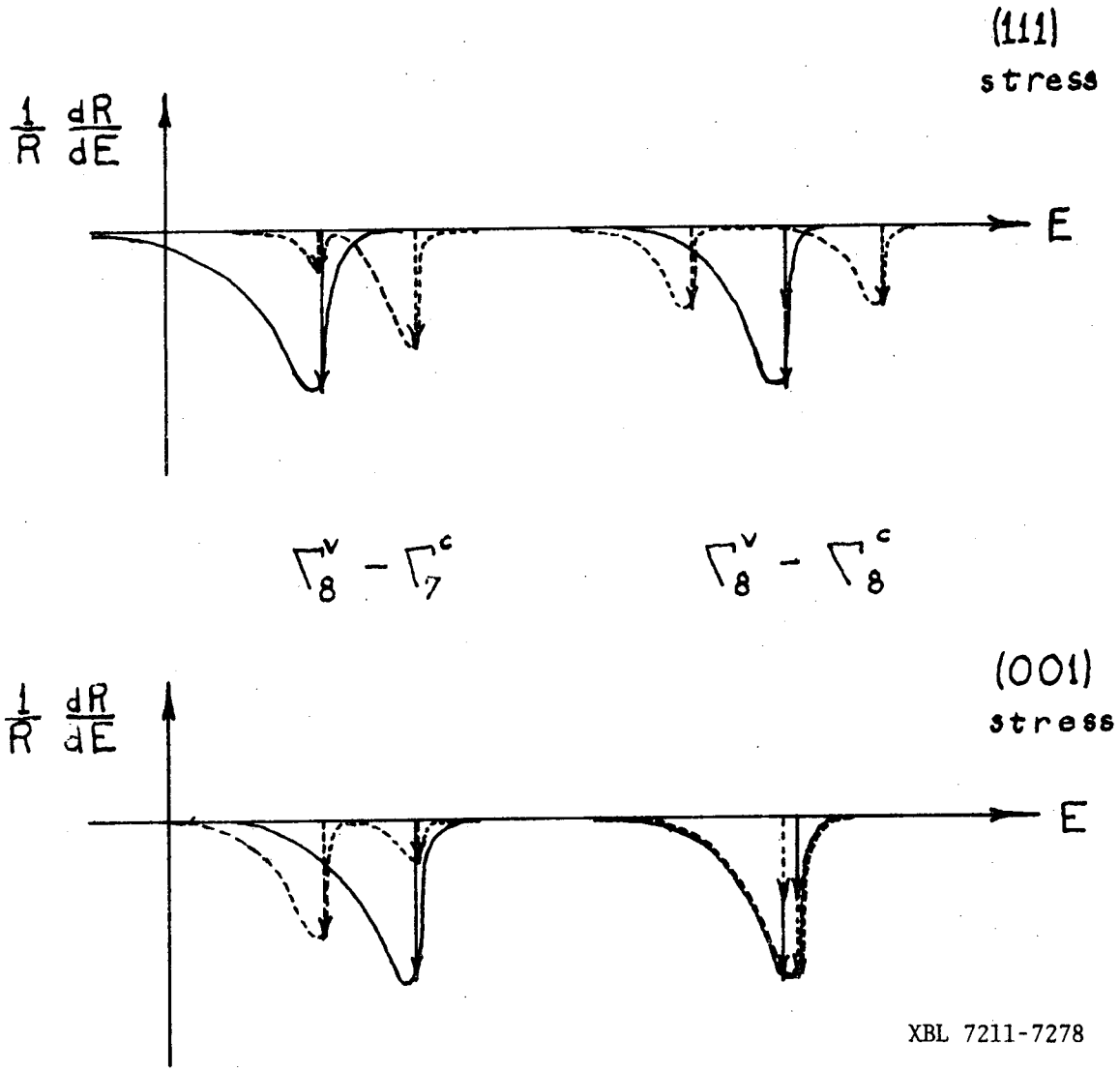

Fig. 21. Shifts of Γ_{15}^v-Γ_{15}^c peaks under stress, for light polarized parallel to stress (——) and perpendicular to stress (----). (Assume M_0 critical points.)

distinguish X' transitions in the experimental spectrum from Δ' transitions, as we shall see later.

The splittings for Γ states, after ref. 9, are shown in Fig. 18, and using the lineshape analysis scheme again we have indicated in Fig. 21 how the Γ peaks might look with and without stress.

After describing the treatment of the samples, the most crucial part of the entire experiment, we will use the conclusions of the present section to interpret the main features of our data.

C. Samples and Surface Preparation

1. Orientation and Cutting.

To fit in the stress apparatus, to use as much of the light beam ($\sim$ 1 mm $\times$ 8 mm) as possible, and to maximize stress (force per unit cross-sectional area), the samples were cut into long rectangular prisms with a square cross-section. The long axis was the stress axis, (001) or (111), and the reflecting face of both samples was $(1\bar{1}0)$. This means that the polarization perpendicular to the stress axis for the (001) sample was (110) and for the (111) sample was $(11\bar{2})$. Since the crystal is cubic to begin with, the particular reflecting face is not crucial for this experiment, so long as it is perpendicular to the stress axis.

Orientation was done by x-ray diffraction with the crystal waxed to a goniometer shaft using a hard wax (no. 70C cement). The goniometer could be mounted directly on the carriage of a diamond wheel saw without losing its orientation. Two parallel cuts about 3 mm apart were made. The 3 mm slice was then rewaxed, reoriented along a

perpendicular direction, and cut again with two parallel cuts, thus producing a bar 3 mm × 3 mm. In a similar manner, the ends were cut off, leaving a rectangular rod about 13 mm long. Thus 3 orientations and 6 cuts are necessary.

2. Grinding and Polishing

Unfortunately the cutting procedure could not be relied upon to give faces or ends that were sufficiently perpendicular to each other, the error being sometimes as much as a few degrees. So a polishing mount was used whereby the orientation of the sample with respect to the polishing plane could be changed by a small screw.* (See Fig. 22a) Furthermore, the central shaft of this polishing holder could be mounted on an x-ray diffraction machine for orientation.

The following procedure was used for grinding and polishing the samples. (1) With the hard wax, stick the sample to the shaft of the adjustable polishing holder, and orient it to the desired crystallographic axis with the x-rays. (2) Grind and polish this long face, starting with #0 emery paper (kerosene) or 400 mesh SiC paper (water) and ending up with .05μ alumina (water). Care must be taken not to grind too much of the sample away, so it won't come out too thin. (3) Repeat the procedure with an adjacent long face, perpendicular to the original one. After orientation and polishing, the two faces should be perpendicular within a degree. (4) Using a second, simpler polishing holder (Fig. 22b), polish the other two long faces down to .05μ alumina.

---

*We are indebted to Dr. Paul Richards and his group for the use of this device.

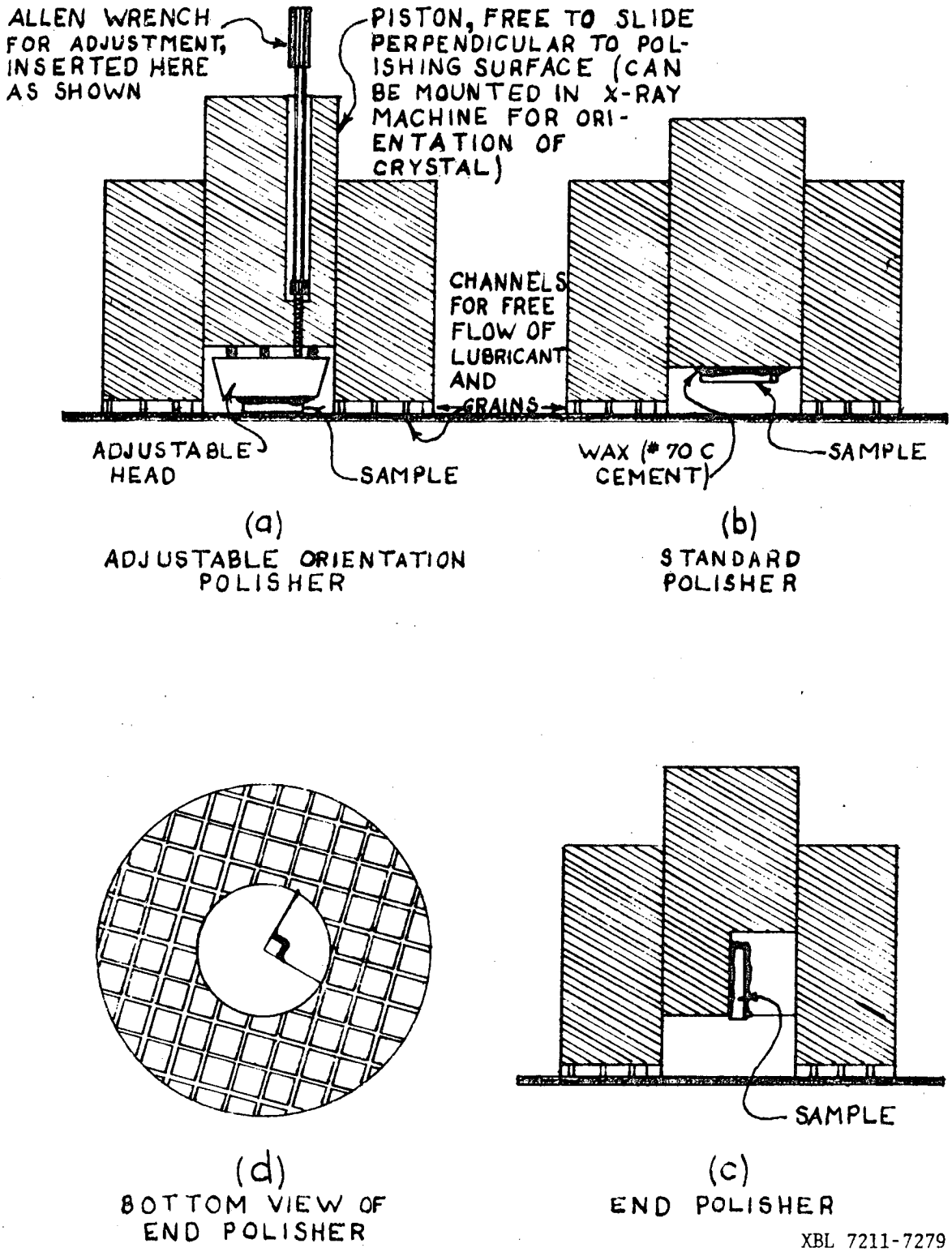

Fig. 22. Polishing devices for uniaxial stress samples.

This device insures that the polished face comes out exactly parallel to the back face which is stuck to the bottom of the piston with wax. (5) The ends are particularly important. They must be both parallel to each other and perpendicular to the sides. After polishing the sides, the sample is mounted in the end-polishing piston shown in Fig. 22c,d. Only a few tenths of a millimeter is left protruding from the bottom. The end is polished down to 1μ alumina, since it should be smooth in order to have uniform stress. The other end is polished in a similar manner.

The wax can be cleaned off by soaking in several baths of methanol for a day or two. There should be no nicks on the edges of the polished sample, as they may act as points of concentration of stress, leading to breaking of the sample.

The final dimensions of our samples were: (001): .23 × .19 × .85 cm.; (111): .21 × .21 × 1.42 cm.

3. Chemical Polishing

Just before mounting, the sample was polished for 90-120 sec. in the solution used by Zucca:[10]

3 parts	HNO_3
1	HF
4	H_2O

WARNING: Acids are dangerous and HF is particularly dangerous. Seek advice before using and take all precautions.

The sample was rinsed by displacing the polishing solution with H_2O and CH_3OH, then dried by blowing it lightly with N_2.

4. Mounting and Gluing

Immediately upon chemical polishing the sample is carefully mounted in the pistons in the sample holder frame, using freshly mixed white epoxy. (Clear epoxy makes it hard to see what you're doing.) At this point the sample holder (stress frame, Fig. 4) is being held upside down, and the weight of the inside shaft is on the sample. If the sample rotates smoothly in the piston holes at either end, then the glue will set well and the distribution of stress will be reasonably uniform. (Use teflon-coated tweezers to handle the sample.) Rotate the sample to the approximate position desired. Now, making sure there are a few pounds of pressure on the sample (corresponding to .01 - .1 kilobars), tighten the nut that locks the shaft in place. The stress frame may now be carried to and mounted in the dewar, which contains N_2(g) and which is immediately flushed and refilled several times until the atmosphere is clean again. The stressing levers are set up, but before actually attaching the levers to the pull shaft of the sample holder, balance the levers using the lead weights. This is so that a zero stress reading will not be in error because of the weight of the levers. Attach the pull shaft, and taking care to keep a small pressure always on the sample ($< .1$ kb) so that it will not shift while the glue is drying, release the nut so that the levers now pull on the sample. In this state the glue is left to dry 12-24 hrs. ($\frac{1}{2}$ hr. if a heat lamp can be properly applied to the sample). It is probably good to keep a slow flow of N_2 gas coming up from the bottom

and venting through a one-way valve at the top, in order to carry any glue vapors away during setting.

Because of possible hysteresis effects which we observed, it is desirable to measure the spectra with increasing stress. Even the ~ 2 kb we applied before cooling to test the sample mount may have been a mistake, since we detected a slight polarization dependence in our zero stress 5° curve measured after this test.

All stress data were taken at He temperature (5°), because in this low temperature region temperature variation of the band structure is negligible and life-time broadening effects are minimized.

D. Experimental Results

1. Description and Interpretation of Results

In Figs. 23 and 24 are the data for logarithmic derivative reflectivity for various levels of (111) and (001) uniaxial stress. In each figure the curves for $\underset{\sim}{E}$ parallel to stress (———) and $\underset{\sim}{E}$ perpendicular to stress (-----) appear at the same time.

Enlarging upon the work of Zucca,[2] et.al., we can interpret the general shape of our zero-stress spectra as the superposition of two lineshapes separated by the spin-orbit splitting of the valence bands. Each of these two shapes can be seen as a composite of an M_0 shape (positive swing) and an M_1 shape at slightly higher energy (negative swing), by putting together the critical point shapes of Fig. 19. The result is shown in Fig. 25a. This is the simplest and most likely combination in terms of what we know about the band

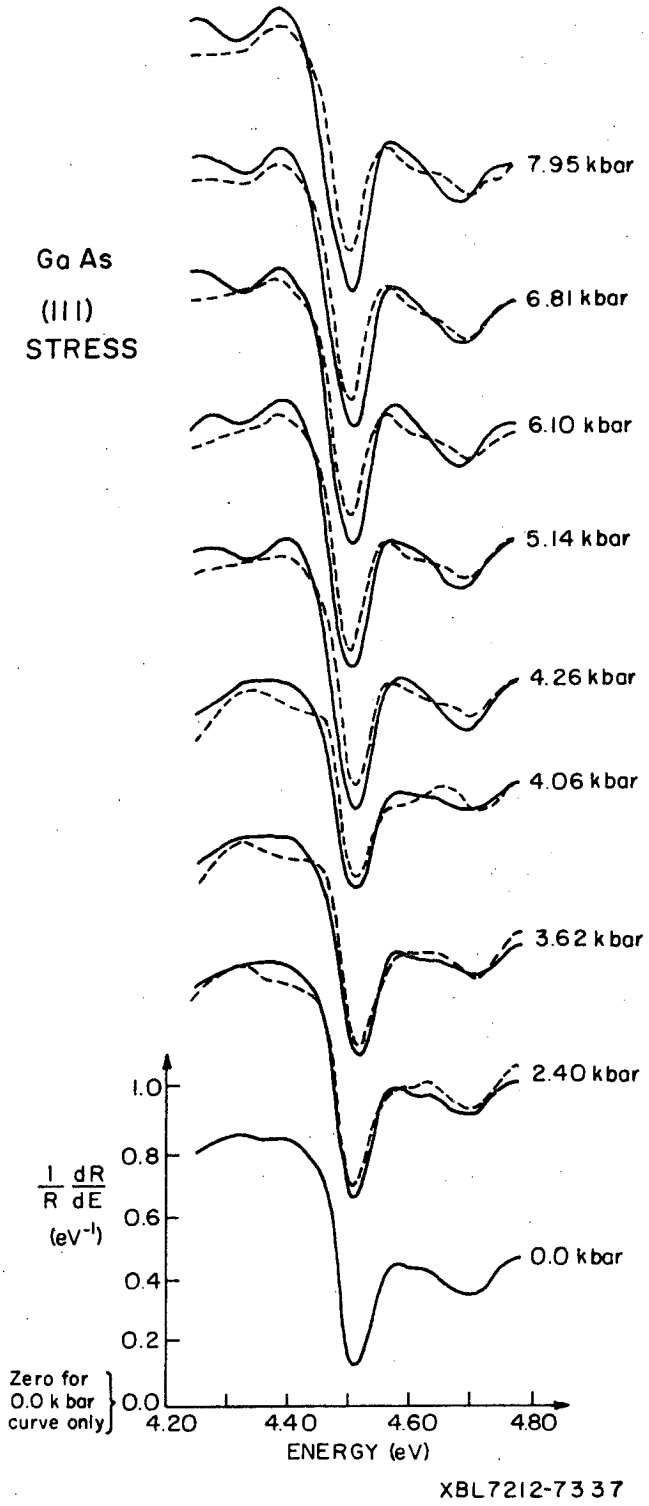

Fig. 23. Derivative reflectivity at 5°K of the E_o' peaks of GaAs, for various levels of (111) uniaxial stress. The solid curve is (1/R) dR/dE for light polarized parallel to stress; the dashed curve is for light polarized perpendicular to stress.

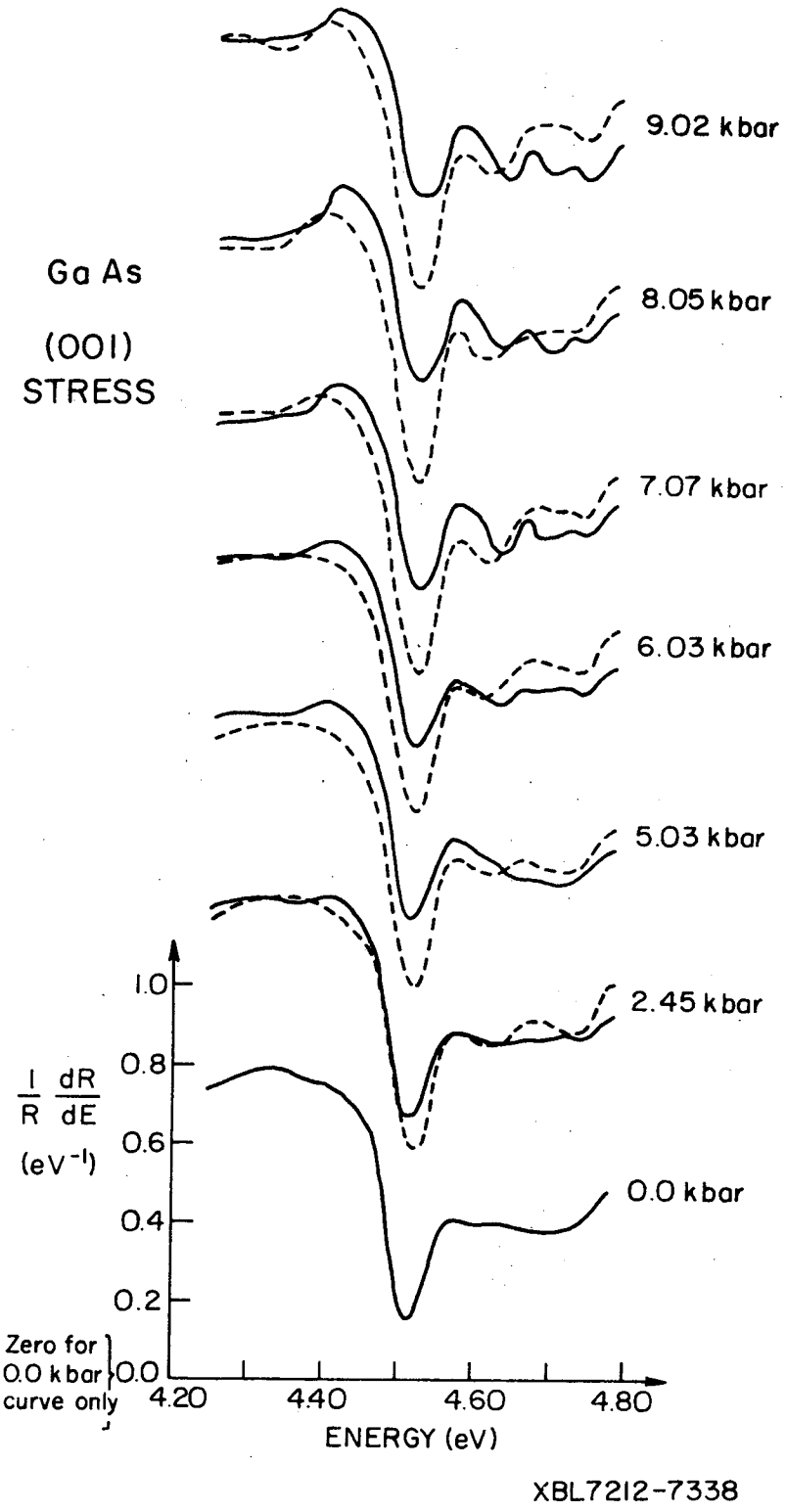

Fig. 24. [Same caption, except replace (111) by (001).]

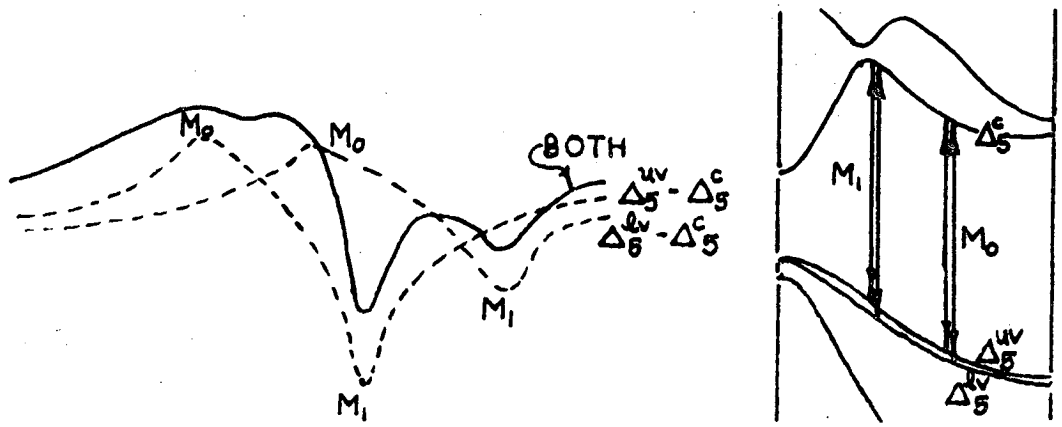

Fig. 25(a). An explanation of the E_0' lineshape in the unstressed GaAs crystal.

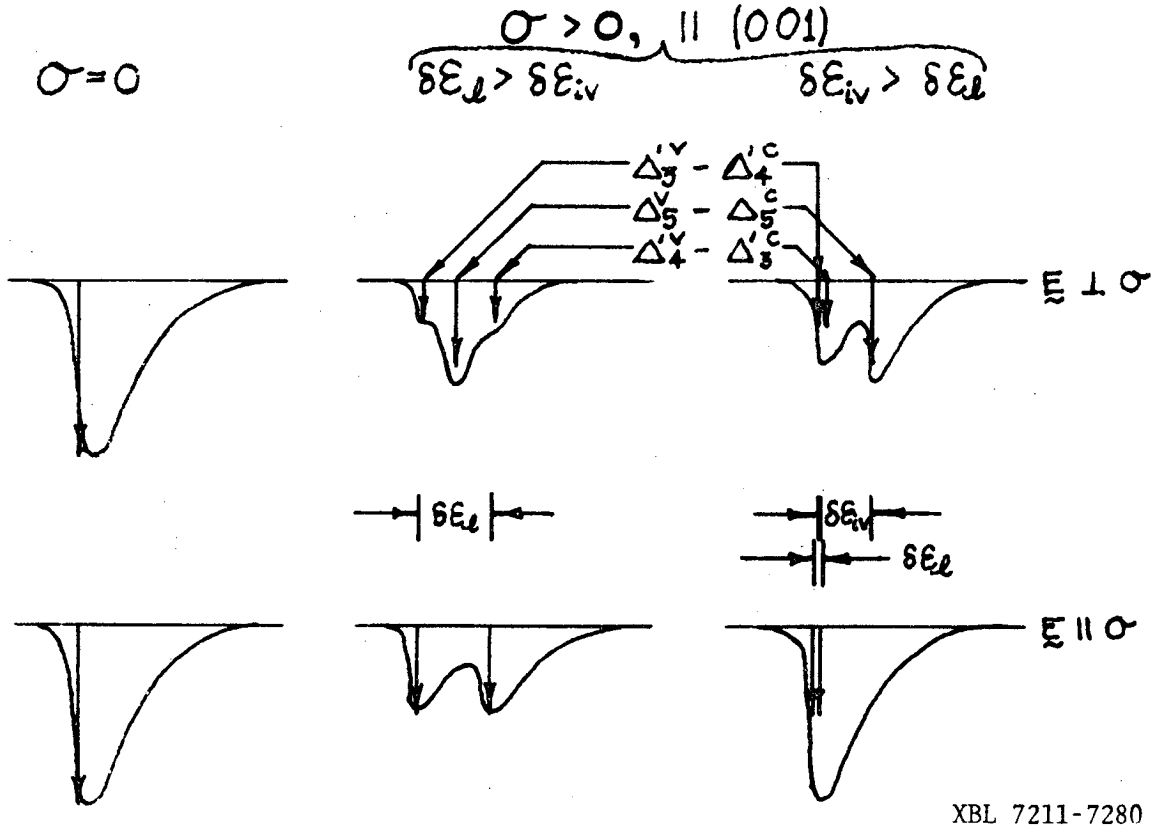

Fig. 25(b). Effect of relative magnitudes of $\delta\varepsilon_l$ and $\delta\varepsilon_{iv}$ on the spectrum, for both polarizations.

structure, but not the only possible conclusion. More definitive statements about where the critical points are in the E_0' structure will have to wait for more experimental information and more highly resolved band structure calculations.

Our data strongly indicate that Δ-transitions dominate, regardless of the exact lineshape interpretation that is made. The curves for (111) stress show relatively little polarization dependence of the big downward peak at 4.5 eV, but the curves for (001) stress show a strong polarization dependence. The downward peak begins to broaden considerably for light polarized parallel to stress, as if it were preparing to split, while for light polarization perpendicular to stress the peak remains fairly narrow. The second downward peak, at 4.7 eV, shows even more marked behavior, with new peaks appearing in the (001) curves for both polarizations.

Referring to Fig. 16, we interpret the behavior of the 4.5 eV downward peak as follows: (1) Under (111) stress, there is little polarization dependence, and a slight broadening of the peak for both polarizations with increasing stress represents the local splitting of Δ_5', at all six locations in the Brillouin zone. Although quantization of this broadening is somewhat of an arbitrary procedure, we have estimated the rate of broadening at .0011 eV/kbar ± .0006. The shift in both peaks for compressive stress is estimated as -.0026 eV/kbar ± .0015. (2) Under (001) stress, the peak in the parallel-polarized spectrum broadens much more than that in the perpendicular-polarized spectrum. This fact indicates that the local

splitting of Δ_5' is more important than the intervalley splitting between Δ_5' and Δ_5. The broadening of the parallel-polarized peak represents the local splitting of Δ_5', and we have estimated its rate at .0043 eV/kbar ± .002. Figure 25b gives our explanation of how the peak is expected to split, for the two possible cases of $\delta\varepsilon_{local} > \delta\varepsilon_{intervalley}$ and $\delta\varepsilon_{\ell} < \delta\varepsilon_{iv}$; clearly our data favors the former case. Estimates for other parameters are: .0011 ± .0008 for the intervalley splitting under (001) stress; .00075 ± .0005 for the average shift of both peaks together ("center of gravity" shift).

2. Deformation Potentials

In Eqs. (28) and (29) we give the analytical expressions for the energy shifts of the Δ_5 and Δ_5' levels under (111) and (001) stresses in terms of the quantum mechanical matrix elements, derived from the general theory of Sec. A. The definitions of these matrix elements, or deformation potential parameters, are given in Eq. (30).

(001) stress

Δ_5, $\underset{\sim}{k} = \pm k\hat{z}$

$$\delta\varepsilon_{\Delta}(001) = \frac{1}{\sqrt{3}}(s_{11}+2s_{12})\sigma\, \mathcal{D}_1^1 + 2\,\frac{(s_{11}-s_{12})}{\sqrt{6}}\,\sigma\mathcal{D}_1^3 \qquad (28a)$$

Δ_5, $\underset{\sim}{k} = \pm k\hat{x}, \pm k\hat{y}$

$$\delta\varepsilon_{\Delta'}(001) = \frac{1}{\sqrt{3}}(s_{11}+2s_{12})\sigma\, \mathcal{D}_1^1 - \frac{(s_{11}-s_{12})\sigma}{\sqrt{6}}\,\mathcal{D}_1^3$$

$$\pm\ \frac{(s_{11}-s_{12})\sigma}{\sqrt{2}}\,\mathcal{D}_3 \qquad (28b)$$

(111) stress

Δ_5'

$\underset{\sim}{k} = \pm k\hat{x}, \pm k\hat{y}, \pm k\hat{z}$

$$\delta\varepsilon_{\Delta'}(111) = \frac{1}{\sqrt{3}}(s_{11}+2s_{12})\sigma\mathfrak{D}_1^1 + \frac{s_{44}\sigma}{3}\mathfrak{D}_1^5 \pm \frac{2s_{44}\sigma}{3}\left|\mathfrak{D}_4\right| \qquad (29)$$

s_{11}, s_{12}, and s_{44} are the elastic compliance constants. We have used the values of Huntington:[51] $s_{11} = 1.264 \times 10^{-11}$, $s_{12} = -.04234 \times 10^{-11}$, and $s_{44} = 1.86 \times 10^{-11}$ $cm^2 dyne.^{-1}$ The deformation potentials are the matrix elements:

$$\mathfrak{D}_1^1 \equiv \left(u_{-1/2}, \frac{D_{xx} + D_{yy} + D_{zz} + d_{zz}}{\sqrt{3}} u_{-1/2}\right)$$

$$\mathfrak{D}_1^3 \equiv \left(u_{-1/2} \frac{-D_{xx} - D_{yy} + 2D_{zz} + 2d_{zz}}{\sqrt{6}} u_{-1/2}\right)$$

$$\mathfrak{D}_1^5 \equiv \left(u_{-1/2} (D_{xy} + D_{yx}) u_{-1/2}\right)$$

$$\mathfrak{D}_3 \equiv \left(u_{-1/2}, \frac{D_{xx} - D_{yy}}{\sqrt{2}} u_{-1/2}\right)$$

$$\mathfrak{D}_4 \equiv \left(u_{-1/2}, \left(\bar{D}_{xz} + \frac{1}{2} d_{xz} + \bar{D}_{yz} + \frac{1}{2} d_{yz}\right) u_{+1/2}\right) \qquad (30)$$

where $u_{\underset{\sim}{k},-1/2}$ and $u_{\underset{\sim}{k},1/2}$ are the two Bloch functions of states belonging to the same Δ_5 in the zinc blende crystal. The D_{ij}'s are the

deformation operators defined in Eq. (17). We have defined the matrix elements $\mathfrak{D}_1^1, \mathfrak{D}_1^3$, etc., according to the scheme of E. O. Kane.[44] In this scheme, the subscripts j indicate that $\mathfrak{D}$ is the matrix element of an $h_\alpha^{(j)s}$, the superscript stands for the repetition index s and indicates the representation to which h would belong in the point group of Γ, T_d.

The energy shifts in Eqs. (28) and (29) are the absolute energy shifts for a particular band; thus the deformation potentials in Eq. (30) refer to a specific band also. From an experiment like ours we can only obtain the shift in relative energies of the bands, and thus all experimental energy shifts discussed are relative ones. The relative local and intervalley splittings are given below in terms of the absolute energy shifts of Eqs. (28) and (29).

$$\delta\varepsilon_\ell^{rel} = \left| \left(\delta\varepsilon_{\Delta_4'^c} - \delta\varepsilon_{\Delta_3'^v} \right) - \left(\delta\varepsilon_{\Delta_3'^c} - \delta\varepsilon_{\Delta_4'^v} \right) \right| , \tag{31a}$$

$$\delta\varepsilon_{iv}^{rel} = \left| \left(\delta\varepsilon_{\Delta_5^c} - \delta\varepsilon_{\Delta_5^v} \right) - \frac{1}{2} \left[\left(\delta\varepsilon_{\Delta_4'^c} - \delta\varepsilon_{\Delta_3'^v} \right) + \left(\delta\varepsilon_{\Delta_3'^c} - \delta\varepsilon_{\Delta_4'^v} \right) \right] \right| . \tag{31b}$$

These quantities are illustrated in Fig. 25b.

A fine quantitative analysis of our data is not possible because of the complexity of the spectra. However, based on the above equations, we have estimated the deformation potentials as follows in Table VI.

TABLE VI

Estimated relative deformation potentials for the $\Delta_5^{\ell v}$, $\Delta_5^{uv} - \Delta_5^c$ transitions in the E_0' region of GaAs. (Tensile stress, or positive stress.)

$\mathcal{D}_1^1$	=	-.08 eV
$\mathcal{D}_1^3$	=	-.07
$\mathcal{D}_1^5$	=	+.5
$\lvert \mathcal{D}_3 \rvert$	=	+.3
$\lvert \mathcal{D}_4 \rvert$	=	+.05

These values may be in error by ± 50%, due to the smallness of the experimental shifts, as well as to uncertainty in the criteria for measuring peak widths and splittings.

Note that these values are really the differences of the $\mathfrak{D}$'s for the two bands between which the transition occurs, namely the upper valence bands and the lowest conduction band.

3. Other Critical Points

Based on available band structure calculations such as that of Walter, et.al.,[37,38] we can rule out the possibility that Λ critical points contribute structure to the E_0' region. However, as mentioned in Sec. B, there is a very definite possibility that Γ transitions from the valence bands to the upper conduction bands affect the spectrum in this region. The Γ_8^v-Γ_7^c energy has been put by various authors at 4.52 eV,[4,52] 4.6 to 4.8 eV,[53] and 4.75 eV.[37] Although any structure due to Γ should be minor compared to that due to Δ, the resolution and sensitivity of our wavelength modulation spectrometer leads us to examine our spectra for structure characteristic of Γ transitions.

Some evidence of Γ transitions can be found in our spectra. The data reveal a more complex picture of the E_0' region than explainable on the basis of Δ transitions alone. In particular, toward the higher energy part of our spectra (4.6 to 4.8 eV), there is polarization dependence for both (001) and (111) stresses. According to Figs. 18 and 21a, this is evidence of the Γ transition, since the other possibility, transitions along Λ, was excluded above. The development of the peaks with stress in this portion of the spectra is somewhat confusing, but one possibility is that the peaks due to Γ_8^v-Γ_7^c and Γ_8^v-Γ_8^c are hidden in the larger Δ peaks, particularly in the region near 4.7 eV. Higher stress, somewhat better resolution, and a detailed

lineshape analysis might allow identification of these critical points. In view of the complexity of the spectra and our limited range, however, we cannot make decisive conclusions about the Γ transtions at this time.

The main downward peak at 4.5 eV, whose shape according to our method of analysis derives from an M_1 critical point, has another possible interpretation: could it be the result of the M_1 point at X, enhanced in the reflectivity because of a large matrix element? This is not likely, since theoretical calculations, including John Walter's*, do not give a substantially different dipole matrix element for transitions at X than at (.3,0,0), which would be necessary to overcome the smaller joint density of states at X. Our data add experimental weight to the conclusion that X is not responsible for the main strength of this peak. This can be seen as follows: The parallel-polarized spectra for (001) stress arises only from Δ' or X' transitions (ignore possible small Γ contributions), namely those with $\underset{\sim}{k}$ perpendicular to stress. Further, the broadening and shortening of the major downward peak at 4.5 eV with increasing stress has been explained above as representing the local splitting of these states. But X' does not undergo local splitting, as mentioned in Sec. B. Thus this structure, and its spin-orbit partner at 4.7 eV, should be assigned to Δ, not X, symmetry.

---

*Carmen Varea de Alvarez, private communication.

E. Discussion

The usefulness of this kind of experiment in band structure studies is limited by two interrelated physical facts: the occurrence of many weak critical points close together, and lifetime broadening which smears out the critical points. These limitations are amply illustrated by our results. With still higher resolution (we were at the limit of our equipment, ~ 30 Å) we might have distinguished, at lower stress, a few more of the small peaks created by the stress. In order to insure that all line widths are intrinsic to the sample, a higher resolution should be tried; by this we mean a smaller modulation amplitude combined with smaller entrance and exit slit widths. Also, non-uniform stress can create an artificial broadening of the critical points.

Perhaps we are depending too much on the picture of sharp critical points and one-electron transitions to explain the structure in this region. There may be many-body effects too large to be treated in the perturbation or lifetime-broadening limit and too complex to be treated by simple exciton theories. However, the optical spectra calculated from band structures on the assumption of one-electron transitions give good agreement with major peaks, especially when excitons are taken into account, so why shouldn't we expect agreement for small peaks? There may still be a lot of new information to be gained on the basis of the one-electron approximation.

The simplest many-body effect is the formation of excitons. We should understand more about how they form in parts of the zone away from Γ. Hyperbolic, quasi-bound excitons have been found in the E_1 structure and are attributed to the $\Lambda(M_1)$ transitions. Along Δ, do excitons occur associated with the M_1 or M_0 points within the zone, or with the valley at X? In view of the fact that our main M_1 peak shows shape and temperature dependence characteristic of Coulomb effects, the answer to this question would provide further evidence about the identity of these peaks.

As with the experiment, theoretical curves are needed with finer resolution. So far, in complex higher energy regions like E_0', there has not been a lot of attention given to displaying the exact location of each critical point in calculated derivative reflectivity spectra. Actually, this is very hard work because a non-noisy and finely - detailed joint density of states curve requires a very fine mesh of points in the Brillouin zone, as well as computation of the joint density of states at small intervals of $\hbar\omega$. Current calculations[37] typically use 20,000 points in 1/48 th of the zone to calculate $\varepsilon_2(\hbar\omega)$ at intervals of .1 eV. A more detailed calculation would be very useful, however, because it would immediately reveal the role of the various critical points in the derivative spectrum and in particular show us what shape each critical point should produce. When the corresponding small structure is found in the experimental curve, the theory curve will tell us what part of the structure represents the critical point energy, enabling more accurate energy

measurement. This in turn will provide accurate critical point energies and also, more of them, so that more pseudopotential parameters may be used and the band structure calculation improved.

If we obtain a more highly-resolved experimental spectrum but comparable pseudopotential results are not available, we might take another tack: determine ε_1' and ε_2' in the E_0' region as Braunstein and Welkowsky[4] have done. The line shapes in these curves, and their shifts and splits with stress, may be more immediately recognizable.

There will be many more uniaxial stress experiments done in the visible and ultraviolet regions for semiconductors, since, as we have found, such experiments contain a gold mine of information. Ours is the first in the E_0' region of a III-V semiconductor combining wavelength modulation with uniaxial stress, but we anticipate that more work will be done in this area soon.

ACKNOWLEDGMENTS

The author is indebted to Prof. Yuen-Ron Shen for his advice, guidance, and criticism, as well as to Stanley Kohn, Dr. Yves Petroff, Dr. Peter Yu, and Dr. Jackson Koo for their assistance and helpful discussions. We also owe gratitude to Dr. Ricardo Zucca, whose diligent work provided the starting point for this thesis.

We also thank Prof. Marvin L. Cohen, Prof. L. M. Falicov, Carmen Varea de Alvarez, Dr. John Walter, Jim Chadi, Dr. Yvonne Tsang, and Prof. C. Y. Fong for many essential discussions that helped us further understand the theoretical basis of the work.

The other people in the group of Prof. Shen, as well as other members of the Physics Department and IMRD, were very kind, both in assistance to my work and in discussions of areas which expanded greatly the scope of my education at Berkeley.

The author also expresses great appreciation for the work done by Alice Ramirez, Gloria Pelatowski, and others in the final preparation of this thesis.

REFERENCES

1. The most comprehensive history and survey of the field is: Manuel Cardona, Modulation Spectroscopy (Academic Press, New York, 1969), 358 pp., and references therein.
2. Ricardo R. L. Zucca and Y. R. Shen, Wavelength-Modulation Spectra of Some Semiconductors, Phys. Rev. (B) 1, 2668 (1970).
3. K. L. Shaklee and J. E. Rowe, Wavelength Modulation Spectrometer for Studying the Optical Properties of Solids, Appl. Optics 9, 627 (1970).
4. M. Welkowsky and R. Braunstein, Interband Transitions and Exciton Effects in Semiconductors, Phys. Rev. (B) 5, 497 (1972).
5. Kerry L. Shaklee, J. E. Rowe, and Manuel Cardona, New Evidence for the Existence of Exciton Effects at Hyperbolic Critical Points, Phys. Rev. 174, 828 (1968).
6. J. E. Rowe, Manuel Cardona, and Kerry L. Shaklee, Derivative Spectrum of Indirect Excitons in AlSb, Sol. St. Comm., 7, 441 (1969).
7. John P. Walter, Ricardo R. L. Zucca, Marvin L. Cohen, and Y. R. Shen, Temperature Dependence of the Wavelength-Modulation Spectra of GaAs, Phys. Rev. Lett., 24, 102 (1970).
8. Jackson Koo, Y. R. Shen, and Ricardo R. L. Zucca, Effects of Uniaxial Stress on the E_0'-peak of Silicon, Sol. St. Comm., 9, 2229 (1971).
9. D. D. Sell and E. O. Kane, Identification of Γ Transitions in the E_0' Region of Germanium by Piezoreflectance Measurements, Phys. Rev. (B) 5, 417 (1972).

10. Ricardo R. L. Zucca, Wavelength Modulation Spectroscopy of Semiconductors, Ph.D. thesis, University of California, Berkeley California, Jan. 1971.

11. Ricardo R. L. Zucca, John P. Walter, Y. R. Shen, and Marvin L. Cohen, Wavelength Modulation Spectra of GaAs and Silicon, Sol. St. Comm., 8, 627 (1970).

12. C. Y. Fong, Marvin L. Cohen, R. R. L. Zucca, J. Stokes, and Y. R. Shen, Wavelength Modulation Spectrum of Copper, Phys. Rev. Lett., 25, 1486 (1970).

13. C. Y. Fong and Marvin L. Cohen, Energy Band Structure of Copper by the Empirical Pseudopotential Method, Phys. Rev. Lett., 24, 306 (1970).

14. J. Stokes, Y. R. Shen, Y. W. Tsang, M. L. Cohen, and C. Y. Fong, Wavelength Modulation Spectra of Single Crystals of Copper and Gold, Phys. Lett., 38A, 347 (1972).

15. Carmen Varea de Alvarez, John P. Walter, Marvin L. Cohen, J. Stokes, and Y. R. Shen, Wavelength Modulation Spectra and Band Structures of InP and GaP, Phys. Rev. (B) 6: 1412 (1972).

16. Stephen L. Adler, Quantum Theory of Dielectric Constant, Phys. Rev., 126, 413 (1962).

17. S. E. Stokowski and D. D. Sell, Reflectivity and (dR/dE)/R of GaP between 2.5 and 6.0 eV, Phys. Rev. (B) 5, 1636 (1972). (We also have seen the spin-orbit splitting of E_1, but we had to rule it out because our resolution, ~50 Å, did not justify trusting this little dip.)

18. Marvin L. Cohen and Volker Heine, The Fitting of Pseudopotentials to Experimental Data and Their Subsequent Application, Solid State Physics 24, II (Academic Press, New York, 1970).

19. B. O. Seraphin and N. Bottka, Band Structure Analysis from Electroreflectance Studies, Phys. Rev., 145, 628 (1966).

20. M. Garfinkel, J. J. Tiemann, and W. E. Engeler, Piezoreflectivity of the Noble Metals, Phys. Rev., 148, 695 (1966).

21. D. D. Sell and P. Lawaetz, New Analysis of Direct Exciton Transitions: Applications to GaP, Phys. Rev. Lett., 26, 311 (1971).

22. Fred H. Pollak and Manuel Cardona, Peizo-Electroreflectance in Ge, GaAs, and Si, Phys. Rev., 172, 816 (1968).

23. See (1) H. Ehrenreich and H. R. Philipp, Optical Properties of Ag and Cu, Phys. Rev., 128, 1622 (1962). (2) B. R. Cooper, H. Ehrenreich, and H. R. Philipp, Optical Properties of the Noble Metals. II, Phys. Rev., 138, A494 (1965).

24. J. M. Ziman, Principles of the Theory of Solids, (Cambridge University Press, Cambridge, 1965), chap. 8.

25. Charles Kittel, Introduction to Solid State Physics, 3rd ed., (John Wiley & Sons, N. Y., 1966), chap. 8.

26. S. N. Jasperson and S. E. Schnatterly, Photon-Surface-Plasmon Coupling in Thick Ag Foils, Phys. Rev., 188, 759 (1969).

27. Andrew R. Melnyk and Michael J. Harrison, Theory of Optical Excitation of Plasmons in Metals, Phys. Rev. (B), 2, 835 (1970).

28. Andreas Otto, Excitation of Nonradiative Surface Plasma Waves in Silver by the Method of Frustrated Total Reflection, Zeitschrift für Physik, 216, 398 (1968).

29. G. B. Irani, T. Huen, and F. Wooten, Optical Properties of Ag and α-Phase Ag-Al Alloys, Phys. Rev. (B), 3, 2385 (1971).

30. Marie-Luce Thèye, Investigation of the Optical Properties of Au by Means of Thin Semitransparent Films, Phys. Rev. (B), 2, 3060 (1970).

31. Donald Grant Howard, Cyclotron Resonance Studies in Silver, Ph.D. thesis, Univ. of Calif., Berkeley, Calif., 1959.

32. J. M. Morabito,Jr., R. Steiger, R. Muller, and G. A. Somorjai, in G. A. Somorjai, ed., The Structure and Chemistry of Solid Surfaces, p. 50-1, (John Wiley & Sons, N.Y., 1969).

33. A. M. Mattera, R. M. Goodman, and G. A. Somorjai, Low Energy Electron Diffraction Study of the (100) Face of Silver, Gold, and Palladium, Surface Science, 7, 26 (1967).

34. N. V. Smith, Photoelectron Energy Spectra and the Band Structures of of the Noble Metals, Phys. Rev. (B), 3, 1862 (1971); Richard Y. Koyama and Neville V. Smith, Photoemission Properties of Simple Metals, Phys. Rev. (B), 2, 3049 (1970).

35. C. N. Berglund and W. E. Spicer, Photoemission Studies of Copper and Silver: Theory, Phys. Rev., 136, A1030 (1964); Photoemission Studies of Copper and Silver: Experiment, Phys. Rev., 136, A 1044 (1964).

36. M. Garfinkel, J. J. Tiemann, and W. E. Engeler, Piezoreflectivity of the Noble Metals, Phys. Rev., 148, 695 (1966).

37. John P. Walter, Electronic Structure and Dielectric Properties of Cubic Semiconductors, Ph.D. thesis, Univ. of Calif., Berkeley, Calif., Nov. 1970.

38. John P. Walter and Marvin L. Cohen, Calculation of the Reflectivity, Modulated Reflectivity, and Band Structure of GaAs, GaP, ZnSe, and ZnS, Phys. Rev., 183, 763-772 (1969).

39. M. Cardona, Fundamental Reflectivity Spectrum of Semiconductors with Zinc-Blende Structure, J. Appl. Physics Suppl., 32, 3151 (1961).

40. H. C. Gatos and M. C. Levine, Chemical Behavior of Semiconductors: Etching Characteristics, Progress in Semiconductors, 9, 1, (London, 1965).

41. Manuel Cardona, Kerry L. Shaklee, and Fred H. Pollak, Electro-reflectance at a Semiconductor-Electrolyte Interface, Phys. Rev., 154, 696 (1967).

42. J. Zak, ed., The Irreducible Representations of Space Groups, (W. A. Benjamin, New York, 1969), 271 pp.

43. G. E. Pikus and G. L. Bir, Effect of Deformation on the Hole Energy Spectrum of Germanium and Silicon, Sov. Phys.-Sol. State, 1, 1502 (1960). (English translation)

44. Evan O. Kane, Strain Effects on Optical Critical Point Structure in Diamond-Type Crystals, Phys. Rev., 178, 1368 (1969).

45. Fernando Cerdeira, Effect of Deformations on Electronic and Vibronic Properties of Zincblende and Diamond-Type Semiconductors, Ph. D. thesis, Brown University, Providence, R.I., July 1971.

46. Michael Tinkham, Group Theory and Quantum Mechanics, (McGraw-Hill, New York, 1964), 340 pp.

47. George F. Koster, John O. Dimmock, Robert G. Wheeler, and Hermann Statz, Properties of the Thirty-Two Point Groups, (M.I.T. Press, Cambridge, Mass., 1963), 104 pp.

48. Eugene P. Wigner, Group Theory and Its Applications to the Quantum Machanics of Atomic Spectra, (Academic Press, N.Y., 1959).

49. Victor Rehn and D. S. Kyser, Symmetry of the 4.5 eV Optical Interband Threshold in GaAs, Phys. Rev. Lett., 28, 494 (1972).

50. J. E. Wells and P. Handler, Piezorefleetivity of Gallium Arsenide, Phys. Rev. (B) 3, 1315 (1971).

51. H. B. Huntington, The Elastic Constants of Crystals, Solid State Physics 7, (Academic Press, N.Y., 1958), p. 213.

52. M. L. Cohen and J. C. Phillips, Spectral Analysis of Photoemissive Yields in Si, Ge, GaAs, InAs, and InSb, Phys. Rev., 139, A912 (1965).

UNIVERSITY OF CALIFORNIA

Lawrence Berkeley Laboratory
Berkeley, California

Date Sept. 10, 1973

ERRATA

TO: All recipients of LBL-1125

FROM: Inorganic Materials Research Division and
Technical Information Division

SUBJECT: LBL-1125, "Wavelength Modulation Spectroscopy of Some Semiconductors and Metals," Jeffrey Andrew Stokes (March 1973)

Please make the following corrections on subject report.

Page 2, line 16 reads: the Fermi distribution, $_{k,\ell}$ is the energy of a state with wave

It should read: the Fermi distribution, $\mathcal{E}_{k,\ell}$ is the energy of a state with wave

Page 6, line 22 reads: ground variation of the slope. The shape of ε_1^1 and ε_2^1 at each type

It should read: ground variation of the slope. The shape of ε_1' and ε_2' at each type

Page 32, replace with attached corrected figure.

Page 35, replace with attached corrected figure.

Page 43, line 13 reads:

The Gap sample, according to Dr. Foster, was vapor grown in a PCl_3

It should read:

The GaP sample, according to Dr. Foster, was vapor grown in a PCl_3

C. Experimental Results

The derivative spectra of Cu, Ag, and Au measured at He temperatures in Figs. 7, 8 and 9, along with the logarithmic derivative reflectivity calculated from the pseudopotential theory.[12,13,14] The overall agreement of theory and experiment is good, in particular in the region of the large dip in (1/R)dR/dE at the onset of interband transitions, except in the case of Ag, where the dip in the theory curve is .22 eV higher in energy than in the experimental curve. The reflectivity and its logarithmic derivative were obtained from the band energies and pseudowave-functions by first calculating R and its derviative. In calculating the matrix elements for $\varepsilon_2(\omega)$, the contributions of the p and s electrons of the outermost core shell (3s, 3p for Cu; 4s, 4p for Ag; 5s, 5p for Au) were explicitly included. With this step the agreement in the region of the interband onset is very good, but without it $\varepsilon_2(\omega)$ in this region is way too low as shown[12] in Fig. 10. In the case of silver, the theory and experiment curves agree in general shape, and it is anticipated that fitting the pseudopotential parameters to our data instead of to a photoemission "density of states"[14,34] will produce better agreement as to the energy of the onset.

In each of the spectra, the first structure that occurs as we move up in energy is a sharp negative dip in the slope, and right after each dip R'/R swings positive (Au and Ag) or goes through a sharp maximum just before it reaches zero (Cu). To the right of the large dip in each spectrum we find a variety of structures, which are

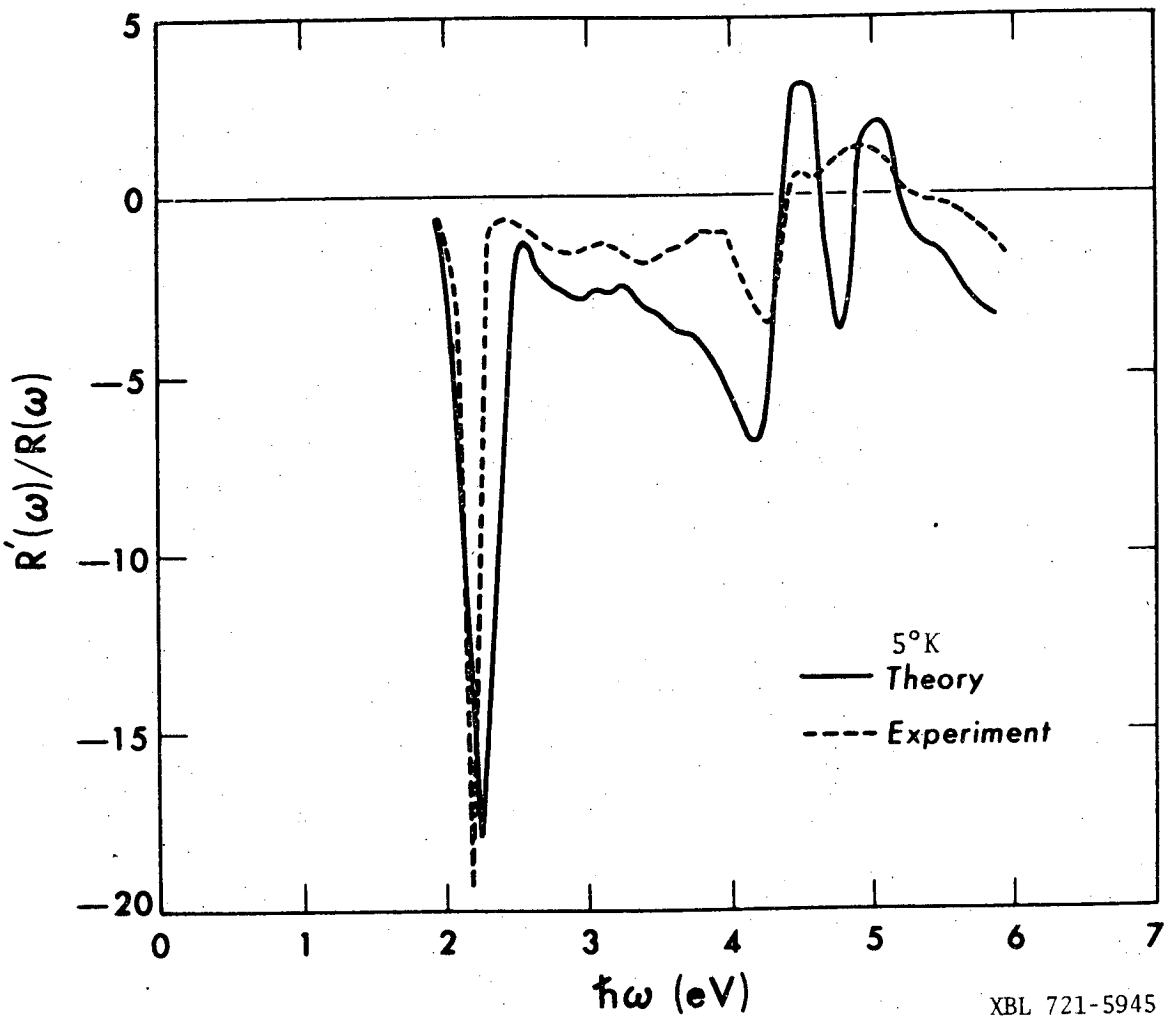

Fig. 7. Theoretical and Experimental Wavelength Modulation Spectra of Copper.

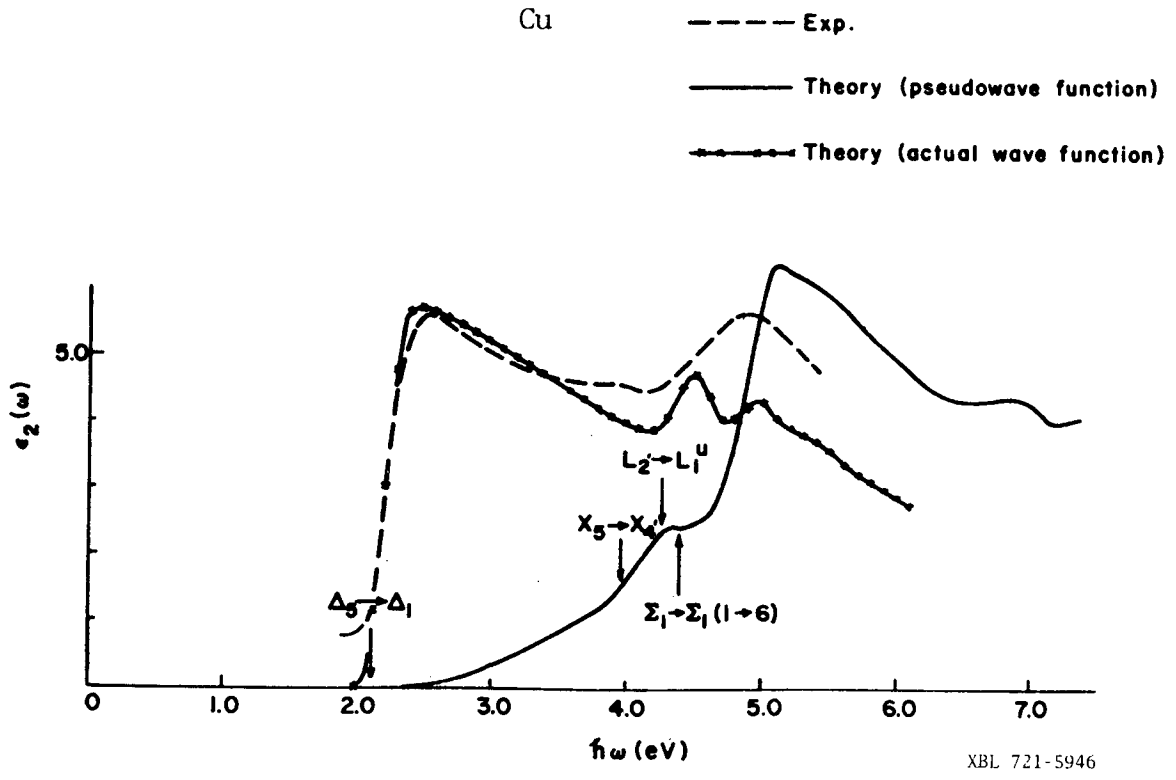

Fig. 10. Comparison of Theoretical Calculations of ε_2 at the Interband Threshold with an Experimental Result.[2] (From Ref. 12; data is that of Gerhardt, et.al., as cited in Ref. 12.).

small in comparison to the dip, but there is not otherwise any striking similarity in the three spectra in this region.

Using the pseudopotential results as a guide, we can interpret some of the features of the experimental spectra. We start with copper[12] (Fig. 7). The large dip between 2.1 and 2.3 eV is produced by the lowest interband transitions, which originate from the bands just below the conduction band and end up on the Fermi surface. Most of these transition occur near Δ in the Brillouin zone. The bump in the data at 3.1 eV is explained by a volume effect, near X with final states in the conduction band just above the Fermi surface. Other volume effects and an osculating point ($\Sigma_1 - \Sigma_1$, band 3 to band 6, numbering the bands according to the single group notation) could acoount for the small structures at 3.6 eV and 3.8 eV. (We note that, because of the coarse mesh of points in the Brillouin zone used for calculating the joint density of states, volume effects may be emphasized in the theoretical result.) In the pronounced structure around 4.0 eV we can locate two critical points, on the basis of both the theory and our line-shape analysis scheme described in Chapter I. These are: an M_1 point, $X_5 - X_4$, (bands 4, 5 to band 6), at 3.97 ± .02 eV; an M_0 point, $L_2' - L_1^u$ (band 6 to band 7) at 4.32 ± .04 eV. Above 4.25 eV, the experimental spectrum agrees with the theory in shape but not in magnitude. We can tentatively assign the bumps near 4.5 and 5.0 eV to volume effects; also, an osculating point may contribute to the lower energy bump.

TECHNICAL INFORMATION DIVISION
LAWRENCE BERKELEY LABORATORY
UNIVERSITY OF CALIFORNIA
BERKELEY, CALIFORNIA 94720